Surface interaction characterisation of microbial fuel cell organism Shewanella oneidensis.

Shah, Maia Kierann

Swansea University
Prifysgol Abertawe

Surface interaction characterisation of the microbial fuel cell organism *Shewanella oneidensis*

Maia Kierann Shah

MPhys MRes

Multidisciplinary Nanotechnology Centre
College of Engineering

Submitted to the University of Wales in fulfilment
of the requirements for the Degree of Doctor of Philosophy.

2011

Summary

In order to develop MFCs to their full potential, the mechanisms by which organisms such as *S. oneidensis* transfer electrons extracellularly need to be researched and understood, and key to this are the physical and chemical interactions between the cell surface and the surrounding environment, including other cells, minerals and MFC-relevant substrates. The research presented here characterises the physical interactions of anaerobically grown *S. oneidensis* MR1 under varying chemical conditions, using aerobically grown cells in identical experiments for comparison.

An array of experimental methods are used, including techniques for estimating cell concentration for growth profiles, ζ-potential of cells in solution, and Atomic Force Microscopy imaging of cells in different growth phases. A novel method using Surface Plasmon Resonance is used to quantify the kinetics of binding of cells to surfaces approximating MFC electrodes. This method is assessed for suitability and reviewed as a potential answer to other research problems based on cell-device interfaces. Finally, novel force spectroscopy using custom-made mineral probes is used to gather mechanical data about cells of *S. oneidensis* MR-1 and to quantify the interaction of cells with iron oxide and graphite.

The results show the differences in growth profiles between aerobically and anaerobically grown cells. Different results were also seen for aerobically grown and anaerobically grown cells in preliminary SPR studies using poly-L-lysine, and in the force spectroscopy results including adhesion force and Young's moduli. The effects of pH and salinity on cell surface interaction were investigated using measured isoelectric points from the zeta-potential studies as a guide and found to change the measured values of Young's modulus, and the maximum change in SPR response, for both types of cell.

The demonstrable effects of ambient chemistry on cell-cell and cell-surface interaction provide a reference point for bio-device design with the potential for multi-organism devices utilising the multiple electron transfer pathways of S. oneidensis MR1. The use of SPR for real time measurement of whole-cell binding to electrode-approximating surfaces and the resultant interaction kinetics is established as a novel, repeatable and accessible way of investigating cell-surface interaction.

Declaration

This work has not previously been accepted in substance for any degree and is not being concurrently submitted in candidature for any degree.

Signed (candidate): .....

Date: 10-10-2011

Statement 1

This thesis is the result of my own investigations, except where otherwise stated. Other sources are acknowledged by the use of explicit references. A list of references is included.

Signed (candidate): .....

Date: 10-10-2011

Statement 2

I hereby give consent for my thesis, if accepted, to be available for photocopying and for interlibrary loan, and for the title and summary to be made available to outside organisations.

Signed (candidate): .....

Date: 10-10-2011

Acknowledgments

Firstly this thesis is dedicated to Eva Thomas, my grandmother.

I would like to take the opportunity to express my immense gratitude to Swansea University and the Multidisciplinary Nanotechnology Centre. In particular I would like to thank my supervisor Dr. Chris Wright for his support and guidance throughout my studies. I would also like to thank the following for their technical guidance and moral support: Dr. Dale Rogers, Dr. Martin Brown, Dr. Mark Penny, Dr. Shuyeng Chen, Dr. Ian Armstrong, Dr. Richard Bayliss, Dr. Lewis Francis, and finally my office/lab partners in crime (and lifesavers) Dr. Lydia Powell and Dr. Kimberley Bell.

Finally, I cannot express enough gratitude for my family and my friends, who have listened, read, supported and cheered me on throughout every single stage of my work. Thankyou.

List of Figures

List of Tables

Abbreviations Used

AFM	Atomic Force Microscopy
ATP	Adenosine Triphosphate
BSA	Bovine Serum Albumin
DNA	Deoxyribonucleic acid
JKR	Johnson Kendall Roberts theory
MFC	Microbial Fuel Cell
mIgG	Mouse immunoglobulin G
OM	Outer Membrane
PSPD	Position Sensitive Photodetector
SEM	Scanning Electron Microscopy
SPM	Scanning Probe Microscopy
SPR	Surface Plasmon Resonance
STM	Scanning Tunnelling Microscopy
TEM	Transmission Electron Microscopy

1. Introduction

One of the defining challenges of the century is the need for safe, clean and renewable energy sources. Demand for energy is growing just as fossil fuels are becoming harder to obtain leading to rising costs for businesses and domestic users. In addition to this, the problem of increasing carbon dioxide levels and the associated climate change add urgency to the need to wean humanity off fossil fuels and traditional combustion methods of energy production. In tackling this challenge innovative answers are required to make renewable energy sources cost effective and up to the job of powering our world.

To this end, some changes will need to start on the small scale. This thesis is concerned with bacteria which can be used to generate electricity. The current output recorded for this bacterium is small-scale, of the order of mA according to the literature (as will be described), but it is a stepping stone on the way to harnessing existing natural energy production.

The organism in question is *Shewanella oneidensis* MR-1, described in detail in section 1.2.6. This study has identified key questions about the effects of environment on this organism, and its interactions between cells themselves and between cells and important substrates. In this first chapter the context of study and the aims and objectives of this thesis are outlined. The following chapter describes the experimental methodology. Chapters 3, 4 and 5 present and discuss the results and their significance in line with pre-existing results in the literature. Chapter 6 discusses the findings, their relevance, and to what extent the questions asked in this chapter have been answered.

1.1 Biotechnology

There is a wealth of "engineering" in the natural structures of the world we inhabit: some motile bacteria swim using a molecular motor to drive an extending flagellum as a form of propellor[1]; the lotus, lauded in mythology for its purity, is now known to have leaves which are nano-structured to repel dirt[2]; and DNA self-assembles from its component nucleotides guanine, adenine, cytosine and thymine paving the way for the "assembly" of living beings[3].

Biotechnology has long existed as the adaptation of the natural world for technological development. It can generally be divided into two main areas: biomimetics and bioinspiration, and biocomposite technology. The biomimetic process has, for example, given us Velcro (inspired by burdock clinging to dog hair) and colour changing car body paint based on the nanoscale structuring of iridescent butterfly wings. These are examples in which biology has provided a precedent that can be mimicked with inorganic materials or in inorganic devices. Biocomposite technology uses biological systems directly and at some point has an organic/inorganic interface. Often the interface is the crux of this technology, as it is in biosensors: these devices usually detect the presence of a substance through the effect it has on an organic molecule which is part of an organic/inorganic interface, thus triggering an electrical signal in the sensor[4].

Biocomposite engineering itself can be exemplified on the nanoscale. In 2007 Ruiz-Hitzky and his team published a report in Advanced Materials detailing the progress of development of nanoscale organic/inorganic hybrid materials that they termed "bionanocomposites"[5]. These novel materials were formed from naturally occurring polymers and inorganic solids with at least one dimension on the nanoscale, and the authors described not only manufacture but also potential applications. The two desirable attributes for

such materials are biocompatibility and biodegradability. The main areas of impact for such biohybrids are biomedical: building structures to aid regeneration of tissues or even bone, and environmental: such materials can biodegrade more easily than wholly inorganic constructs. Further to this, functional bionanocomposites, which can be used in optical, electrochemical or photoelectric systems, are described. As the authors intimate, there is a wealth of possibilities in this area as there is an abundance of natural polymers to use in synergy with inorganic materials. Further research could conceivably provide a multitude of composite materials with varying components and production processes in order to improve properties and multi-functionality.

There is also arguably a third area of biotechnology: wholly biological technology where biological systems have been manipulated to suit human design criteria. Genetic engineering is an example of this, in particular the manipulation of stem cells for gene therapy or organ transplant solutions.

As technology has allowed us to view and understand how biological systems operate on the nanoscale, the resulting knowledge has been tied into what we understand on the macroscale. This is certainly the case in molecular biology and bacteriology: a nanometre is 10 times larger than an Angstrom, Å, a unit of measurement often used to describe atomic radii or the length of chemical bonds. Thus, macromolecules (large molecular structures made up of hundreds of atoms) can be perfect raw material for nanoscale design. Molecular biology is the study of biology on a molecular (near-nano) scale, looking at how biological molecules interact. Once again, DNA research and genetics are excellent examples of the impact of molecular biology on macroscale understanding.

Bacteriology also requires the understanding of biology on a small scale. Most bacteria cultivated in laboratory conditions have dimensions between

0.5 and 15μm in diameter or as minimum width and maximum length, depending on their morphology. However the largest known bacterium, *Thiomargarita namibiensis*, grows in chainlike formation of cocci (spherical bacterial components) and can grow up to 750μm in length (just visible to the naked eye). In contrast the smallest, *Mycoplasma pneumoniae*, which can cause a form of bacterial pneumonia, is 0.2μm (200nm) in diameter[1].

One automatically associates bacteriology with medicine and human health science, aided by public perception of "superbugs" such as MRSA (methicillin-resistant *Staphylococcus aureus*) and *Clostridium difficile* and "probiotic" products such as yoghurts that include specifically added live bacterial cultures intended to aid digestion. Bacteriology is not, however, only useful in terms of medical research. Bacteria are important in geology, waste treatment, water management, and also in nanotechnology.

One of the most exciting novel uses of bacteria is in the Microbial Fuel Cell (MFC), in this application electrical energy is generated using microbial metabolic functions[6]. What makes this developing technology even more exciting is the design of MFCs that use waste as a fuel source, even to the point of removing harmful substances from soils (bioremediation) or wastewater. There is no such thing as free energy, but this is energy where the cost in fuel provides the ultimate bonus.

1.1.1 Energy production with waste reduction

One of the greatest challenges facing the global community in the 21st century is the increased demand for energy; caused by widespread adoption of high-energy lifestyles throughout the developed and developing world. Catchy phrases such as "climate change" and "carbon footprint" are ubiquitous as the global consciousness struggles to come to terms with the

finitude of fossil fuels, our greatest source of energy, and the effects of global warming from the use of such fuels.

According to the UK Government Department for Environment and Climate Change the UK's total final user consumption of energy (including all industry, transport, and domestic use) in 2009 was the equivalent of 152.7 million tonnes of oil, the majority of which comes from gas and petroleum[7]. Emissions of greenhouse gases are caused by such electricity production as well as the use of oil derivatives in all forms of motorised transport. Climate change and energy production are two sides of the same problem: can there be renewable, clean energy production that makes a dent in our voracious consumption?

Nuclear energy is often put forward as an alternative to burning fossil fuels. There is a public unease about nuclear power plants due to their connection to the development of nuclear weapons and the Chernobyl disaster of 1986. Even more pressing a disadvantage is the production of nuclear waste by nuclear power plants. This problem with waste is actually common to all traditional methods of power production, and is another reason why renewables such as Wind and Solar power are termed "clean".

Modern society is incredibly wasteful and alongside our need for energy is the need for clean water. There is plenty of water on the Earth, but that which is drinkable is a precious commodity that needs to be managed appropriately. Methods exist which make undrinkable water suitable to drink, such as desalination, but when these methods are used on a large scale they are huge consumers of energy. Using so-called "grey water", a term for water that has already been used in domestic activities such as laundry, for watering plants or washing cars is one way to cut down on clean water consumption. The ideal situation would be finding a method of removing waste products from polluted water, allowing the water to be used again.

The ultimate answer to these two major problems: clean energy production and the removal of water pollutants, would be a method that combines the two. As will be discussed later in this chapter, Microbial Fuel Cell research has taken steps toward this goal.

1.2 Microbiology in biotechnology

Humans coexist with a wide spectrum of microbial faunae, some of which are inherent in the human body, within the digestive system for example[1]. The use of microorganisms in human systems and technology has a rich history. Microbial processes were harnessed when yeasts such as *Saccharomyces cerevisiae* were used in the production of beer, bread and wine by the first farming cultures[8]. These staples have sustained people throughout thousands of years of human history. Cheese is created using a process that begins when bacteria convert milk sugars into lactic acid. Today bacteria are even being promoted as aids to digestion that can be taken as over the counter preventatives for bloatedness in the form of yoghurts. Despite human reliance on microbiota, the science of microbiology has only developed over the last 350 years; beginning in the late 1600s with the first time man ever saw single-celled organisms[1]. This man was Antoni van Leeuwenhoek who, using a microscope of his own design, viewed and described minute creatures or "animalcules" that could not be seen with the naked eye.

In the 1800s Frederick Cohn founded the sub-discipline of Bacteriology: he proposed the first taxonomic system for labelling the bacteria he studied. The contributions of Louis Pasteur and Robert Koch in the same century rooted microbiology firmly in science with the understanding of microbe

reproduction, pasteurisation for food preservation, vaccination for disease prevention, and the germ theory of disease[9].

Currently, microbiology is an ever-expanding science involving the study of microbial habitats, metabolism, physiognomy, function and environmental interactions. Such studies have benefits for medicine and health science in understanding the effects of microbial faunae on humans (virology, medical microbiology); in understanding the use of microbes in industrial processes for food manufacture and agriculture; even the corrosion of metals and the formation of our chemical environment require reference to microbial action to be fully understood. However the story does not end there, as microbiology offers an insight into true "bottom-up" technology: designs that have evolved over millennia which we can finally dismantle and recreate in order to further our own development of devices and systems on the nanoscale.

1.2.1 Bacteria and Biophysics

The lives of microbes offer insights into physics on a cellular scale. The means of propulsion for motile bacteria are a brilliant example of microbial physics, and biochemistry, in action. Motility comes at a premium in terms of energy use and thus it must be worthwhile for the bacterium. Some bacteria swim, using flagellar motion, others are motile without flagella (gliding motility), or use chemotaxis, whereby the chemical gradient of the environment causes a randomly moving cell to move according to the chemical bias[1]. These mechanisms for motility are one way in which cells adapt to their environment. Mitchell and Kogure wrote a mini-review in 2005 describing the efforts of biophysicists to understand bacterial motility and the advantages of this understanding[10]. The review describes tools

and techniques for studying bacterial motility, looking at how these approaches further investigation of the mechanisms employed by bacteria and how these mechanisms are achieved by bacterial design and affected by environmental factors.

1.2.2 Microbial Surfaces

The surface of a microbe serves as its interface with its environment. The bacterial cell membrane or cell wall defines the extent of the cell and functions to maintain the integrity of the cell, as well as to control the uptake and excretion of substances to or from the cell. Thus the functioning surface of a unicellular organism is vitally important to its survival.

In general bacteria can be grouped into two types: gram-negative and gram-positive. The definition of these comes from gram staining; in this procedure (named after Christian Gram who developed the process in 1884) gram-positive bacteria appear purple and gram-negative bacteria appear pink after staining with a basic dye (such as crystal violet) and treatment with ethanol. Differences in the cell wall structure cause ethanol to decolourise gram-negative cells, but not gram-positive ones[9]. Gram-positive cells are bounded by cytoplasmic membranes with a rigid outer layer of peptidoglycan whereas the walls of gram-negative cells are more complex multilayer structures comprising a cytoplasmic membrane, one or more layers of peptidoglycan and an outer membrane[1]. Studies of the cell wall have been greatly helped by the introduction of electron microscopy, with the existence of the outer membrane (OM) being confirmed by electron microscopy of thin sections, such as that shown in figure 1.1.

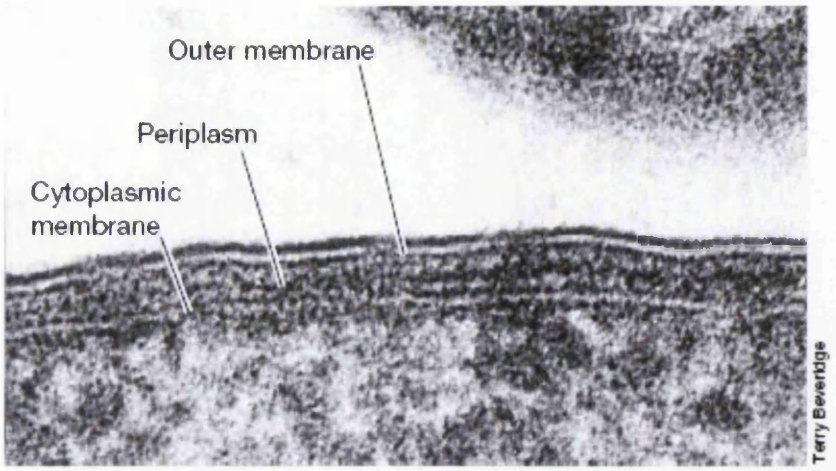

Figure 1-1:*Thin section transmission electron micrograph of the cell envelope of Eschericia coli with the outer membrane, periplasm and cytoplasmic membrane labelled. From Brock Biology of Microorganisms Unit 1 Chapter 4 by Madigan, Martinko, Dunlap and Clark*[11].

The cytoplasmic membrane acts as a highly selective permeability barrier of about 6-8 nanometres in width. Its general structure is that of a phospholipid bi-layer, whose homogeneity is broken up by membrane proteins that act to bind substrates, process large molecules and allow transport of materials into and out of the cell (e.g. metabolites, waste). The strength of the cell wall is usually due to the peptidoglycan layer, and it is this strength that maintains the cell's structure and rigidity[1]. The presence of peptidoglycan between inner and outer membranes was shown using lanthanum-stained thin sections[11]. It is thought that in the vast majority of bacterial cells, with only a few possible exceptions, the maintenance of bacterial shape is governed by the cell wall[12]. A diagram showing this structure is shown in figure 1.2.

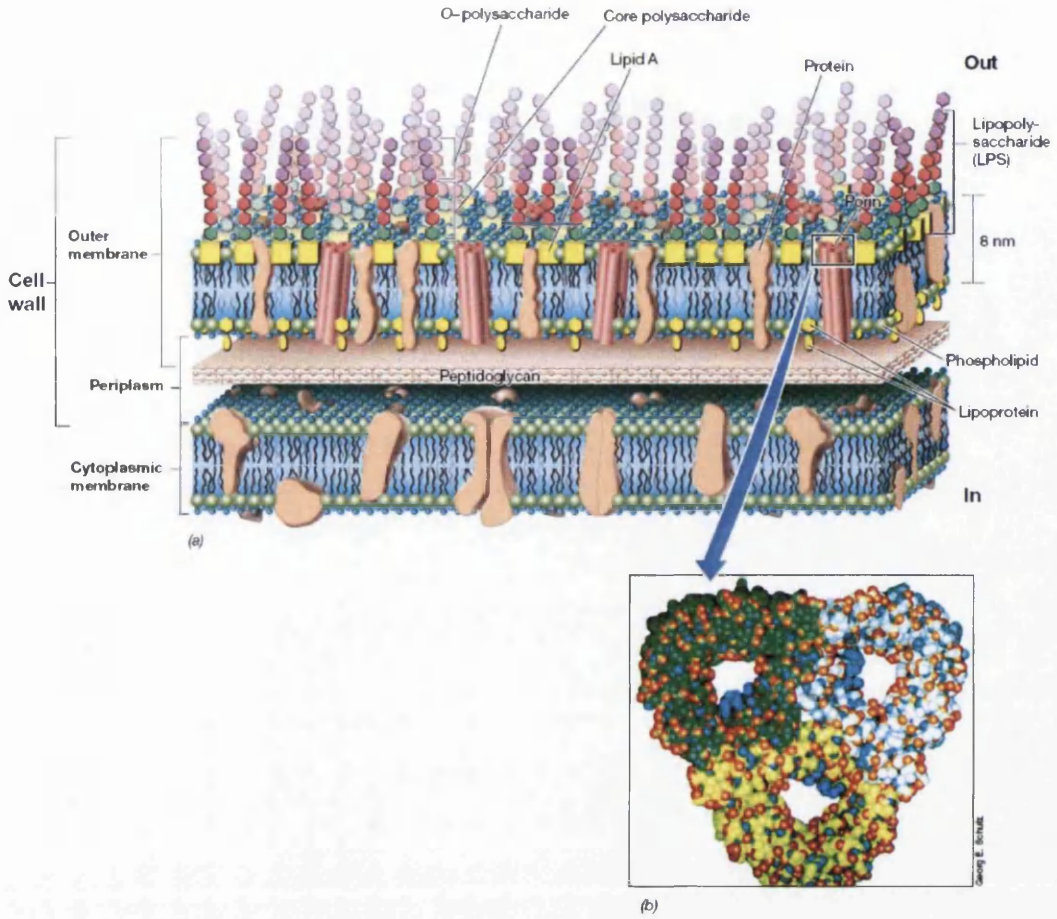

Figure 1-2: *The gram-negative cell wall. In this diagram the differences between the outer membrane and the cytoplasmic membrane can be seen such as the arrangement of membrane components, for example lipopolysaccharides and in the inclusion of porin proteins. Cross section of porin shown in (b). Diagram from Brock Biology of Microorganisms[1] Unit 1, Section 4.*

1.2.3 Metal reducing metabolism

In most organisms metabolism is powered via the respiration process, which allows energy to be produced from food or fuel. The respiratory process produces Adenosine triphosphate (ATP), which carries chemical energy vital for powering processes that would otherwise be energetically unfavourable.

The basic respiratory reaction is a redox reaction: it involves the oxidation of an electron donor and the reduction of an electron acceptor. As a result of

this reaction energy is produced and used to form ATP. For example, in this overview of the aerobic respiration of glucose oxygen is reduced:

$$C_6H_{12}O_6 + 6O_2 \rightarrow 6CO_2 + 6H_2O \quad 1.1$$

The reaction actually takes several stages, forming ATP via a method called "electron transfer phosphorylation" in which a series of protein-mediated reactions result in Adenosine diphosphate (ADP) and inorganic phosphate molecules combining to form as many as 30 molecules of ATP as a result of the oxidation of one molecule of glucose[13].

When the respiration process occurs without oxygen present, electrons must still be transported out of the cell to terminal electron acceptors. The greater the variety of minerals the bacteria can use for this purpose the better as far as species survival is concerned. Competition with other species for resources is less when bacteria can utilise a variety of electron acceptors. One of the most well known examples of such "extracellular respiration" is the electron transfer between microbial cells and minerals in their environment. In the review paper Extracellular Respiration, Gralnick and Newman present various examples of the title phenomenon[14]. As they discuss, the underlying molecular mechanisms are the basis for extracellular respiration and dictate the strategy by which a bacterium respires. Four potential pathways for extracellular respiration are put forward: direct contact between protein on the cell surface and the extracellular substrate, contact between the cell and substrate via an electrically conductive appendage, and two types of chemically mediated respiration. The chemically mediated strategy can either cause the cell or substrate to approach via chemical gradients (chemotaxis) or can be enacted at a distance using a chemical shuttle.

From the point of view of the cell, the terminal electron acceptor must simply be a material that the cell has the capability to reduce either through direct

contact or through the production of mediating chemicals[15]. Certain bacteria are known to use metals and metal oxides in their environment as the terminal electron acceptors in their respiratory process[16]. This ability enables them to live in anoxic or low oxygen environments such as marine sediments and oxygen depleted soil[17]. The exogenous transfer of electrons where oxygen is not available has been termed "electrogenesis" by Logan[18]. The types of bacteria he terms "exoelectrogens" will transport electrons out from within the cell body to an external terminal electron acceptor.

1.2.4 Biotechnological Applications of Microorganisms

As mentioned above, there are numerous applications for which microorganisms can be used in biotechnology. Some of these are outlined in more detail in this section to give an idea of the breadth of applications.

1.2.4.1 Microbial Synthesis

Bacterial systems can process inorganic materials in their environment by transporting them into cells and then expressing them either intra- or extra-cellularly in another form, thus synthesizing inorganic material on the nanoscale[19]. Nanoscale materials or "nanoparticles" are of interest due to their novel optical, photoelectrochemical, and electronic properties. For example: quantum dots are nano-scale semi-conductor crystals. These particles exhibit the characteristics of a confined semi-conductor and as such they have distinct optical qualities. The energy of photons they can absorb is dictated by their size, and so under UV light for example they will re-emit photons of specific energy levels and hence fluoresce with a unique colour. Larger quantum dots tend toward the red end of the spectrum with smaller quantum dots at the blue end. These materials have applications as tags for

biological macromolecules, or in other nanodevices as part of a circuit. They can be produced by a variety of bacteria. *Schizzacharomyces pombe,* for example, will produce cadmium selenide nanocrystals when challenged with cadmium in solution[20].

Gericke and Pinches investigated a number of different microorganisms, including bacteria, yeast and fungi, for their ability to produce gold nanoparticles[21]. One of their conclusions was that controlling the parameters of production in order to manufacture nanoparticles of consistent sizes and shapes would remain difficult until the cellular mechanism of synthesis was fully understood. To that end, they tried changing parameters such as pH, temperature, and growth stage of cells for two fungal cultures. They found that for these cultures pH affected the nanoparticle size, and growth stage affected the number of nanoparticles. Findings like this are a demonstration of how environmental factors and stage of growth are important considerations for studies of living things in bionanotechnology.

It is not only dot-like nanoparticles that can be manufactured with microbial synthesis: Kumar and colleagues describe use of a bacterium, *Magnetospirillium magnetotacticum,* as a catalyst for producing multi-walled carbon nanotubes[22]. Interestingly the nanotubes produced were of consistent diameters, around 13nm. This works because "The MS-1 bacterium synthesizes intracellular, linear, single-domain magnetic nanoparticles through highly regulated biomineralization" and these nanoparticles, which do not aggregate due to cellular structures, become the catalyst for the lateral alignment of carbon nanotubes on the silicon oxide substrate. This technique shows further potential for biosynthesis as the nanoparticles synthesized are then used to influence the production of other, more complex, structures.

1.2.4.2 Corrosion Protection

The process of rusting or metal corrosion is an electrochemical reaction where the surface of the metal has sites that become "corrosion cells" with different sites on the surface acting as anode and cathode. The anodic sites produce metal compounds such as oxides: metal atoms on the surface have become ions and formed bonds, for example with oxygen. Concurrently the cathodic sites will take part in electrochemical reactions, such as the reduction of oxygen gas. The metal oxide may form a surface coating, preventing exposure and therefore limiting corrosion when the oxide film is complete. However corrosion also causes degradation: for example rust will flake away from iron, exposing new surfaces to the phenomenon. Microbially influenced corrosion (MIC) is the name given to processes by which corrosion rate is accelerated due to the presence of bacteria, for example acid producing bacteria accelerating the corrosion of carbon steels. Microbial action can also inhibit corrosion (this is called microbially influenced corrosion inhibition or MICI), an example being the prevention of pitting of Al 2024 in the presence of certain *Shewanellae* strains[23].

1.2.4.3 Antibiotic Production

Penicillin is widely recognised as the first antibiotic ever produced: it came from the mould *Penicillium notatum*[9], famously observed in 1928 by Alexander Fleming to inhibit the growth of bacteria. Antibiotics are produced by microorganisms as a method of removing competing microorganisms from their vicinity. A large number of important antibiotics used in modern medicine were discovered in studies between 1939 and 1963, largely from organisms commonly found in soil and air. Other *Penicillium* species have also been used to produce penicillin.

Antibiotic production is one of the key properties of *Streptomyces* species, with about 50% of *Streptomyces* species that have been isolated being able to produce antibiotics[1], and at least 500 different antibiotics being classified from these bacteria.

1.2.4.4 Bioremediation

Increased industrialisation has resulted in the pollution of our environment: soils and water are contaminated with heavy metals and industrial toxins in many sites worldwide. The process of environmental clean-up may simply be summarised as removing the unwanted pollutants, however in practice it is a lot more complicated. Contaminants may be so ingrained in the environment at a particulate level that in order to remove them they must first be processed into a more manageable form. In an example described by Wall and Krumholz in 2006, uranium contaminants, in the form of soluble uranyl salts, can be reduced to the insoluble mineral uraninite by bacterial action, causing the uranium to be immobilised[24]. In this way, the uraninite can be removed from the soil, instead of remaining in the groundwater, possibly moving with water flow to contaminate other areas. Such natural attenuation is known as bioremediation. An assessment of the use of this and other means of natural attenuation at a Brazilian oil refinery showed biodegradation of regulated compounds, such as benzene and toluene and mixed hydrocarbons, by local microbiota, and suggested that encouraging this process could be part of the overall plan for site decontamination[25]. As well as biodegradation of pollutants, indigenous microorganisms can be used for environmental assessment: the response of such organisms to pollutants may be monitored as a bioindicator in a specified area[26]. Approaches like this need to be part of a bigger picture approach including

geographical and ecological information about the contaminated site coupled with an understanding of the chemistry of the contaminants.

1.2.5 Microbial Fuel Cells and Biosensors

As well as observing microbial action in response to environmental factors, the response of microbes to their environment can be used integrated into the man-made devices. The interface between microbes and inorganic components can be key to the utilisation of microbial response for biosensors and for the exploitation of microbial respiration in devices such as microbial fuel cells.

1.2.5.1 Microbial Fuel Cells

Microbial fuel cells (MFCs) generate "bioelectricity"[27] from biomass using bacteria. The MFC reactor is set up to take advantage of the release of electrons from the bacteria during respiration. The concept of a biofuel cell is not a new one, in fact Lewis's *Symposium on Bioelectrochemistry of Microorganisms*, 1966[28], refers to work by Potter in 1911: in Potter's study a comparison was made of the potential difference between electrodes immersed in a live bacterial culture and a sterile culture respectively. The system he used contained six battery cells, each with one yeast-glucose half-cell and one glucose half-cell, and may be considered the first ever MFC.

In a recent review[29], Debabov discusses the molecular mechanisms behind extracellular electron transfer with a view to the development of MFCs. Specifically the review focuses on two organisms that have been the subject of many MFC studies: *Shewanella oneidensis* and *Geobacter sulfurreducens.*

Originally MFCs were designed using electrochemical mediators such as thionine, methyl viologen and neutral red among others. Their role is to

shuttle electrons from the bacterial cells to the electrode within the MFC. In 2002, however, Kim et al. released a paper describing a mediator-less MFC[30]. This was part of a revolution in MFC design based on bacteria that could transfer electrons directly to electrodes without a terminal electron acceptor added. Electricity production by *G. sulfurreducens* using electrodes as electron acceptors was reported by Bond and Lovely in a 2003 paper[31]. In 2006 this was developed further by the same group using genetic analysis of *G. sulfurreducens* in relation to its extracellular electron transfer specifically to electrodes[32]. The expression of conductive nanowires by *G. sulfurreducens* was also shown to be beneficial to current production in fuel cells with this organism[33]. Research has also been conducted into the ability of a selected microbial consortium to generate energy from wastewater[34]. The variety of organisms used within MFC systems can affect their efficacy and output, and in fact MFCs have been shown to select groups of organisms that can self-mediate electron transfer[35].

The limitations of MFCs are being pushed further and further, however there are discussions of the problems in MFC design and limiting factors: cathodic activation, ohmic and mass transport losses and substrate crossover[36], fuel diffusion, limits to maximum power density from internal resistance, and fuel oxidation at the anode surface[37].

1.2.5.2 Biosensors

The premise behind a biosensor is that a biological component that has a known response to a specific chemical stimulus is used to generate a signal in a connected sensor system[9]. The obvious applications are in environmental monitoring and medical diagnostics.

In some cases the biological component can be a whole cell, in others enzymes harvested from biological cells are used. To get an idea of this dual approach to biosensors using bacteria or bacterial components, consider Svitel's Review from *Biotechnology Letters*, 2006[4], describing how bacteria from the genus *Acetobacter* and the genus *Gluconobacter* have been used in biosensors as whole cells, as well as having enzymes harvested from them for use in biosensors. At the time of writing Svitel pointed out that there was only one commercially available *Gluconobacter* enzyme, which illustrates why using whole *Gluconobacter* cells has been popular: cells can be grown cheaply and the various enzymes each cell has do not need to be isolated but can be used in their natural environment, the cell surface. The ratio of enzymatic activities is hard to control however, when using whole cells, and for that reason some designers of biosensors would rather use isolated enzymes. Despite being more difficult to manufacture, enzyme based biosensors are desirable for their greater selectivity. *Gluconobacter* and *Acetobactor* whole cell and enzyme sensors are used in various studies reviewed by Svitel to detect the presence of a variety of analytes including glucose, ethanol, fructose and lactose.

When cells are used in biosensors their response to the analyte is due to the necessary biological process of metabolism: *Gluconobacter* feed off glucose and so they have a metabolic response to its presence and are geared towards detecting and utilising it, hence Gluconobacter produces enzymes which respond to sugars. Another example of this is the use of denitrifying bacteria, which metabolise nitrogenous compounds, to detect nitrate in a microsensor as described by Larsen in 1996[38]. This paper is not a review but rather details the process of developing the microsensor: the bacteria were isolated from soil and sediments, their capacity for nitrate reduction was tested, and the microsensor was finally constructed of a capillary

containing a culture of these bacteria connected to a nitrogen oxide detector. The bacteria reduced any nitrate to nitrogen oxide (in the presence of acetylene), which was then detected. The amount of nitrogen oxide detected was proportional to the amount of nitrate present. The bacteria were simply used to functionalise the nitrogen oxide detector to detect nitrate levels instead.

1.2.6 Shewanella oneidensis MR-1

Although the gram-negative γ-proteobacteria *Shewanella oneidensis* MR-1 is able to respire in the presence of oxygen, it is this organism's ability to thrive in anoxic environments with suitable alternative electron acceptors that makes it interesting[39]·[40]. First isolated from Lake Oneida in New York State, USA, it has become the subject of a great deal of research, resulting from its ability to reduce ambient metals and metal oxides as part of its anaerobic electron transfer process[15]. The wealth of information about *S. oneidensis* means that it can be used as a model or reference organism, although perhaps *Pseudomonas aeruriginosa* and *Eschericia coli* strains are more traditional choices for research in characterising gram-negative γ-proteobacteria[39].

The species *Shewanella oneidensis* was described for the first time in Venkateswaran's 1999 paper on the genus *Shewanella[41].* Preceding this paper, MR-1 was classified as a strain of the species *Shewanella putrefaciens* since its original classification in 1988. However genetic analysis of MR-1 compared with *S. putrefaciens,* performed by Venkateswaran and colleagues, showed MR-1 to be deserving of reclassification as a distinct species. The first part of the paper describes numerous assays with various *Shewanella*

species in order to develop a schema of their characteristics for identification of distinct species within the genus.

The description of *S. oneidensis* MR-1 was further expounded in 2002 when Heidelberg et al. published the genome sequence of the organism[42]. The authors of this paper note that *S. oneidensis* MR-1 is "an important model organism for bioremediation studies because of its diverse respiratory capabilities". In fact it is these respiratory capabilities and the variety of electron transport systems reported in the bacteria that made MR-1 interesting enough for this group to study its entire genome. The findings of this paper were used to support later research including a comparison of genomes of various γ-proteobacteria[39], in which predictions were made about genomic similarities and differences amongst this taxonomic group.

1.2.6.1 Extracellular electron transfer

Not only is *S. oneidensis* a dissimilatory metal reducer, but also it is highly adaptive to circumstance and environment, employing one or several pathways to export electrons to extracellular acceptors. In section 1.2.3 the four main possible pathways of extracellular electron transfer were discussed for bacteria in general. All four methods are potentially used by *S. oneidensis* under certain circumstances. In situations where the external electron acceptor is insoluble, such as a solid mineral surface or an electrode, it has been shown that electron transfer can occur through direct contact between cell and surface, or remotely through chemical shuttles[43]-[44]. The utilisation of conductive nanowire appendages, similar to the pili of *Geobacter metallireducens*[45], has even been posited since the pili on *S. oneidensis* MR-1 have been shown to be conducting using STM[46]. However it must be said

that there is no evidence demonstrating that they have a specific role in electron transfer thus far.

To form direct contact between cell and an insoluble electron acceptor the cells must adhere to the surface of the electron acceptor. There must be enough attraction between the cell surface and the substrate surface for the cell to attach despite any repulsive forces, such as steric interaction. In comparison with *E. coli*, *S. oneidensis* was found to implement specific bonding mechanisms with goethite (an iron hydroxide mineral with formula FeO(OH)), meaning that the latter organism was more strongly bound to the goethite surface, but only when grown anaerobically[47]. Cells of each organism were attached to glass beads coated with amino-silane such that the silane would act as linkers between the cells and bead. The beads were then used as colloid probes in AFM force studies, in which the cell-coated probes were brought into contact with the mineral surface. The strength of adhesion for the *S. oneidensis* probe was also shown to increase with contact time, suggesting that the cells optimised their surface to interact specifically with the goethite once it was clear that this specific pathway was open to them. The difference in force curves of aerobic and anaerobic *S. oneidensis* probes show that the anaerobic cells have a more rapidly increasing affinity for goethite, supporting the hypothesis that the cells adaptive respiratory functioning responds to environmental circumstances[48].

It is apparent that *S. oneidensis* can bind to electron accepting surfaces via mineral specific proteins, such as outer membrane (OM) polypeptides suggested by Lower et al[49] on the basis of AFM force profiles. The sawtooth shape of retraction profiles of cell probes was interpreted by Lower's group as the unfolding and breaking of protein linkers between cell and substrate. Various approaches to the interpretation of AFM force curves are described in greater detail in Section 1.4.

It has been shown that *S. oneidensis* MR-1 can reduce metal oxides at a distance. Nanoporous glass beads were adapted by precipitating ferric hydroxide (glass beads incubated in iron chloride solution, precipitate formed through addition of potassium hydroxide) and the ability of cells to reduce iron within these beads was assessed using energy-dispersive x-ray spectroscopy (EDS) and transmission electron microscopy (TEM) to characterise the beads before and after suspension with cells[50]. Despite being unable to directly contact the interior pores of the beads, *S. oneidensis* was able to reduce more than 85% of the iron, demonstrating its ability for extracellular electron transfer at a distance.

1.2.6.2 Surface characterisation, studies so far:

The surface structure of *S. oneidensis* MR-1 has been characterised under various circumstances with a variety of methods. However a comprehensive survey of these studies is lacking, as is an understanding of the cellular interface as a whole. The general composition of bacterial surfaces has been described earlier in this chapter. There are specific surface features of *S. oneidensis* however that are vital to the organism's functionality, and these are under scrutiny both as isolates and in situ.

The effect of environment on cell surface characteristics and cell structure must be understood in order to optimise ambient conditions for devices using the organism.

1.2.6.3 Other key studies

S. oneidensis cells grown aerobically and anaerobically exhibit different morphology, as studied by AFM and surface enhanced Raman spectroscopy

(SERS). In a study by Biju, nanoscale structures on the OM of *S. oneidensis* MR-1 cells were shown to be present when the cells were grown in the absence of electron acceptors, however these structures disappeared when electron acceptors were abundant[51]. The variation in cell morphology depends on the availability of the electron acceptors and appears to be physical evidence of the mechanisms of extracellular electron transfer via OM surface proteins. In a study by Elias et al. the variability in dissolved oxygen under certain aerobic culture conditions, i.e. shake flasks, was shown to cause cells to exhibit electron-acceptor-inhibited characteristics even when grown in oxygen[52]. The paper recommended that bioreactors, with their ability to monitor and control dissolved oxygen concentration, will produce more homogenous microbial cultures, in which all cells will exhibit electron-acceptor-abundant morphology and composition, as determined by mass spectrometry and 2D gel proteomic analysis.

Interestingly, temperature can have a direct affect on cellular morphology, as demonstrated by Abboud et al using epifluorescent microscopy and protein analysis, as well as optical density for assessing concentrations of cells over time[53]. Decreasing the temperature from 22°C to 3°C increased the lag time, whilst increasing the doubling time from 40 to nearly 70 hours, it is worth noting that the lag time depended on the temperature at which the inoculum had been grown: if the inoculum was grown at 3°C, the lag time for 3°C cultures was reduced to 48 hours. The cold cells were not rod-like so much as filamentous, up to 16μm in length (average 8.57μm) compared with those grown at 22°C which averaged 1.7μm in length. The presence of spheroplast structures in the cold cell cultures was also noted. The variance in phenotype depending on temperature suggests that as well as diverse methods of achieving respiration *S. oneidensis* MR-1 has diverse mechanisms of growth and propagation, depending on environment.

Biffinger et al. explored the effect of pH on growth and electron transfer capabilities of *S. oneidensis* MR-1 in their 2008 study. The case for relevance to MFC design was made, as most MFCs operate at around pH 6 to pH 8. When comparing the *S. oneidensis* DSP10 strain with MR-1 it was found that the former had a greater energy output at neutral pH, but not at pH 5. DSP10 cultures exhibited a significant reduction in riboflavin concentration at pH 5, leading Biffinger to suggest that the synthesis of mediators by cells for electron transfer is affected by pH, and that MFC output will depend on the ability of bacteria to produce mediators rather than just on the concentration of bacterial cells[54].

1.3 SPR and ζ-potential studies of cell properties.

At the micro and nano scale surface properties start to become more important than bulk properties[55], and thus the surface interfacial physiology of the cell is an important area of study to understand its interactions with its environment. One of the important functions of the cell surface is adhesion, or non-adhesion to selected surfaces. In laboratory situations, microbial cultures can be grown on solid or in liquid media, illustrating the adaptive nature of microbes, which can grow attached to a surface or planktonically in suspension.

ζ-potential provides a way of predicting whether or not cells are likely to stay separate in solution or flocculate, forming clusters of cells. As a parameter related to surface charge, ζ-potential allows researchers to learn more about the cell surface and its impact on cellular life. Surface Plasmon Resonance (SPR) by contrast offers information about functional cellular binding to a substrate, rather than to other cells. Both ζ-potential and SPR provide results that vary with environmental factors such as temperature and the ionic strength and pH of the suspension. This illustrates the connection between

cells and their environment: the electrochemical environment informs the properties of the cells, as described in section 1.3.2. Both ζ-potential and SPR can be used to monitor environmental effects on cellular qualities such as surface charge or propensity for substrate binding.

1.3.1 Surface Plasmon Resonance

The principles of Surface Plasmon Resonance (SPR) have their origin in the phenomenon of total internal reflection. When light travelling through a medium of high reflective index impacts upon an interface with a medium of lower reflective index at an angle greater than θ, the critical angle, it is totally reflected back into the original medium at the same angle. This is classically demonstrated in practical terms using a ray of light and a glass prism. The ray of light travels through the prism and can be transmitted wholly through the second interface (glass to air), partially transmitted and partially reflected, or totally reflected from this interface. The effect on the transmission of the light beam by the interface is governed by the incident angle. Effectively at a specific angle the interface acts as a mirror.

Surface Plasmon Resonance explores a similar effect using glass coated on one side with a thin metal film. Research into the absorption of light by thin metal films shows that although there would be no net loss in the energy of the light beam on total internal reflection (TIR) an electrical field intensity called an evanescent field wave would be generated by the impact of photons on the surface of the second medium, as shown in figure 1.3. In Turbadar's work in 1959 it was shown that at the thickness of film required for zero reflection, no light would be transmitted[56]. The normal component of the complex amplitude of emerging light, theoretically, is shown to be normal to the surface; hence the resulting wave propagates

along the surface. This is the evanescent wave, or "surface plasmon" exploited in Surface Plasmon Resonance.

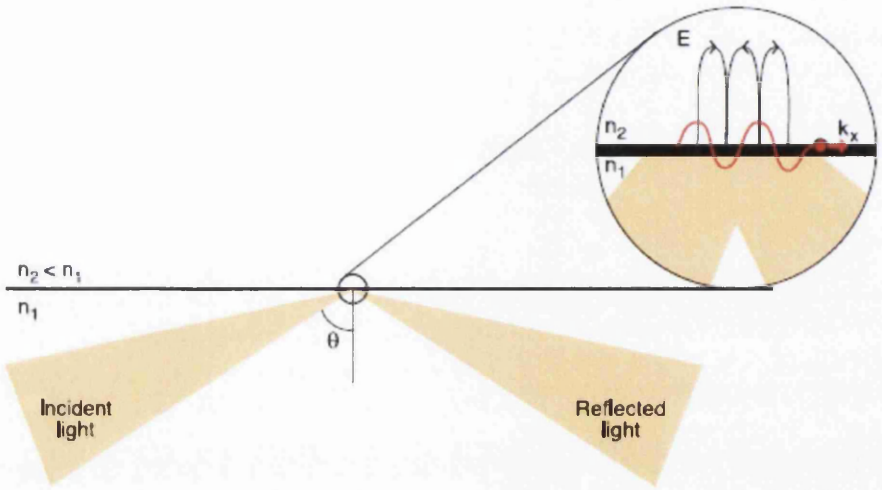

Figure 1-3: *From Biacore Technology Note 1[57]. Total internal reflection for non-absorbing media. The field E is a result of electrical field intensity oscillation. The evanescent wave that results has a wavevector* k_x.

This effect can be amplified by constructing the media interface with specific properties. If the interface between the two media is coated with a conductive layer (a metal film) of appropriate thickness then the p-polarised component of the evanescent wave is able to move through the conducting layer. Thus it may then excite electromagnetic surface plasmon waves that move within the conductor surface that is in contact with the medium of lower refractive index. If the metal film is non-magnetic, the surface plasmon wave will also be p-polarized and will create an enhanced evanescent wave as shown in figure 1.4 below.

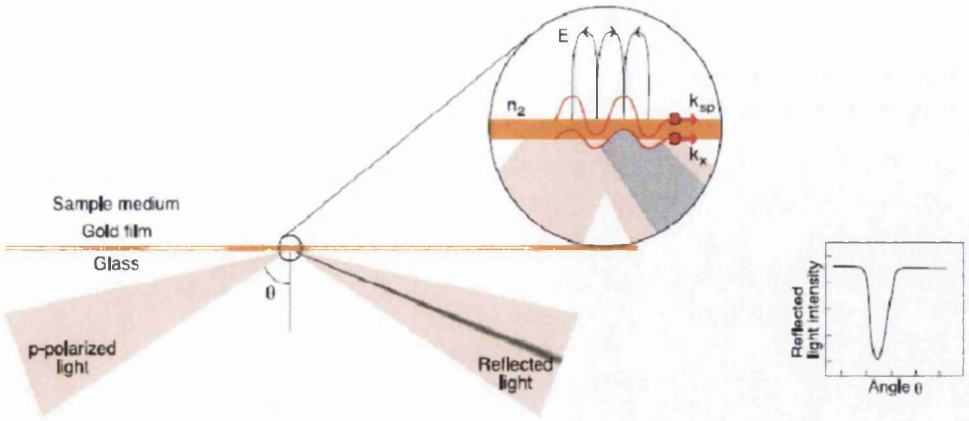

Figure 1-4: *From Biacore Technology Note 1[57]. The p-polarised light incident on the surface is totally reflected however there is a dip in light intensity at the particular reflection angle, dependent on the surface Plasmon wave. This is detected in SPR.*

The intensity of light reflected from the interface is reduced at a specific angle, the angle of resonance, due to the energy taken up in the generation of surface plasmons[58]. The resonance angle (or SPR angle) is highly dependent on the nature of the interface and thus reflects any changes in the metal surface layer.

The premise behind SPR detectors is that functionalising the metal layer (usually gold) with different organic groups changes the angle at which the SPR phenomenon occurs and the change in this angle can be measured. The response of the SPR angle shows changes in the metal film surface and thus can be used to measure interaction of different molecules with those bound to the film[59]. The change in angle is indicative of a change in the refractive index of the material near the surface. In the BIAcore series of apparatus the change in refractive index is recorded as "response units" (RU). The response, R, of the SPR sensor can be given as:

$$R = R_0 + R_{buffer} + R_{binding} \qquad 1.2$$

Where R_0 is the background or baseline level, R_{buffer} is the response due to the sample buffer, and $R_{binding}$ is the response due to the actual binding of material to the surface[60].

The SPR detector has varied applications in organic and biochemistry, including immunosensing[61]. Especially since information about molecular binding can be gathered by attaching various groups to the gold surface and measuring changes in SPR angle for SPR response. As well as stoichiometric binding information, SPR sensors can be used for kinetic analysis and the determination of association/dissociation constants[62],[63],[64]. It has even been used for the detection of whole cells[58, 65] binding to a surface, as described further in section 3.1.2.

SPR detectors can be used for assays of varying complexity. The change in SPR angle (also measured in response units, RU) will change when a new buffer is put in contact with the surface, however if any particles in that buffer attach to the surface, then some of that change will remain even when the system returns to the original buffer. In this way SPR can be used for a simple yes/no binding assay confirming whether or not a specific substance has bound to the surface. Modern systems such as those from BIAcore keep the surface under flow of a running buffer. Qualitative measurements such as yes/no binding or comparisons between levels of binding are relatively straightforward: quantitative results are more difficult as the binding must be able to fit a model so that adhesion rates can be calculated[66].

1.3.1.1 Binding and kinetic models

Adhesion in SPR can be studied in a static system, or under constant flow. Systems such as the BIAcore range of SPR detecting apparatus use controllable flow rates as a parameter which can be changed in order to

study its effect. Low flow rates mean a greater contact time, which may cause an increase in binding, and higher flow rates may not allow enough contact time between sample and substrate. A higher flow rate may also increase dissociation of sample from the substrate, due to the forces exerted by buffer flowing past.

The binding of the analyte to the sensor surface can be described as the interaction of two components, A and B to form a complex AB, where A is in the injected analyte and B is the surface immobilised material.

$$A + B \leftrightarrow AB \tag{1.3}$$

Thus there is a rate of formation of complex, AB, and also a rate at which the complex decouples into A and B. These are analogous to the rate of association of analyte to the surface and the rate of dissociation of analyte from the surface. The former is dependent on the concentrations of A and B, whereas the latter is dependent on the concentration of the complex AB. Thus the association rates of analyte will depend on the concentration of analyte injected, but the dissociation rates are independent of this concentration[67].

The rate of change of concentration of complex AB can be written as:

$$\frac{d[AB]}{dt} = k_a[A][B] - k_d[AB] \tag{1.4}$$

where k_a (also called k_{on}) and k_d (also called k_{off}) are the association and dissociation constants respectively. Since the concentration of AB is the same as the amount of analyte bound to the surface, it can be said that [AB] = R and so the rate of change in response R can be thought of as:

$$\frac{dR}{dt} = k_a C[R_{max} - R] - k_d R \tag{1.5}$$

where C is the concentration of the analyte, and the concentration of surface immobilised substance is given by the maximum value of R (i.e. saturation of binding sites) less the value of R recorded, in other words the number of unused binding sites[67].

Most models consider one-on-one binding, in other words binding of one particle of analyte to one site on the sensor surface. More complicated analysis of interaction takes into account scenarios such as more than one ligand, mass transfer, and heterogenous samples. Often in published research the kinetic analysis is skimmed over, with no association or dissociation rates calculated, and a simple comparison between total change in RU is drawn on in order to highlight the more successful interactions[64, 68, 69]. This comparison is enough for purpose in many cases, as long as it is done consistently. However, since there is much more information about the process of binding that can be gleaned from comparisons of association and dissociation rates and equilibrium, the kinetic analysis is worth looking at.

The rate of adhesion of particles to a surface will decrease as accessible space on the surface becomes rarer since the particles already on the surface will obstruct new particles' access to the surface. At some point the number of particles detaching from a surface in a given time will match the number attaching to the surface in that time, with the system achieving an equilibrium state. If no more particles flow into the system, then the detachment rate will decrease the total numbers attached until such time as only strongly fixed particles, which will not detach under normal circumstances, remain.

Karlsson uses linear transform methods to find values for the association and dissociation rate constants, and this may be thought of as the starting point for any analysis of similar data[70].

The linear transform analysis has its limits, for example if the data does not adhere to the first order rate equation a plot of the rate of change in response against response will produce a curved plot, making it harder to determine k_a. The case has been made for using exponential curve fitting in order to determine association parameters instead. Exponential curves can be fitted with great success, however the selection of experimental data is key, since the changeover from ordinary buffer to sample solution will entail the influence of changes in temperature and bulk refractive index. These can be minimised experimentally but as shown they can affect the accuracy of the fit. In work by Gill et al, the requirements of the method were explored including minimum exposure times, to ensure enough data for a representative fit[71]. These were shown to be dependent on concentration for the association constants (not the dissociation, which is independent of concentration). The importance of quality of data was also stressed.

In later work, Karlsson exploits competition between two ligands in order to observe interactions of a ligand of low molecular weight. Since detector response is proportional to the mass of the analyte, observation of binding for a low molecular weight (<5000Da) is not possible under common experimental practice. In order to detect ligands of low molecular weight, Karlsson uses two ligands: one of observable high molecular weight (hmw), the other with a low molecular weight (lmw), which both bind to the immobilised receptor[60]. When recording the equilibrium constants for the hmw ligand, both in the presence and absence of the lmw competing ligand, the difference is due to the binding sites being taken up by the lmw competitor. Karlsson gives a detailed explanation of the theory and then uses two model experimental systems based around interactions with antibody functionalised surfaces to illustrate the method. The competition

method is furthered by Nieba et al in an attempt to get past the problem of rebinding and multivalent binding in SPR experiments[72].

Part of the problem with the more simplistic models for binding is that they assume a 1:1 interaction of analyte with surface sites, leading to a first order time dependence. As well as Nieba's paper on using a method based on competition binding to analyse more complex binding scenarios, there is work by O'Shanessy and Winzor that outlines reasons behind deviations from first order kinetics[73]. They found that it was most likely to be due to non-uniformity of binding sites.

When researching the effect of a particular component of the methionine repressor protein MetJ in *E. coli*, the SPR sensor surface was functionalised with an idealised operator fragment of DNA, rather than unprocessed DNA[74]. The component under study, S-adenosylmethionine (SAM) increases the affinity of MetJ for operator DNA, whereas similar molecules with a slightly different structure do not. Through comparison with these analogous molecules the researchers were able to suggest that the effect of SAM on the binding of MetJ is electrostatic in origin, since the other molecules in the study each contained a positively charged atom in a different location to that within SAM molecules. In this work rate constants were calculated using the BIAcore evaluation software for SAM and the analogues used for comparison. It was found that the data did fit well with the software's pseudo first order model, despite the fact that the interactions were multi-component.

1.3.1.2 Biological and Whole Cell SPR studies

Whole cell studies using SPR are more rare than studies of biological components such as isolated proteins or antibodies and antigens[64],[66]. In

the latter the interaction of functional macromolecules can be observed directly, and without the complication of non-specific interactions occurring. The role of type IV pili of *P. aeruginosa* cells has been investigated using SPR without flow conditions, comparing the attachment of whole cells of the wild type strain to a gold surface with that of a pili-deficient mutant, and a mutant with pili that cannot be retracted. The kinetics of attachment were observed from the change in the angular minimum of the reflected light as plotted against time. Although each curve displayed the same basic shape: rapid increase and subsequent slower decrease in attachment, there were differences between each type. The pili deficient and wild type start off with a high attachment, and a more rapid detachment than the strain with the un-retractable pili, which does not decrease in attachment. This suggests that the pili are involved in microbial attachment to the surface, and that retractable pili are used by the wild type for temporary surface binding[62]. This research was conducted under static conditions and flow over the surface was, therefore, not considered.

Using the same static SPR system, the adhesion of living cells of *P. aeruginosa* was compared to the adhesion of cells killed by thermal shock to a gold sensor surface functionalised with mercaptounadecanoic acid. The dead cells were found to be easily removed from the surface by rinsing, unlike the living cells, which maintained a presence on the surface, suggesting that active adherent function was not present in the dead cells[63].

BIAcore instrumentation has been used in a variety of whole cell studies, including research into the binding of tooth colonising bacteria under environmental conditions. In one study BIAcore sensor chips were functionalised with salivary agglutinin, with the subsequent adhesion under steady flow of mutants and wild type *Streptococcus gordonii* cells compared in order to evaluate the role of the gene sortase A (srtA) in cell wall binding[68].

It was found that srtA acts as an accessory gene in order for the cells to express adhesin proteins, since mutants missing srtA were still able to adhere to agglutinin but with less success than the wild type. Agglutinin was also the functional surface species used to investigate the effect on *S. mutans* adherence of surface adhesin P1[69]. In this study the adhesion of whole *S. mutans* cells to the agglutinin functionalised SPR sensor surface was demonstrated to be disrupted by the addition of monoclonal anti-P1 antibodies, and inhibited yet further in the presence of polyclonal anti-P1 rabbit immune serum.

Using similar experimental methods, the binding of *S. sanguis*, *S. mutans* and *S. mitis* to saliva functionalised sensor surfaces was observed using SPR. Association and dissociation rates for the bacterial cells were calculated using a concentration dependent binding study for each type to calculate the association constant, which was then used with BIAcore's BIAevaluation software to calculate the dissociation rates from curves[75]. *S. sanguis* had both the highest association rate and the highest dissociation rate, however *S. mutans* had the highest equilibrium constant (association constant divided by dissociation constant).

Some approaches to whole cell studies are not as straight forward experimentally as injecting cells over a functionalised surface. Several studies take very different approaches including immobilising cells onto the sensor surface first and then flowing sample molecules over the functionalised surface[76], incubating sample molecules with whole cells before injecting the molecules unbound by the cells (separated using centrifugation) over a specified surface to see if the sample was changed by the presence of the cells in order to use SPR to detect cellular contamination [77], and using different experimental hardware such as fibre optic SPR sensors[78].

1.3.2 Zeta (ζ) Potential and Microbe-microbe Interaction

The surface charge of a microbe is a vital property of the cell wall, which is important for maintenance of cell shape and turgor, growth and division, and allowing the right constituents into and out of the cell[12]. All particles have surface charge properties to some extent, even if they have no net charge. Bacteria are known to have negative surface charge due to the ionised functional groups of cell surface macromolecules; in gram-negative bacteria these groups are phosphoryl and carboxylate groups as part of surface lipopolysaccharides. The surface charge can also be affected by extracellular polysaccharides. The surface charge of relatively small particles such as bacteria cannot be measured directly, however the ζ-potential of small particles in solution treated as a colloidal system can be used as a measure of surface charge[79]·[80].

In order to visualise what ζ-potential actually represents, imagine a negatively charged particle in a salt buffer, it is easy to imagine that the positively charged ions will be attracted to the negative particle surface. In that way it will form a layer of positive ions, which in turn will attract negative ions, which form another layer of charge. The opposite case can be imagined with a positively charged particle and all the resulting charges swapped, resulting in a layer of counter-ions (opposite charge to surface) and a further layer of co-ions (same charge as surface)[81]. In fact, even particles which have an overall neutral charge may have a charge distribution across the surface that will attract ions of the opposite charge to that area and these ion layers will still form. Thus the description of the surface of such a particle in solution is actually quite complicated; the particle surface is overlaid with the Stern layer (the counter-ion layer) and then the second ion layer, these form the electrical double layer.

The perimeter of the electrical double layer is called the shear plane or slipping plane, this is where the bulk solution begins, although the charges in the second ion layer are part of the diffuse layer of charge interaction with the bulk solution[79]. The size of the electrical double layer and therefore the measurements of each distinct particle boundary are dependent not only on the surface charge of the particle but also on the ionic strength of the bulk solution[79]. Figure 1.5 shows how the different layers are related for a negatively charged particle. The zeta potential (ζ-potential) is related to the surface charge: it is the potential difference in mV between the particle surface and the plane of shear (known also as the slipping plane, although this is more commonly for large flat surfaces[79]).

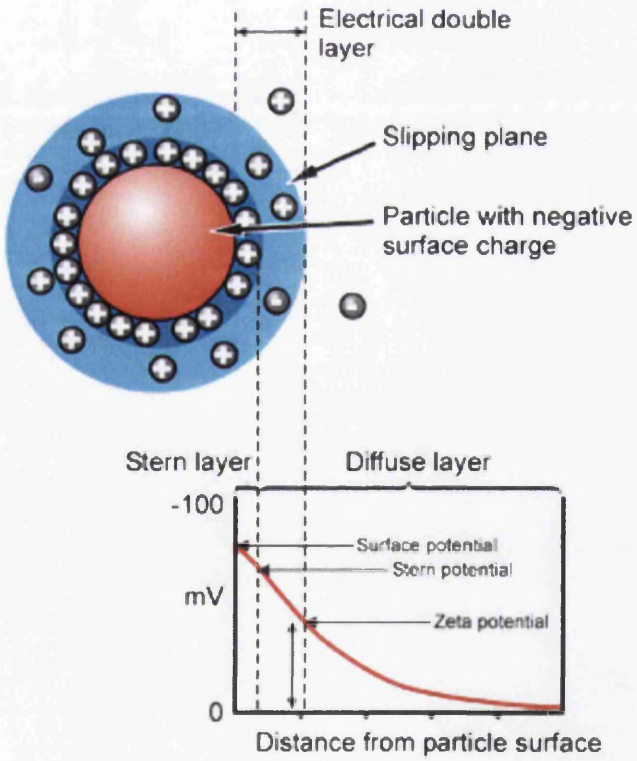

Figure 1-5: *Diagram showing zeta potential as the difference in potential from the particle surface to the slipping (or shear) plane, from Malvern Instruments' website[82].*

The ζ-potential is inherently dependent on pH, since the pH affects the net charge of a particle as it affects the ionisation of the molecular groups on the particle surface[81]. For a colloidal system there is a pH value at which the net charge of the particle (and thus the ζ-potential) is equal to zero, this is called the iso-electric point and can be estimated from graphs of ζ-potential against pH. Large ζ-potentials of ±30mV indicate that the particles in the suspension will repel one another more than they will attract one another, and hence the suspension can be thought of as stable. This means that the particles will remain separate within the suspension. An unstable suspension, where the attractive forces between particles may be greater than the repulsive force of like charge, will result in particles gathering together or "flocculating". If flocculation continues, when the particles are dense enough compared to the host solution they will fall under gravity and form a sediment layer, leading to phase sedimentation between colloid and suspension media. Sedimentation can also occur due to coagulation in the case of particles being less dense or comparatively dense compared to the suspension media, in this case the coagulated particles will eventually become large enough and heavy enough to sink, leading once again to phase sedimentation[81].

The prediction of suspension stability from ζ-potential allows an insight into the adhesive quality of the suspended particles, especially in respect to one another. More extreme pH values (highly acidic or highly alkaline) will result in greater surface charge, increasing the repulsion of like charges between particles and decreasing any tendency to flocculate. The isoelectric point is the point at which the suspension is most unstable, and at this pH the particles are most likely to attract one another and link together. Understanding how the isoelectric point and stable regions of high ζ-potential relate to the native or artificially induced pH of cells can shed light

on their propensity for sticking together or keeping their distance from one another in different chemical environments.

1.3.2.1 Measuring ζ-Potential

When an electric field is applied to a solution containing particles with electric charge, the charged particles will necessarily be affected by the electric field. These electrokinetic effects can be measured in a colloidal system where one phase is made to move with respect to the other (e.g. solid particles with respect to liquid or vice versa). Two of these effects are more appropriate for a fixed surface: streaming potential, where fluid is forced past a fixed surface, generating a potential, and electo-osmosis, in which an electric field is applied to make the liquid move past a fixed surface[81].

In order to measure the ζ-potential of suspended particles a different approach must be taken, since the position of the particles cannot be fixed. One method is to use the effect of sedimentation potential. This can be measured when the particles settle either due to gravity or during centrifugation. The downward movement of the particles forces the electrical double layer to become a dipole, the sum of these dipoles resulting in a measurable potential difference between the top and bottom of the suspension[79]. From this observed potential the ζ-potential can be estimated.

Another method of using electrokinetic effects to calculate ζ-potential is electrophoresis. This is the effect whereby an electrical field is applied to the solution, causing the particles to move within it. Their speed of motion is measured and from this their electrophoretic mobility, i.e. their velocity in a unit electric field, is gained. The experimental set up requires a method of measuring the particles' velocity so that an average mobility can be

calculated. One popular method in modern research is electrophoretic light scattering (ELS), as used by Malvern Instruments[79]. Two coherent beams of light cross paths in a capillary cell holding the sample suspension. An interference fringe pattern is formed at this intersection of the light beams, which is interrupted by particles moving under the applied electric field. The amount of light scattered is detected, and the frequency of fluctuations in this detected signal is related to the velocity of the particles under study. The particles will be subject to random (Brownian) motion as well[83], however the system is set to measure only the component of motion due to the electric field. The resulting data is a distribution of mobility, a spectrum of particle mobility rather than a single averaged value.

The measurement of electrophoresis requires that an electric field is applied to the system such that the particles will move with respect to the liquid in which they are suspended. However, as the electric double layer is fixed to the particle it does not move with respect to the particle. The surface plane of shear is the region where the liquid first begins to move with respect to the particle[79]. The potential at this plane, which can be regarded as the effective surface of the particle, is the ζ-potential. Electrophoretic mobility (μ_E) is then used to evaluate the ζ-potential using one of two approximating equations: Huckel's or Smoluchowski's[84] both of which are derived from Henry's equation:

$$\mu_E = (4\pi\varepsilon_0)\frac{\varepsilon_r\zeta}{6\pi\eta} f_1(\kappa a), \qquad 1.6$$

which becomes

$$\mu_E = \frac{2\varepsilon\zeta}{3\eta} f_1(\kappa a) \qquad 1.7$$

Where ε_0 is the permittivity of a vacuum, ε_r is the relative permittivity (dielectric constant) of the suspension liquid, ε is the product of ε_0 and ε_r, η is

the coefficient of viscosity of the suspension liquid and $f_1(\kappa a)$ is a correction factor depending on the particle shape (usually assumed to be near spherical), with a being the particle radius.

The approximation put forward by Huckel sets the correction factor $f_1(\kappa a)$ to 1 ($\kappa a \ll 1$), whereas that of Smoluchowski uses $f_1(\kappa a) = 1.5$ ($\kappa a \gg 1$). Thus Huckel's equation is:

$$\mu_E = \frac{2\varepsilon\zeta}{3\eta} \qquad 1.8$$

and Smoluchowski's equation is simply:

$$\mu_E = \frac{\varepsilon\zeta}{\eta} \qquad 1.9$$

The ζ-potential can therefore be calculated by rearranging Smoluchowski's equation for ζ, using measured values of the electrophoretic mobility μ_E, so long as the particle under study has a relatively thin double layer compared to the particle size[83].

$$\zeta = \frac{\eta\mu_E}{\varepsilon} \qquad 1.10$$

Smoluchowski's equation, and Henry's equation from which it derives are based around rigid particles with a well-defined slipping plane. Dague et al set out in their 2006 paper to show that since cells can be viewed as soft bioparticles, rather than rigid particles, a different approach is required for studying their electrophoretic mobility[85]. The main problem with the rigid particle approximations is that the cell surface is not homogenous, but rather it features a variety of molecular species, some of which may extend through what would otherwise be a distinct double layer, which means that the cells have an ambigious slipping plane. The paper's authors evaluate the "softness" of cells with and without polymer fringes, using modelling

methods based on theory developed by others from their group in previous papers.

1.3.2.2 ζ-potential studies of biological systems and whole cells

In 2000 Wilson et al were invited to write a review of methods of measuring bacterial cell surface charge using ζ-potential measurements[83]. Electrophoretic Light Scattering methodology was reviewed in depth with regard to bacterial samples. The review outlined several studies in which ζ-potential of bacterial cells is measured in order to derive conclusions about intercellular interactions and interaction between cells and ambient surfaces.

In a study by van Loosdrecht et al in the late 1980's[86] twenty-three different microbial strains were studied in order to compare their hydrophobicity with their electrophoretic mobility (as a measure of the electrostatic state of the bacterial surface) since these qualities affect cellular adhesion. Arguably this study was one of the first to compile electrokinetic information alongside hydrophobicity in order to develop a more comprehensive understanding of the forces involved in cellular adhesion. Interestingly, although no correlation was apparent between electrophoretic mobility and adhesion, combining these data with hydrophobicity measurements by contact angle demonstrated that when cells are more hydrophilic, surface potential becomes a bigger factor. Increasing hydrophobicity was found to match increasingly negative potentials. It is noted that hydrophobic cells with small electrokinetic potentials would be likely to clump together and therefore be absent from the harvested, refined cell sample, and as these qualities would prevent the cells from spreading or colonising it could also be argued that there would not be many of them to be observed anyway. Considerations like this lend perspective to the results,

which overall seem to show that terrestrial and shallow-water organisms are more adherent under optimal growth conditions, whereas deep water or oceanic organisms are more adherent under challenging conditions, in this case starvation. Quite sensibly, the author suggests that this may encourage microbial migration when times are hard, either by detaching from habitat substrates, or by attaching to organisms or materials that may transport cells to more habitable environments.

Using ζ-potential and hydrophobicity studies, the adherence mechanisms of different strains of *Streptococcus sanguis* and *Streptococcus mutans* were compared by Satou et al[87]. Electrophoretic mobility was measured for both the bacterial cells and dental restorative particles and the ζ-potential calculated using Smoluchowski. The number of *S. mutans* cells adherent to dental restorative plates increased as the ζ-potential became less negative, suggesting that electrostatic interactions play a part in this organisms adherence. *S. sanguis* did not show a correlation between ζ-potential and numbers of cells adhering to the restorative plates, however numbers of *S. sanguis* cells adhering to the plates did increase with contact angle, suggesting a greater role for hydrophobic interactions for the adhesion of this organism.

Electrostatic interactions did not seem important for the adhesion of *P. aeruginosa* to stainless steel, as investigated by Vanhaecke et al[88]. There was no correlation between electrophoretic mobility of the cells and the number of cells adhered after incubation of the plates with cell suspensions, as measured by bioluminescence assays. However hydrophobicity, as measured by hydrocarbon and contact angle methods, did affect the adhesion rates determined in this study.

As well as medical and dental applications, such information about cell interactions can be used in geology: microorganism migration is looked at in

order to predict the usefulness of bioremediation by microbes in specific geological sites, with hydrophobicity and surface charge affecting microbial movement through geological formations. In one study the movement of P. aeruginosa through dolomite was found to depend on growth phase. Cells in the stationary phase had higher ζ-potential than those in logarithmic growth and stationary phase cells were furthermore found to adhere to dolomite to a greater extent as well[89].

1.4 Atomic Force Microscopy

1.4.1 History of Surface Probe Microscopy

Surface Probe Microscopy or SPM is any microscopic technique that involves near-surface scanning with a designed probe. Originally these techniques were furthered in order to map surface features at a size too small to be resolvable using optical microscopy techniques[55]. Although the most obvious application for SPM is imaging, different types of SPM are used for sensing, measurement of surface properties, and manipulation of surface features, even on the atomic scale[90].

The first successes of SPM were found with the Scanning Tunnelling Microscope. Binnig and Roehrer's 1987 paper provides a first hand narrative account of the origins and development of this microscope[91], for which they won the Nobel Prize for Physics in 1986. It was an implementation of the phenomenon of tunnelling, in which electrons may jump across energetically forbidden gaps with a probability depending on the size of the gap and the potential difference across it[80]. A current produced as a result of that tunnelling can be measured and hence the STM: electrons tunnel between a nanoscale tip and a surface, with an increase in tunnelling (and hence current) when the separation decreases (i.e. over raised surface

features) or when the potential difference between tip and surface is higher (for example if the surface or tip are charged) the change in tunnelling current is translated into a topography of the surface showing surface features and surface charge properties. However, the surface must be either conducting or semi-conducting in order for STM to provide useful images.

A further application of the concept behind STM in combination with the stylus profilometer was Atomic Force Microscopy (AFM), introduced in 1985[92]. AFM was developed in order to be able to see topography for insulating surfaces: unlike STM, AFM does not require samples to be conducting. The main differences between AFM and the other SPM techniques are the ease of sample preparation and that surface interaction is achievable with AFM.

In the first few years of use AFM produced high resolution images of stiff inorganic material, with resolution on the angstrom scale achieved, for example in Marti et al's study of highly ordered pyrolytic graphite and sodium chloride, both covered in paraffin oil to prevent surface effects due to moisture[93].

In recent years the study of biological systems using AFM has exploited both the imaging and force measurement applications of AFM. The minimal sample preparation and physiological conditions have allowed the imaging of the surface of dormant and germinating spores of fungi[94], the photosynthetic transmembrane pigment-protein complexes of phytobacteria[95], and even different surface layers of bacteria[96].

1.4.2 Basic operation of the Atomic Force Microscope

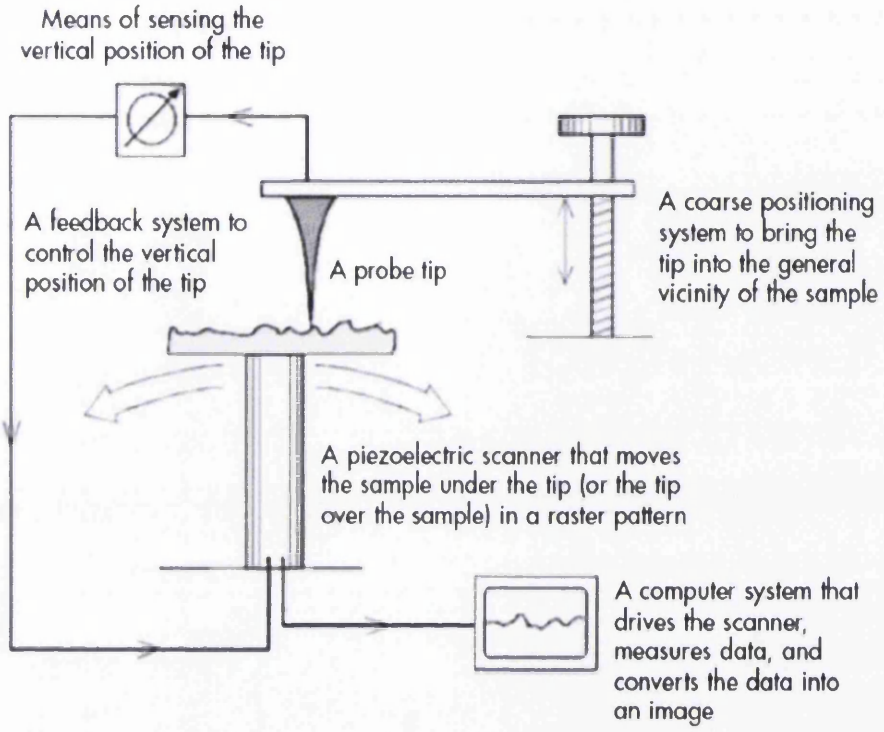

Figure 1-6: *Basic AFM set up. Diagram from Veeco's "A Practical Guide to SPM"[97].*

The set-up of the AFM is shown in the diagram above. For basic AFM studies a sharp tip is fixed at the end of a cantilever. The cantilever is lowered until the tip's interaction with the surface causes the cantilever to flex. This deflection is most commonly measured using the optical deflection scheme, shown below in figure 1.7, whereby a beam from a laser diode is reflected from the end of the cantilever to a PSPD (position-sensitive photodetector)[98].

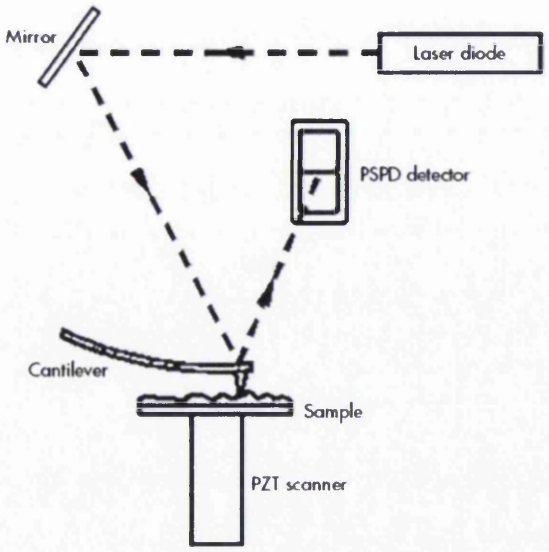

Figure 1-7: *Optical deflection scheme of AFM, from Veeco's "A Practical Guide to SPM"[97].*

The AFM is then used to take surface images by raster-scanning the tip in lines across the surface, forming an image from topographical data line by line. The AFM can also be used for slightly varied applications such as force-distance curves and manipulation of surface features.

The forces that cause the deflection of the cantilever are dependent on the tip sample separation, as the diagram below shows:

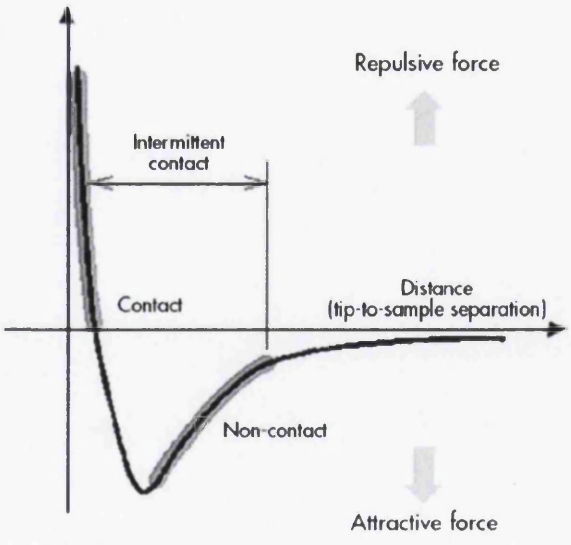

Figure 1-8: *Force against separation between tip and surface. From Veeco's "A Practical Guide to SPM"[97].*

At a large distance, there is very little force between the tip and sample. However as the tip-sample separation decreases, so the long range attractive forces increase. Then as the tip comes into contact with the surface, the force becomes increasingly repulsive. The repulsive and attractive regimes correspond to different modes of AFM operation, which are discussed in the next section.

1.4.3 Atomic Force Microscopy techniques

There is more than one approach with which atomic force microscopy measurements can be obtained: these different AFM operating modes are dependent on the type of cantilever and probe used as well as the feedback system employed. The specific requirements of the sample to be studied will inform the choice of which mode to use. The three principle modes of AFM are described in section 1.4.3.1 to 1.4.3.3. There are also a number of related microscopy techniques using different probe qualities, which are summarised in section 1.4.3.4.

1.4.3.1 Contact

Contact mode is a static mode of AFM operation, in which the cantilever only moves in response to interaction with the surface. When in contact with the surface, the feedback signal is the force on the lever which causes the cantilever to bend, detected as laser deflection by the PSPD[98]. The cantilever is deemed to be in "contact" when the cantilever-surface system is in the repulsive regime of the inter-molecular force curve.

AFM tips that are used in contact mode can be subject to strong lateral forces resulting in damage to the tip or deformation of the surface. The effect of lateral forces is exploited in Lateral Force Microscopy (see section 1.4.3.4).

1.4.3.2 Tapping (Intermittent contact)

In the tapping mode of operation, also known as intermittent contact mode, the cantilever oscillates at its resonant frequency and thus contact with the surface is intermittent. The system experiences feedback as damping of this oscillation. As the duration of contact is a small fraction of the oscillation period any lateral force effects are greatly reduced. This means that tapping is more suitable than contact for imaging soft surfaces (e.g. organic and biological samples).

A by-product of tapping mode has become one of its strengths: not only is topographical data obtained from the change in force, but also amplitude and phase data are obtained and give their own information about the sample.

The amplitude will actually be maintained at the same level, however the voltage required to alter the z height using the piezoelectric system is recorded. This can be displayed and will usually show greater contrast of surface images than the topographic image. The phase data is the difference between the phase of the measured oscillation and that of the driving oscillation of the cantilever. This can provide information on surface properties such as adhesion and friction.

1.4.3.3 *Non-contact*

Although this is often considered the same as intermittent conctact, this mode has some different applications and can be defined separately. In non-contact imaging, the cantilever is oscillated above the surface, never coming into contact[99]. Instead it operates in the attractive regime of the inter-molecular force curve. The advantage of this mode is that it does not risk any damage to the surface, however a disadvantage is that it can be difficult to bring the cantilever near to the surface and yet keep it distant enough to not "jump into contact" with the surface due to the attractive forces between tip and sample. In ambient conditions such a jump could even be caused by a capillary bridge between water on the tip and on the sample[99]. The force is detected in the same way as for tapping mode.

1.4.3.4 *Related force microscopy methods*

The distribution of electrical charge on a surface can be studied in a non-invasive/non-destructive manner by using non-contact force microscopy to probe the long-range electrostatic Coulomb forces. In order to eliminate the influence of charge from other sources of tip-sample interaction forces Electrostatic Force Microscopy (EFM) has been developed in which an AC voltage is applied between tip and sample. The frequency of oscillation of this signal is far lower than that of the cantilever oscillation. The force gradient between the tip and sample is measured experimentally, and its oscillation depends on the charge on the surface, allowing the surface charge to be mapped. Interestingly the study of the charge decay over time is often used to look at surface characteristics particularly charge mobility[100].

Although lateral force effects are often seen as a disadvantage when scanning using contact mode AFM, they can be specifically exploited to give

information about the friction of a flat surface in Lateral Force Microscopy (LFM) also referred to as frictional force microscopy[98]. In LFM, regions with different friction exhibit different contrasts when imaging, although the line profile is not the same in the trace and retrace, reflecting the "push or pull" of the cantilever as it scans. The result is both normal and lateral force data being obtained[101].

1.4.4 Force Measurements

As the tip moves across the surface it experiences forces of attraction or repulsion depending on its proximity to the surface and the composition of the surface. This interaction can also be used to measure the tip's adherence to the surface at a specific point, providing information about the surface properties locally. The interaction between tip and sample at its most basic is due to van der Waals forces, as well as electrostatic forces, and in ambient conditions there is a capillary effect due to moisture on the surface.

To measure this interaction the tip is lowered into contact with the surface at one point or sequentially over a series of points, to a specified set point, and then raised from the surface. The force of the interaction is measured throughout this down-and-up motion, resulting in a force curve. These resulting graphs have distinctive shapes for different interactions[102]. A surface that repels the tip will give a different force curve to one that is "sticky" from the tip's point of view. The presence of compressible layers, or breaking structures on retraction of the tip, can also be observed.

The force on the cantilever during contact can be described simply by Hooke's Law

$$F = -kx \qquad 1.11$$

in which F is the force, k is the spring constant of the cantilever, and x is the deflection of the cantilever. The force laws governing the interaction between the tip and the sample are expressed in terms of force as a function of the tip-sample distance, D, hence F(D). Often with AFM systems D is worked out from the piezo movement and cantilever deflection rather than independently. On a hard surface, when surface contact is established, at "zero separation", the cantilever deflection is directly dependent on the piezo movement, which is seen in the force curve as a straight line of unit slope[103], also known as the slope of constant compliance[102]. On other surfaces this point of separation can be hard to determine. The rest of the curve shows the forces experienced by the cantilever on approaching and retracting from the surface.

Force studies include the measurement of adhesion forces, the calculation of properties such as elastic modulus of a surface from indentation studies[104], protein folding/unfolding studies, and even the study of cellular creep under a constant compressive force[105].

1.4.4.1 Force in liquid

In aqueous conditions, the problem of the capillary force is eliminated and there is no jump into contact due to moisture bridging the tip-surface gap. In liquid, electrostatic forces can play a much stronger role in the tip-surface interaction[106]. This is because even in water, many surfaces have a net charge, either through the dissociation of groups present on the surface, or through the adsorption of ions onto the surface. An electric field is then present at the surface, the strength of which decreases with distance exponentially. As described in section 1.3.2, the surface charge then attracts a layer of co- and counter-ions forming the electrical double layer[81]. The

interaction of the tip with the surface is subject to electrostatic interaction. There is also an osmotic pressure near the surface due to the concentration of ions, which adds to the repulsive force on the tip.

In a study by Butt, the impact of salt concentration and pH on force curves on mica and glass with tips of varying material, and hence varying surface charge, was observed[106]. For example, increasing the salt (KCl) concentration caused the repulsive force to decrease. The repulsive force also decayed more steeply and the van der Waals component of the interaction was more easily observed. In work by Muller and Engel the effect of pH and electrolyte concentration on measuring biomolecules due to electrostatic forces was found to be significant, suggesting that the environment for investigations needs to be controlled and consistent[107].

1.4.4.2 Measuring adhesion

Adhesion of tips to cells is one way of investigating the cellular surface. Some research has taken the approach of using cells as the probe instead of a regular AFM tip to allow direct measurement of single cell interaction forces with a substrate[108, 109]. Physiological properties of cells such as surface charge and hydrophobicity are found to play an important part in such interactions. The adhesion force is the attractive force maximum on retraction from the surface, relative to the baseline force[102, 110]. However, there is more information to be gained from looking at the curve shape as well as this simple value. When the tip is being kept in contact with the sample during retraction due to adhesion the cantilever is still being removed from the surface, so the range of separation for which the adhesion interaction continues is also important[102].

1.4.4.3 Modelling indentation

Indentation studies can lead to host of mechanical information about whole cells[104], such as elastic moduli, spring constants and even the internal turgor pressure of the cell[111, 112]. Investigation using indentation of surfaces with the AFM requires both the sample surface and a hard reference surface to be probed for comparison. The loading force for the interaction can be varied, allowing a graph of force vs. indentation to be plotted and then analysed. The most commonly used analytical model is based on the Hertz theory[104, 113] and describes the deformation of two homogenous bodies touching under an applied load. There are two other large assumptions for this model: that the indenting body is parabolic in shape, and that the indentation depth is much smaller than the thickness of the indented body, less than 10%. When the material from which the tip is made is much harder than the material of the sample, the elastic interaction is used to calculate the force dependent on the indentation F(h) using the following equation:

$$F(h) = \frac{4E\sqrt{R}}{3(1-\nu^2)} h^{3/2} \qquad 1.12$$

Where h is the indentation depth, E is the elastic modulus of the sample, ν is the Poisson ratio (usually set at 0.5 for biological surfaces[114]), and the tip has a radius of R[103].

Hertz modelling for this interaction has some problems however; it does not take into account the adhesion between the tip and the sample. Thus if tip-sample adhesion is negligible a Hertzian approach is adequate, but if tip-sample adhesion is not negligible it needs to be accounted for in some way.

The Sneddon approach develops the Hertz model for a flat, deformable substrate and a hard indenting tip which can be modelled as a conical shape.

At times Sneddon is used alongside Hertz for comparison[115]. Other possible models include the JKR (Johnson, Kendal and Roberts) model, and a model suggested by Sirghi and Rossi, both of which account for the effect of the adhesion force in indentation[116]. The latter is used in a study on live mice fibroblast cells, under physiological conditions, in which the theoretical predictions for the elastic moduli of cells match well with the force displacement curves resulting from indentation.

The shape of the tip is key to this kind of study, and approximation of the tip shape is required for determining the elastic modulus. Conical and parabolic approximations for the tip are commonly used[104]. It is also likely that the shape of the tip will affect the indentation quality of the sample, for example a sharp tip will exert a more localised force than a rounded tip. The tip should also experience negligible deformation.

The following diagram from the Heinz and Hoh paper which appeared in Nanotechnology in 1999[103] neatly summarises the force equations for various approach and retract scenarios. This paper gives a thorough overview of the force spectroscopy techniques, the origin of the methods and its uses in biology.

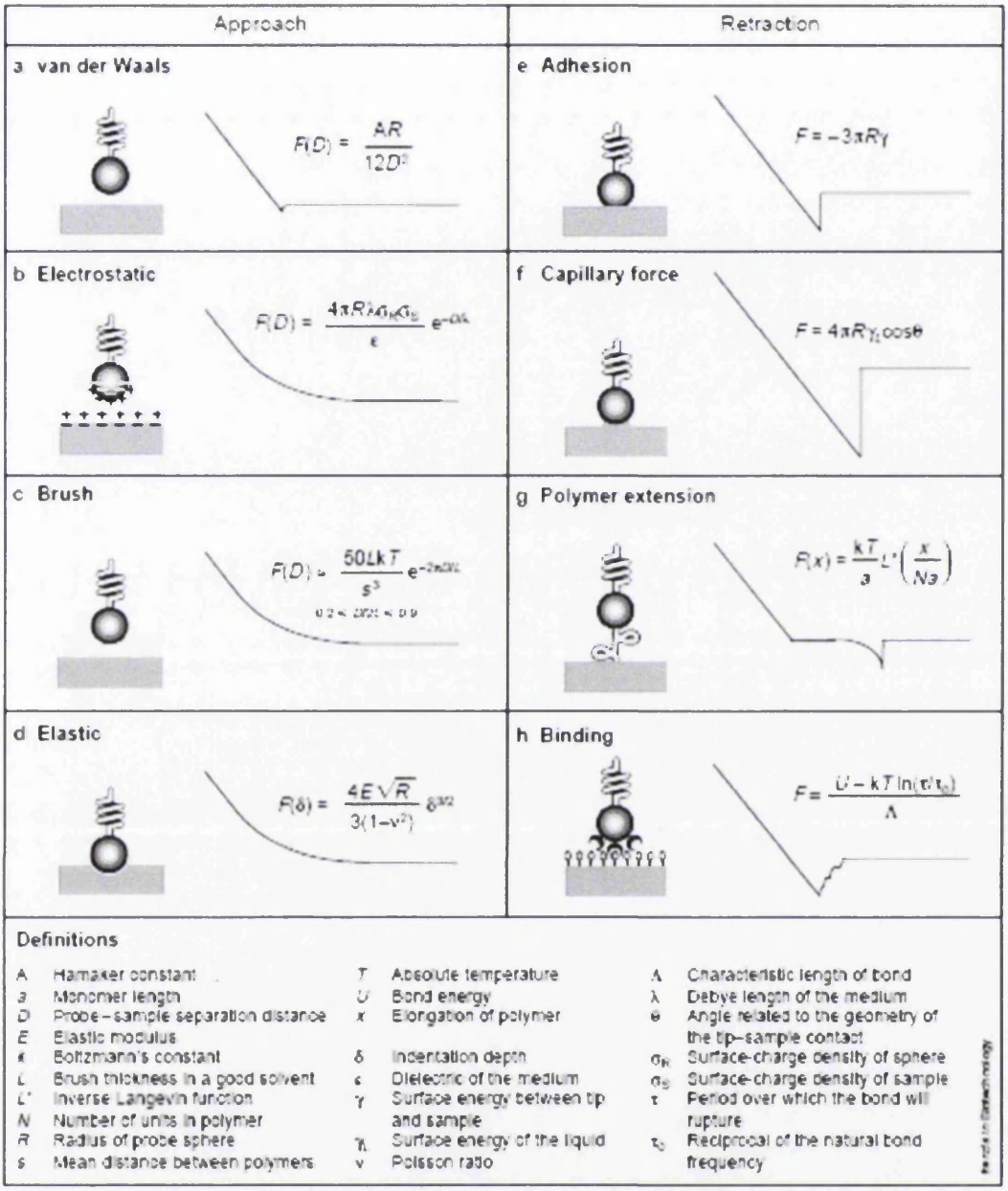

Figure 1-9: *Typical force spectra and the formulae to describe them, from Heinz and Hoh 1999[103].*

As Heinz and Hoh discuss, the next step in elasticity studies is the generation of spatially resolved force data. By compiling data over a variety of points on a surface a force map can be generated, providing information about the changing elastic properties of a surface[115]. An example of this kind of study is the mapping of canine kidney cells by A-Hassan et al, who developed force integration to equal limits (FIEL) mapping, which is

independent of the tip-sample contact point and the cantilever spring constant, and works by relating the work done by the cantilever to a local elastic constant[114].

1.4.5 Atomic Force Microscopy and Biology

There are many studies that use AFM to image the topography of biological surfaces. It is useful to be able to see of what the surface structure comprises with greater than optical resolution. With different AFM approaches the sample's mechanical, chemical, adhesive and electrostatic properties can be studied[110]. In general, biological surfaces are soft in comparison to inorganic surfaces and thus low force setpoints are used in biological AFM studies[80]. Force spectroscopy studies are also used often for characterising biological samples, either to measure adhesion or to calculate mechanical properties, or to look at specific binding between a functionalised tip and surface[117]. Studies of protein or single molecule characterisation have also been conducted with the molecules in situ on a cell surface. Wright et al's paper from 2010 reviews in depth the use of AFM to study cell surface molecules, whole cells and biofilms[118].

1.4.5.1 Liquid imaging

Liquid imaging using AFM requires a suitable scanner if it is to be successful, in order that the liquid does not damage the scanner. The image can be gathered in the same ways as AFM in air but the sample is kept under a liquid layer, usually contained within a liquid cell. The liquid used depends on the nature and purpose of the study, for example using paraffin oil to maintain a water-free environment[93]. When imaging in liquid the laser must be realigned when the cantilever is in the liquid as the change in

refractive index from air to water affects the apparent angle of deflection of the laser from the cantilever. Despite this extra preparation, liquid imaging has great advantages. There are two main reasons for a preference for liquid imaging in biological AFM: firstly the quality of image obtained, and secondly the opportunity to image under conditions that mimic those of living environments. The quality of images produced under liquid have the potential to be better than those in air as the effects of ambient noise are reduced, since vibrations pass more easily through air than through liquid media. This means that greater resolution of surface features can be achieved with liquid imaging.

Sample preparation needs more thought when the imaging is to be undertaken in liquid. It is impossible to use AFM to image material that is floating freely in a liquid medium. Samples must be fixed to the substrate under the liquid. This is where the imaging of living cells becomes much more complex. How can the cells be fixed to a substrate under liquid without interrupting their living processes? This problem has been solved in a number of ways for different reasons, as discussed in the next section.

1.4.5.2 Live cell imaging

Imaging cells that are immobilised usually means that they are no longer living. However, live cell imaging is possible and proffers new insight into the cell surface. Kasas et al imaged cells that were cultivated on glass slides, after being washed and then re-immersed in new media, in 1993[119]. The researchers experienced problems in that the cells were not strongly bound to the surface, with some of them missing from subsequent scans of the same area, presumably due to being knocked off the surface, as well as difficulty in imaging whole cells individually. When rescanning the same area on a cell

surface every five minutes, height changes resembling a wave were seen to propagate across the surface. This change in surface height was argued, alongside microcinematography, as evidence that the cell was alive with some function occurring at its surface.

Kasas also worked on a mechanical entrapment method for living cells, using a Millipore filter with a pore size comparative to the diameter of round cells[120]. This method ensured that the cells would not be removed from the surface by the action of the AFM tip, allowing them to be repeatedly imaged. Subsequently this method has been used in other research, such as the timelapse study of enzyme digestion of the cell wall of *S. cerevisiae* cells[121]. The limitations of this method of immobilisation are the shape of the cells being studied, as rod like cells will not sit in the pores in the same way as round cells, and also the possibility of force measurements being affected by the anchoring method, since the cell is supported in a pore and cannot expand if indented as it might on a flat surface. The amount of cell accessible within the pore may also limit the extent to which cellular living processes can be observed.

Chemical immobilisation of cells for imaging under liquid can also work for live cells. Cells are incubated onto a surface which has been coated in a chemical for adhesive purposes, such as poly-L-lysine[105, 122, 123], or gelatine[124]. Cells partly embedded in agarose gel have also been imaged, without any other buffer as the gel layer was seen to provide suitable local aqueous conditions for the cells[122].

1.4.5.3 Time-lapse AFM

Changes in morphology and life functions of bacteria have been observed through repeated AFM scanning of the same area at different times. In this

way the digestion of *S. cerevisiae* cells by protease has been observed to cause an increase in roughness due to the breakdown of the outer layer of the cells[121]. The variation in cellular topography with growth phase has been observed, alongside a study of response to colistin for *Acinetobacter baumanii* strains, showing a variation from rod-like colistin-susceptible cells to spherical colistin-resistant cells[125]. Time-lapse AFM has also been used to demonstrate the bactericidal application of treatment with low-temperature plasma[126].

Combined AFM and Raman spectroscopy has shown that the amount of material expressed at the cell wall, including proteins, lipids and carbohydrates, changes over time. This corresponds to a change in surface roughness[127]. Using Raman spectroscopy with AFM allows the composition of the surface under study to be explored at the same time as gaining topographical AFM data.

1.4.5.4 Imaging of cellular components

The structure of cellular machinery can be examined using AFM imaging. An example is the imaging of the assembly FliG proteins, functional components of the "nano-motor" that drives flagellar motion in motile cells, on both mica and bilayer membranes used to imitate a cellular surface[128]. Conducted in liquid media this work looks at how these proteins aggregate in terms of size and shape of aggregation under varying circumstances, in order to understand their role in the model of the nanomotor.

1.4.6 Force spectroscopy : biological applications

Force spectroscopy in biology has been used to evaluate cell to tip adhesion, cell probe to surface adhesion, the elastic moduli of cells, the turgor pressure of cells, cell surface charge, forces between biomolecules, forces within biomolecules, and the deformation of cells via constant compressive force[108, 111, 117, 129-134].

Single molecule force studies can involve the probing of individual macromolecules by a sharp or functionalised tip[135, 136]. Once attached in contact to the tip, these molecules can be stretched, the resulting unfolding of the molecules affecting the shape of the resultant force curves. These studies can be conducted in situ, when the macromolecules are present on a cellular surface[137, 138]. Studies in which a specific molecule is immobilised at the tip, such as an antibody, which will "recognise" through binding a co-molecule, such as an antigen, have termed this method molecular recognition force microscopy (MRFM)[117]. This was used in conjunction with imaging of *Bacillus subtilis* spores, where an antibody tethered to the tip was used to bind to a surface antigen after imaging revealed the surface structure of the spores[139].

Research into oral bacteria and their adhesive capability has an obvious application in dental hygiene. Oral *Streptococci* convert sugar the diet into glucan molecules which they use to adhere to dental surfaces and the acid they produce as a by product of their living processes erodes teeth. Research by Cross et al investigated the adhesion on teeth of *Streptococcus mutans* wild type and gene inactivated mutants, which were impaired in their production of the glucosyltransferases (Gtf proteins) that are used in glucan production[128]. It was found that *S. mutans* mainly adheres through glucans in the presence of sucrose. Local glucan adhesion strength has also been shown to increase over time[140]. Other than making one want to

brush one's teeth, this example illustrates how macromolecular mechanical properties (probing the glucan molecules) can be compared with force measurements on individual cells to evaluate adhesion.

Similar studies have looked at polysaccharides on the surface of *Lactobacilus rhamnosus* GG, which promotes health, being a "probiotic" bacterium present in the human body[141]. The surface polysaccharides were investigated because they were reported to contribute to biofilm formation by this bacterium. It was found that several different polysaccharide types were present on the cellular surface.

The polymer brush layer of *Pseudomonas putida* KT2442 was studied using a sharp tip, allowing the effect of salt concentration, from pure water to 1M KCl, on the cell surface polymers to be compared with theoretical predictions[142]. At salt concentrations higher than 0.01M the brush layer became more rigid and compressed and adhesion forces increased. The researchers make a good case for the effect of environment on the conformation and associated adhesion of extracellular polymers.

Salt concentration and pH were also found to be important in work with *Aspergillus niger* spore probes[134]. The adhesion of these cells to mica was measured under varied salt and pH conditions, and a study of the effect of loading force on the adhesion was also carried out. It was found that long-range electrostatic repulsive force was decreased as the pH became more acidic, but this did not correlate with changes in adhesion. These kinds of experiments demonstrate that the interaction is heavily influenced by the environmental conditions.

Other experiments have examined the effect of more complicated substrates, such as work using a yeast cell probe to calculate adhesion to surfaces of varying roughness, including smooth silicon and silicon coated with hydrophilic silica particles of either 110nm or 240nm diameter[143]. A silica

particle probe was also used for comparison on these surfaces. It was found that increasing roughness reduced the silica particle's adhesion, and slightly increased the yeast cell's adhesion. The influence of the loading force applied and the surface hydrophobicity was found to have more impact than the roughness however. The effect of hydrophobicity on interactions between an AFM tip and *Lactobacillus* strains showed that when the cell and tip were both hydrophobic or hydrophilic there were stronger interaction forces than when they had opposing hydrophobicities, with little influence from ionic strength[144].

Elasticity maps of lactic acid bacteria have shown variation in the surface properties of different strains. *Lactobacillus crispatus* and *L. helveticus* showed homogenous stiffness, which was postulated to be due to the s-layers of these bacteria, whereas *L. johnsonii* strains were found to have high adhesion forces, correlating with their polysaccharide dense surfaces. Interestingly one *L. johnsonii* strain showed less adhesion and through imaging its topography showed depressions on the surface, leading the researchers to suggest that its surface has a pattern of bare s-layer areas alongside polysaccharide rich regions[123].

1.5 Aims and objectives of thesis

The organism *S. oneidensis* is important for both microbial fuel cells and biosensor applications. It is also useful as a model organism due to the genomic[42] and interaction[47] research that has been discussed in this chapter. For these reasons *S. oneidensis* merits further research in its own right and as a model organism in the consideration of MFCs and related research. Within MFCs the chemical environment is a key factor in the microbe-electrode interaction. Since *S. oneidensis* is capable of electron

transfer through direct contact and at a distance[50] it is likely that this organism will work in MFCs with varied chemical environments, however in order to control cell-electrode contact, especially with a view to multi-organism MFCs[35], a working knowledge of environmental effects on cell-surface binding is essential.

To begin with a comprehensive microbiological picture of MR-1 growth and colony development in liquid media is needed. To develop this will require monitoring cell population growth, and developing concentration estimates and specific growth rates. Further to this the size, shape and surface features of MR-1 cells over time will be recorded and verified against existing data in the literature[41]. All of these studies will be undertaken for cells grown in oxygen-rich and anoxic environments in order to better understand the necessary metabolic differences between organisms adapting to different environments, and how these differences are manifested physically. This is particularly relevant to MFCs as it *S. oneidensis* MR-1 is maintained in an anoxic environment in the MFC set up. Comparisons between anaerobic and aerobic populations may also provide insight into naturally occuring populations living in lake sediments which are likely to bridge both oxygen-rich and oxygen-depleted zones depending on the depth of sediment and the lake environment[41]. Thus the first aim of this research is to create a comprehensive profile of aerobically and anaerobically grown populations including growth profiles, microbe morphology, and surface charge in relation to chemical environment. Colony growth will be investigated using optical density as a measure of concentration over time, and correlated with dry mass and colony forming units. The physical presentation of the microbes over time will be observed using AFM imaging due to ease of sample preparation. The surface charge will be investigated by calculating ζ-potential from electrophoretic mobility measurements. As well as

monitoring the ζ-potential over time it will be calculated for varying salt concentrations of buffer. All of these assessments will be done for both aerobically and anaerobically grown populations and with two different types of growth media.

Once this context is established the next goal is to assess and measure the interaction of MR-1 cells with surfaces relevant to gram-negative cell binding in general, to metal-reducing metabolism specifically, and to materials used in microbial fuel cells as well. The two methods used as part of this study will be SPR and AFM, the former providing information about cells in solution under flow and the latter providing information about cell-coated surfaces probed both with sharp tips and with mineral colloid probes. The mineral probes will be iron oxide, in order to be able to compare work with that done by Lower et al using cell-coated probes and goethite surface[48], and graphite as this is the material most commonly used to make MFC electrodes[145].

A study of the interaction behaviour of MR-1 when presented with a substrate approximating an MFC electrode will be undertaken in order to demonstrate that cell-electrode interaction kinetics can be quantified before MFC construction allowing design factors such as chemical environment to be considered in isolation. The basis for this study is in work by Lockett et al in which SPR was used to assess binding to a carbon coated sensor surface[146]. This method has only been used so far to assess the binding of DNA arrays to the carbon surface and has never previously been used with whole cells. Describing the non-specific binding of cells to an electrode-approximating surface will be the next challenge and will look to other whole cell SPR studies[69],[63] in order to present the data in line with recent publications.

The overall aim is to present a comprehensive profile of the organism *S. oneidensis* MR-1 and to demonstrate new methods of characterisation with a view to both MFC design and wider characterisation of microbe-manmade interfaces.

2. Materials and Methods

2.1. General laboratory methods

At all stages of study reproducibility, accuracy and safety were the foremost considerations. Preparation of cell cultures and harvesting of cells for sampling was undertaken in a specialist laboratory run according to Biosafety Level 2 guidelines. Glassware and other equipment, where appropriate, was sterilised before use by autoclaving using a steam autoclave (Priorclave, London) at a temperature of 120°C for 15 minutes. Glassware was then allowed to cool to room temperature before being rinsed thoroughly with deionised water. Used glassware was autoclaved in a similar way, then the contents rinsed out and the glassware soaked for at least 2 hours in hot water and Decon 90 glass wash detergent (Decon Laboratories Ltd, Hove, East Sussex), before being thoroughly rinsed and allowed to dry at room temperature.

When preparing media, liquid volumes were measured by either 10-50μL, 50-1000μL or 1-5mL Thermo Scientific Finnpipette adjustable pipetters. Larger volumes were measured using sterile measuring cylinders. Solid ingredients were weighed out to an accuracy of 0.001 grams using a Voyager precision balance (Ohaus, New Jersey, USA).

Unless otherwise stated, chemicals were laboratory grade and sourced from Sigma-Aldrich, Gillingham, Dorset. Laboratory consumables other than chemicals such as glassware were sourced from Fisher Scientific, Loughborough, Leicestershire.

2.2. Bacterial culture

Stocks of *Shewanella oneidensis* MR-1 were subcultured from an original ampoule ordered from NCIMB Ltd, Aberdeen (bacterium account number 14063, reference 49:721). Two types of media were used, each being prepared as solid agar based media, aerobic liquid media, and anaerobic liquid media.

Type of media	Components	Concentration (g/L)
Luria Bertani (LB) agar	Nutrient Agar	25
	LB powder	20
LB aerobic liquid	LB powder	20
	Lactic acid	6.7ml in 1L
LB anaerobic liquid	LB powder	20
	Lactic acid	6.7ml in 1L
	Sodium fumarate	9.6
Tryptone soy (TS) agar	Nutrient agar	25
	Tryptone	15
	Soya protein	5
	Sodium chloride	5
	Dipotassium phosphate	2.5
TS aerobic liquid	Tryptone	15
	Soya protein	5
	Sodium chloride	5
	Dipotassium phosphate	2.5
TS anaerobic liquid	Tryptone	15
	Soya protein	5
	Sodium chloride	5
	Dipotassium phosphate	2.5
	Sodium fumarate	9.6

Table 2.1: *Ingredients for each different type of media used.*

Cells were cultivated initially on agar, with new plates inoculated every 5 days. Agar plates were incubated at 30°C and sealed with plastic film to prevent them from drying out. Fresh agar plates were inoculated from established agar colonies using a sterilised scraper to collect living cells and to deposit them on the fresh agar. Pre-prepared agar plates were made using autoclaved agar mixture made according to the composition shown in table 2.1 and treated with UV light to maintain sterility. They were then sealed and stored.

Aerobic liquid media was poured to a volume of 100ml in 250ml conical flasks stoppered with cotton wool and sealed with foil before being sterilised by autoclaving. Anaerobic liquid media was made up and then heated until boiling. Whilst cooling down in a water bath oxygen-free nitrogen gas (BOC, Guildford, Surrey) was bubbled through the media. Nitrogen gas was also piped into 100ml serum bottles that were then filled with media via a syringe. Once the desired amount of media had been put into the serum bottles they were closed with a rubber injection stopper after "double dosing" with nitrogen to ensure lack of oxygen, and the bottles were sealed with aluminium crimp seals clamped around the lip of the bottle opening. The prepared serum bottles were then autoclaved.

Solid media was prepared in 1L conical flasks, and then autoclaved. Afterwards the media was poured into sterile petri dishes when still hot, under asceptic conditions, and sterilised again under UV light (Bioquell UV lamp, Bioquell, Andover, Hampshire) once set.

Cells were harvested at 20 hours (except during studies where the culture age was varied) and washed by spinning down twice at 6000rpm for 2 minutes, pipetting off the supernatant and diluting the pellet with distilled water each time.

2.3. Initial studies of *Shewanella oneidensis*

2.3.1. Growth curves by optical density

Cells were harvested, as described above, every hour from inoculation for a 24 hour period. The resulting suspension was then diluted: 1ml cell solution to 2ml pure water, for 3 samples. The optical density (OD) of the dilute solution was then measured for each sample using a Unicam UV 300 UV-visible spectrophotometer (Pye-Unicam, Cambridge) at a wavelength of 660nm, with the resulting measurements used to provide an average. This is a method providing results rapidly after minimal sample preparation.

The OD values were then plotted against time to give a curve. As OD is an indication of concentration, this curve demonstrates the growth of cell population over time from inoculation. In order to convert OD to concentration the OD at a specific age of culture was compared with other cell quantifying methods, as described in the next sub section.

2.3.2. Determination of concentration

Concentration of microbes in solution can be determined by three mainstream methods. The first is cell counting using a Haemocytometer. Although this method is the most suitable as it provides a total concentration in cells per unit volume (including both living and dead cells, distinguishing between the two would require staining), it does require viewing the microbes (in a specified volume cell) through an optical microscope in order to count the number of cells per unit volume. Unfortunately, since the size of *S. oneidensis* MR-1 cells is close to the resolution limit of optical microscopy in air this method was not possible using the equipment available to this study.

Without a haemocytometer count, determining the total number of cells both living and dead is a matter of estimation, as the other two methods are a)

colony forming unit (CFU) counts, which takes into account only living cells that can form new colonies, and b) dry weight estimation, which gives a concentration in terms of mass per unit volume not numbers of cells.

In order to determine the number of colony forming units, the sample was first harvested from culture in the same manner as detailed earlier. This was then diluted with varying amounts of M9 salt solution (which halts growth until the sample is plated out) and the resulting solution was plated out onto LB agar.

M9 salt solution	Component	Concentration (g/L)
	Sodium phosphate dibasic	60
	Monopotassium phosphate	30
	Sodium chloride	5
	Ammonium chloride	10

Table 2.2: *Composition of M9 salt solution*

After allowing 24 hours of growth, the number of colonies on the plates was counted. Each separate colony represented one live cell or CFU in the solution used for that plate, and so an estimate of CFU in the original sample could be made using the concentration calculated from each plate. This was done by a simple calculation taking into account the concentration of the solutions and the volume.

Concentration of colony forming units = number of colonies/dilution of sample

Dry weight measurement gives the amount of biomass per unit volume. Weighing boats fashioned from foil were weighed for a baseline mass measurement, and then a specific volume of washed cell solution, harvested as described, was placed in the boat to dry. The mass of the boat and

solution was measured at regular intervals and once the sample was fully dry these measurements converged. When the mass was the same on repeated consecutive weighing, that mass was taken as the biomass of the sample. This method provides a concentration in grams per unit volume. Three foil boats were used and the average of the biomass in each was taken to provide a concentration value, which was then used to convert OD curves into concentration in terms of mass against time.

Once the cell concentration was known in dry mass against time, the curves were analysed further by plotting semilogarithmic graphs, in which the y axis was converted to the natural logarithm of the concentration. In the semilogarithmic plots the exponential growth phase appears as a straight line and the slope of that line is the specific growth rate of the bacterium[1].

2.3.3. Cell size using High Performance Particle Sizer

The size of harvested cells was measured using Malvern Instruments High Performance Particle Sizer or HPPS (Malvern Instruments Ltd, Malvern, Worcestershire) with NIBS DTS software. This uses dynamic light scattering to measure the size of particles in solution. Samples of a minimum volume of 5ml were prepared in "disposable sizing cuvette DTS0012" with care to prevent air bubbles that would affect results. The cuvette was placed into the HPPS cuvette holder and measurement taken.

The results are presented in graph form showing numbers of particles for each size, displaying a peak at the most common particle size. The sharper the peak the more homogenous the sample in terms of particle size.

2.3.4. ζ-Potential

Electrophoretic mobility measurements were made using the Malvern Instruments Zetasizer 2000 (Malvern Instruments Ltd, Malvern, Worcestershire) using electrophoretic light scattering as described in section 1.3.2.1. Cells were harvested by the same method as previously described and made up into solutions of 20ml (2ml of undiluted solution and 18ml of water or saline solution). For the study comparing harvested aerobic and anaerobic cells from LB and tryptone soy growth media, sample solutions were made up in either pure water or salt solution varying from 1M to 0.0001M NaCl, and with a range of pH values from pH 1 to pH 10 (10 values). For the studies of aerobic and anaerobic cells harvested every hour over a period of 24 hours, solutions were made up in pure water at five pH values ranging from pH 2 to pH 10.

For each zeta potential measurement, 20ml of sample solution was injected into the Zetasizer, with care to avoid air bubbles, and 20 measurements were taken with the second ten used to calculate an average for that solution. The ζ-potential was calculated from the measured mobility values using Smoluchowski's equation rearranged to give ζ-potential in terms of viscosity, η, permittivity, ε, and mobility, μ_E:

$$\zeta = \frac{\eta u_E}{\varepsilon} \qquad 2.1$$

ζ-potential and mobility were plotted against pH to show regions of stability/instability. The cell suspension was deemed stable, and therefore more likely to maintain dispersion of cells throughout the buffer at pH values resulting in a ζ-potential of 30mV or higher, or -30mV or lower. The isoelectric point, at which dispersion stability is lowest and cells are most likely to flocculate, for the cells in each solution could also be estimated from

the plot as the point in pH at which the resultant plot line crossed zero on the ζ-potential axis.

The measurement chamber was rinsed thoroughly with pure water between each measurement. Between each set of results the system was double checked by taking measurements with pure water to ensure consistency of results.

2.4. SPR experiments

SPR studies were carried out using a BIAcore X system (GE Healthcare UK Ltd, Little Chalfont, Buckinghamshire) with compatible test surfaces, known as sensor chips, also sourced from the system provider. Sensor chips are able to be functionalised according to established protocols in the BIAcore handbooks. The system was maintained according to the protocols advised by the BIAcore handbooks and a system check was undertaken before each new round of experiments, with any problems being addressed by specific maintenance procedures before repeating the system check to ensure the problems were fixed.

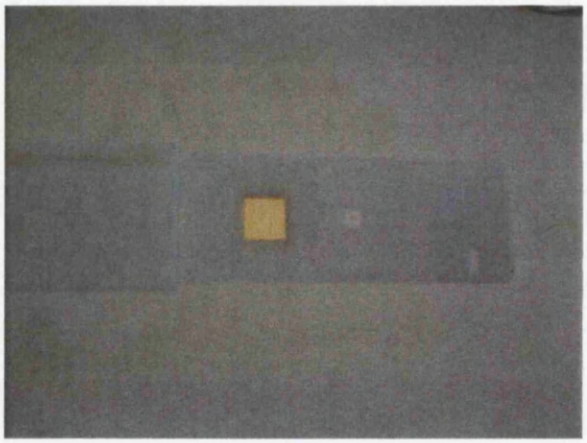

Figure 2-1: *CM5 sensor surface, mounted onto plastic frame to form sensor chip which fits into plastic holder. The holder keeps the surface dust free and covered until installed into the BIAcore system.*

For the first set of experiments the amine-coupling protocol was used to bind poly-L-lysine to the surface of a CM5 (dextran on gold) chip. Samples were dissolved in a basic buffer: 0.01M Hepes, 0.15M NaCl initially, at the appropriate pH, and the same buffer was used as the running buffer in these experiments to prevent buffer effects from affecting the response. Later assays were conducted, changing the buffer salinity, at concentrations of 0.1M, 0.01M, 0.001M and 0.0001M NaCl. Sample injections and running buffer had a flow rate of 20 μL/minute and 30μL of sample was injected at a time.

The net change in response units (RU) from before injection to post-injection was recorded and then averaged over three separate measurements. The change in response was used as an indication of the mass bound, and therefore of the adhesive qualities, of the cells for comparison between samples. After each injection the chip surface was regenerated using a 30μL injection of 1M NaOH. This regeneration protocol was developed in several assays to assess the suitability of different common regeneration solutions.

For the study of binding against culture age for both aerobic and anaerobic growth media, cells were harvested every hour from the growth media and suspended in water at x5 dilution (1ml harvested cells to 4ml pure water). A volume of 30μL of the resulting solution was then injected over a poly-L-lysine functionalised CM5 chip at a flow rate of 20μL. For each sample three different injections were made and the average net change in response calculated. The surface was regenerated after each test with 30μL of 1M NaOH.

The final study required a specially made surface coated with amorphous carbon. Plain gold sensor surfaces (from BIAcore SIA Kit Au) were coated with a layer of amorphous carbon by physical vapor deposition (PVD), using a PVD 75 (Kurt J. Lester Company, Hastings, East Sussex), to a thickness of

2nm for the first surface and 10nm for the second. The resulting sensor surfaces were then mounted onto the plastic supports provided with the bare surfaces, so as to be usable in the same way as pre-prepared BIAcore chips. Sample concentration and flow rate were varied for both aerobic and anaerobically grown bacteria on each carbon coated surface. Regeneration of the carbon surfaces was achieved using BIAcore desorb solution 1, normally used in the BIAcore desorb protocol for maintaining the system, after testing the suitability of the common regeneration solutions and finding that no others were able to regenerate the surface. For comparison cell solutions were also injected over a plain gold, untreated, sensor surface.

2.5. AFM

For AFM studies sample preparation is an important factor. Biological samples can be allowed to dry, but this will affect the results. Thus it is important to view AFM data in context of how the sample was prepared and maintained. AFM imaging in air was undertaken using a Veeco Dimension 3100 (Veeco Instruments, Cambridge). Force measurements in liquid and liquid imaging were undertaken using a JPK Instruments Nanowizard (JPK Instruments, Berlin, Germany).

2.5.1. Imaging

For the most basic tapping mode in air images, cells were harvested in the usual way and then a droplet of solution was placed onto freshly cleaved mica and allowed to dry in air (minimum drying time of half an hour for a droplet of volume 50μL). The mica had been previously affixed to glass sample slides using double sided sticky tape to provide a sturdy base.

Veeco non conductive silicon–nitride tapping cantilevers, with spring constant k=42N/m and frequency f=300kHz, were used at a setpoint of around 1V. Different size images were taken at scan rates appropriate to the sample, using 1Hz as a starting point and decreasing to 0.5Hz or 0.2Hz if necessary. Laser alignment and cantilever oscillation frequency were calibrated before scanning and double checked between sets of image scans.

To match up with the OD/Biomass against time growth curves, an AFM study was conducted with cells harvested every hour for preparation on mica and AFM scanning after drying in air for half an hour.

2.5.2. Probe preparation

Functionalised AFM probes were constructed using the Singer Instruments MSM micromanipulator array, comprising an optical microscope with a moveable chip holder and camera connected to a computer on which images could be saved.

To functionalise a cantilever, a 'tipless' cantilever chip (Park Scientific Contact Tipless Ultralevers, model ULCT-NTHW, Park Systems, Leatherhead, Surrey) was installed into a holder, which was then held in place underneath a glass slide on the microscope. These cantilevers do have small tips, however these are so small compared to the attached colloids that they do not affect the colloid-surface interaction. The glass slide was cleaned thoroughly beforehand. A drop of Loctite UV curing glass bond was put onto one end of the glass slide and spread thinly using a cardboard spreader. At the opposite end of the slide either iron oxide powder or graphite powder was deposited using clean tweezers, and the slide tapped to remove large, loose, clumps of powder. The glass slide was then put into place with the

glue and powder side facing downwards. The set up for the preparation of a colloid probe is summarised in Figure 2.2.

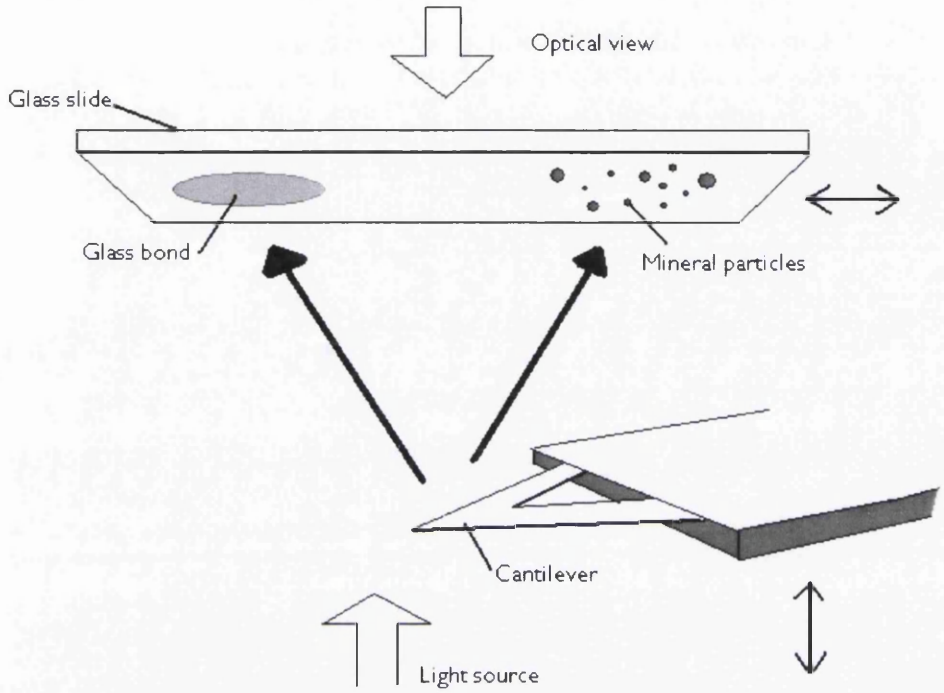

Figure 2-2: *Diagram showing method of attaching mineral particles to cantilever. Cantilever stage can be raised and lowered and the slide stage moved from side to side, in this way the cantilever is brought into contact first with the adhesive and then with the desired particle.*

The position of the powder particles was used to focus the microscope on the lower surface of the slide. The chip holding stage was then raised until the cantilever was just visible, meaning that it was near the surface. The slide stage was moved (using a joystick controller) to bring the glass bond into view above the cantilever. The end of the cantilever was dipped into the glass bond by raising the stage such that the cantilever made contact with the slide. After removing the cantilever from the glass bond it was brought down onto clear glass to remove any excess glue. The slide stage was then moved once more so that the FeO or graphite particles were visible. Once a suitable particle was selected, the cantilever was manoeuvred into place and

then brought up to the slide surface such that the end of the cantilever contacted the particle. On removing the cantilever from the glass slide the particle would be removed as it was now attached to the cantilever. Snapshots of the particle and cantilever were taken just before, during, and after this procedure.

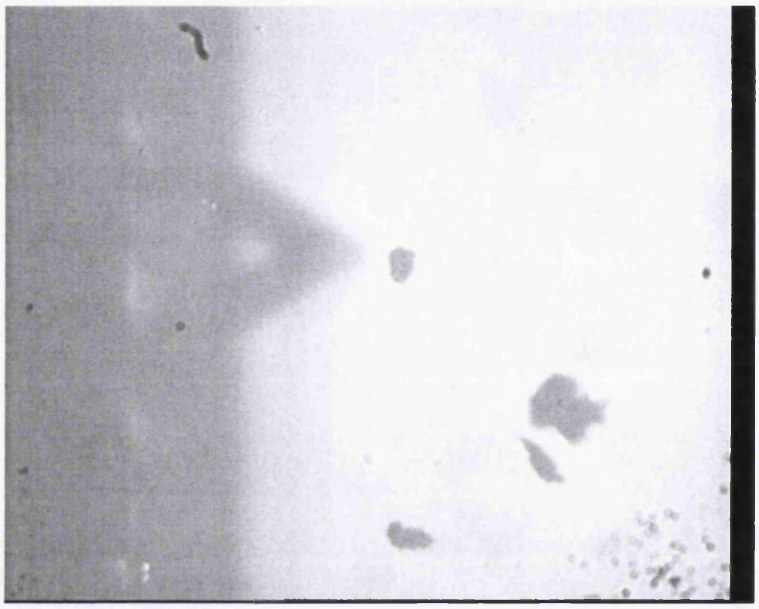

Figure 2-3: *Graphite powder particle shown on glass slide before capture by prepared cantilever. The cantilever is out of focus but visible due to proximity to the surface, with the target graphite particle just in front of the apex of the cantilever. This particle was measured as 5μm by 7.5 μm on the image by comparison with the graticule image.*

Once the particle was attached to the cantilever, the cantilever chip and holder were placed under a UV light source in order to set the glass bond. Meanwhile a snapshot was taken of a reference graticule at the same magnification and focus position so that the scale of the graticule could be correlated with the size in pixels of the saved images, allowing the diameter of the particles to be measured from the "before" pictures pictures with an accuracy of ±0.4μm. Once fixed the cantilevers were imaged under the microscope to confirm the presence of the attached particle, as shown in Figures 2.4 and 2.5.

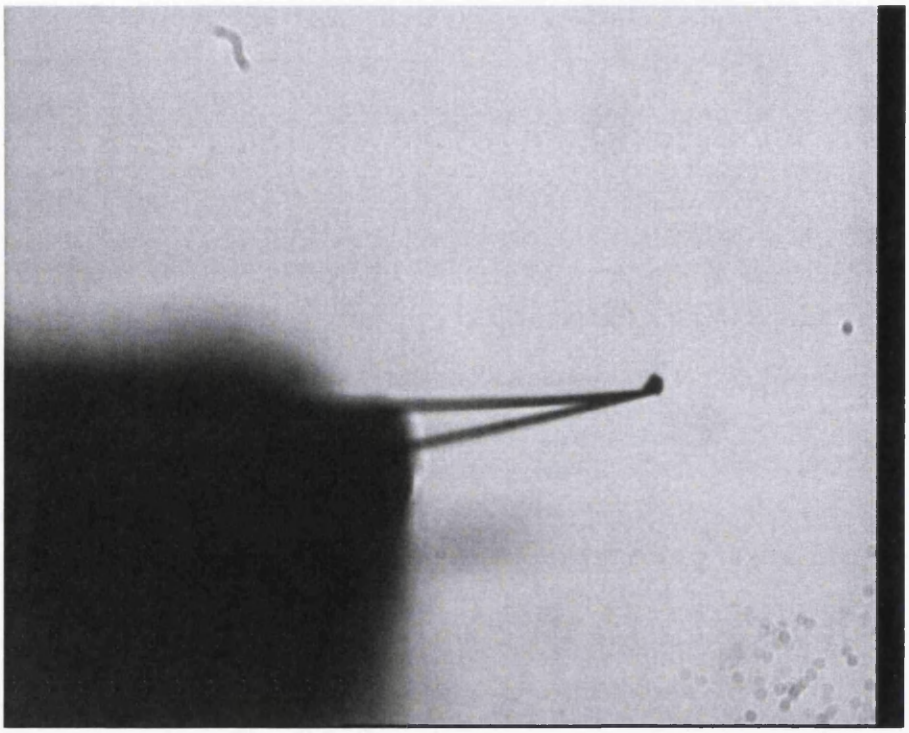

Figure 2-4: *Optical microscope image of iron oxide probe after preparation.*

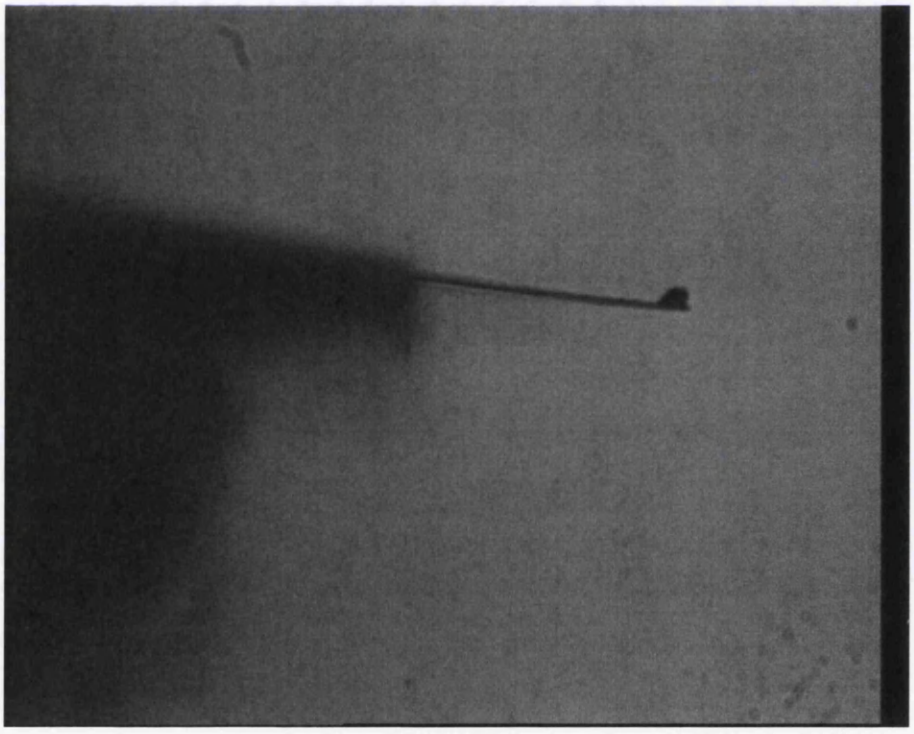

Figure 2-5: *Optical microscope image of graphite probe after preparation.*

From the graticule images, the diameters of the probes be between 4μm and 7μm for the iron oxide probes and 5μm and 6μm for the graphite probes. During use there is a possibility of deformation or damage to the probes, as well as the potential for biological material to become attached to the probe. In order to monitor for such problems the probes were photographed under the microscope in a similar way regularly in between setting up different samples for force studies.

2.5.3. Measuring force interactions

Force curve studies were conducted under aqueous conditions. For the first study harvested cells were deposited onto clean glass coverslips of 25mm diameter and allowed to dry overnight. The coverslips were mounted onto glass slides using capillary forces (a droplet of water was placed onto the slide, with the coverslip placed on top of the droplet). Using silicone gel, a seal was formed between the coverslip and a plastic ring, forming a dish with the sample at the bottom into which approximately 1ml of water or pH adjusted salt solution was pipetted, ready for force curve measurements in liquid.

The JPK Nanowizard scanning software allows thermal tuning of cantilevers in order to correlate the deflection with force via the spring constant. In order to do this the probe was first brought into contact with a hard, bare surface, in this case clean glass, in air. The JPK system then requires the probe to be retracted from surface contact by about 6μm, in order for force spectra to be taken. After taking a force curve on the surface at a default relative setpoint of 0.4V, the calibration protocol could be used to fit a line to the repulsive regime of the curve of deflection against height. This gave the sensitivity in nm/V. The next stage in calibration is the determination of the

spring constant, k, using the cantilever response to thermal noise. The spring constant is in N/m and thus the deflection in V could be converted to an applied force in nN.

Once the calibration had been performed, the probe was used for reference curves on plain glass in the solution to be used for the sample measurements in order to determine which aspects of interactions were due to the sample and which, if any, were due to the glass substrate. For both FeO and graphite probes, aerobically and anaerobically grown bacteria were compared in water, and then in low salt buffer (0.0001M NaCl) at the isoelectric point pH for that type of cell as determined from the ζ-potential studies. The comparison for each began with force ramping, with the relative setpoint varied from 10nN to the maximum force at which serviceable data could be garnered, and a speed based study, under which the approach time was varied from 0.5s to 5s. These investigations suggested appropriate speed of approach and force to be applied for useful force spectra to be obtained. Using these values two hundred curves were taken for each probe/sample/buffer combination over two 30x30μm areas.

3. General characterisation of *Shewanella oneidensis*

This chapter provides a comprehensive study of measurable qualities of *S. oneidensis* MR-1 comparable with those in the literature for other bacteria, such as colony growth and ζ-potential as an indicator of surface charge. This is the first study to show comparisons of growth for aerobically and anaerobically grown MR-1 bacteria in this way, as well as the first to detail the effect of pH and salt concentration on the ζ-potential of MR-1.

3.1. Colony growth and population estimates

The numbers of colony forming units and biomass at 20 hours are summarised in the table below, along with the optical density at 20 hours, for both aerobic and anaerobic growth media.

Growth condition	Colony forming units/L	Dry weight (g/L)	Optical Density
Aerobic	10^{10}-10^{11}	1.5	0.52
Anaerobic	10^{10}	0.43	0.27

Table 3.1:*Equivalent measures of concentration at 20 hours of growth.*

From these data a conversion factor for transforming optical density into concentration by mass can be calculated. For aerobically grown cells this factor is 2.9, and for anaerobically grown cells it is 1.6.

Figures 3.1 and 3.2 show plots of mass against time using the conversion of optical density measurements to biomass. The error bars on these curves show one standard deviation either side of the mean value. The errors are far larger for the aerobically grown inoculum, however the values, in g/L, for the aerobic cultures reach a maximum more than four times that of the maximum for the anaerobic cultures. Since the mass is indicative of concentration, the larger maximum for the aerobically grown cells demonstrate that cell numbers at their maximum are higher for the

aerobically grown cells than for the anaerobically grown cells, despite the same volume of medium being used. Therefore, it can be surmised that the aerobic environment fosters a more successful cell colony in terms of size. It must also be considered that the aerobic cultures were kept in shake flasks, with the aim of consistently oxygenating the whole culture, whilst the anaerobic cultures were static. In fact the cells of the anaerobic culture could be observed as a residue in the base of the serum bottles as well as the clouding of the medium due to the presence of cells.

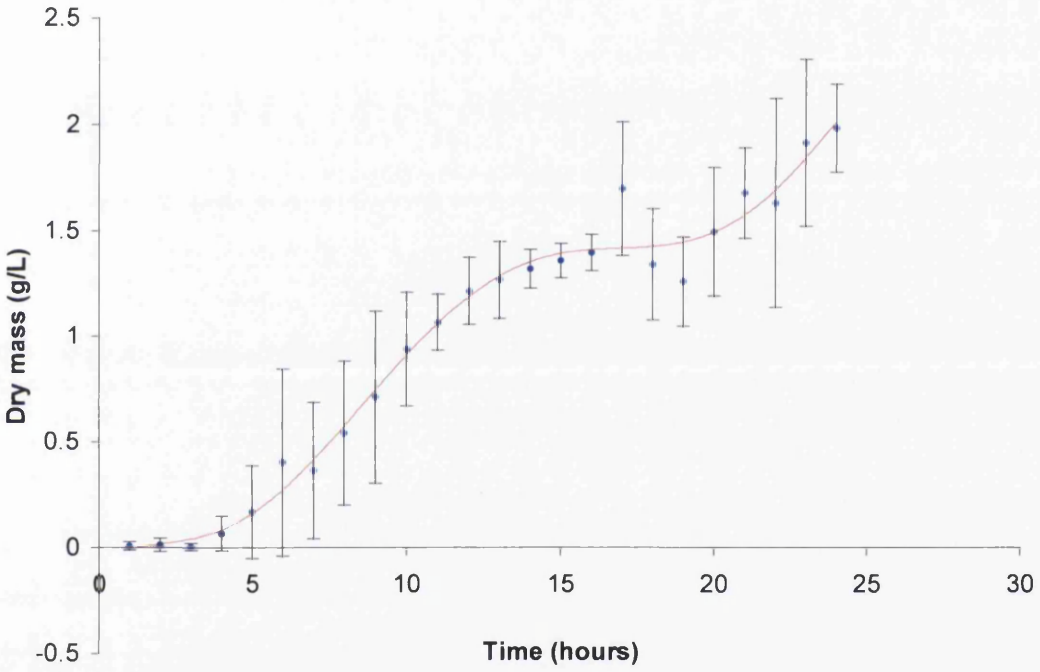

Figure 3-1: *Mass against time for aerobically grown MR-1 cells, as calculated by conversion from optical density measurements. Errors shown are one standard deviation from the mean. Line of best fit, 6th order polynomial generated by Excel, shown in red.*

The plot of concentration against time for the aerobically grown bacteria, figure 3.1, shows a lag phase, a phase of growth and then a plateau around hour 15, before growth continues from hour 20 onwards, in what appears to be a second growth phase.

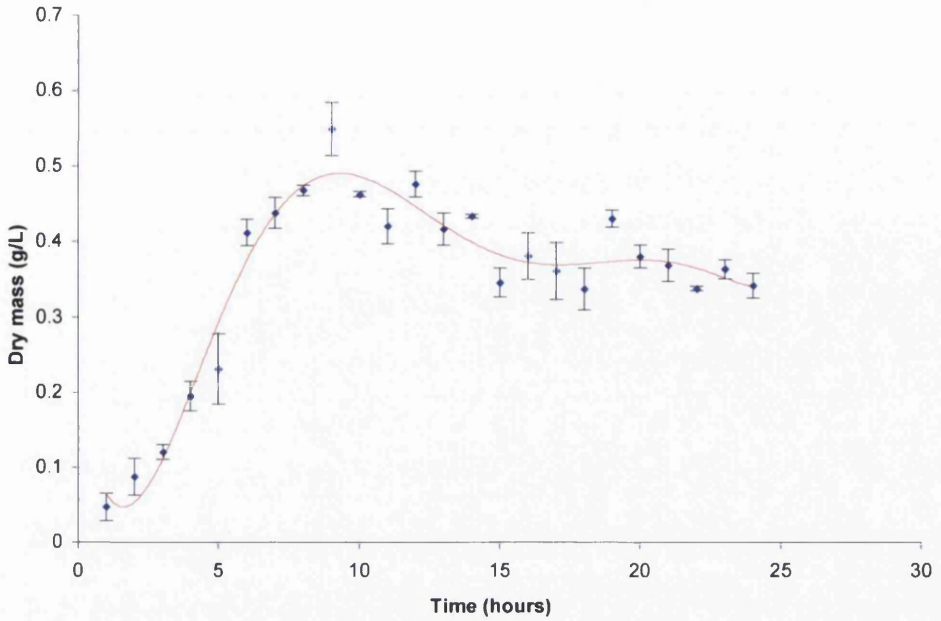

Figure 3-2: *Mass against time for anaerobically grown MR-1 cells, as calculated by conversion from optical density measurements. Errors shown are one standard deviation from the mean for each data point. Line of best, 6th order polynomial, fit shown in red.*

In order to compare the aerobic and anaerobic growth quantitatively the natural logarithm of the concentration was plotted against age of the culture in hours, as shown in Figures 3.3 and 3.4. From this the duration of each growth phase can be measured, excepting the death phase as the method of calculating concentration does not discriminate between dead or living cells and so both dead and living cells are included in the total concentration. For the aerobic cells the lag phase is about 3 hours long, before the exponential phase which continues for three hours, and then the stationary phase starts 6 hours after inoculation. When spinning down the harvested cells, a visible pellet is only seen from 5 hours onwards. For the anaerobic cells the lag time is less than 1 hour, as no lag is seen on the curve. A visible pellet of cells is however only noted from 4 hours onwards. The anaerobic exponential phase is seen from hour 1 to hour 6, after which it enters the stationary phase.

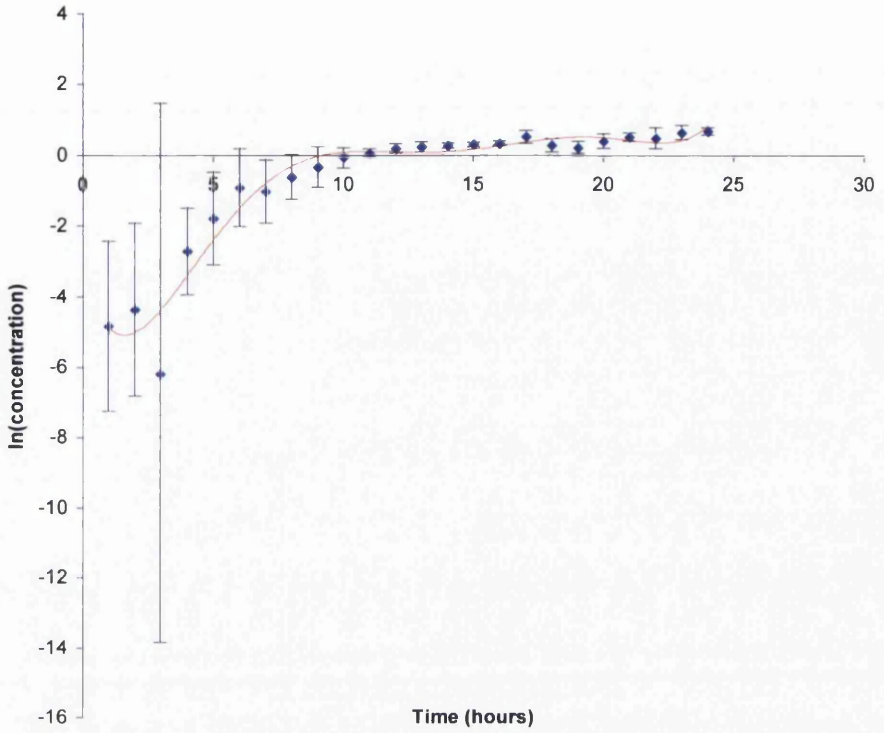

Figure 3-3: *Natural logarithm of concentration against time for aerobically grown MR-1 cells. The errors are calculated by dividing the error in concentration by the concentration, in other words the error is given by* $d(\ln(x)) = d(x)/x$.

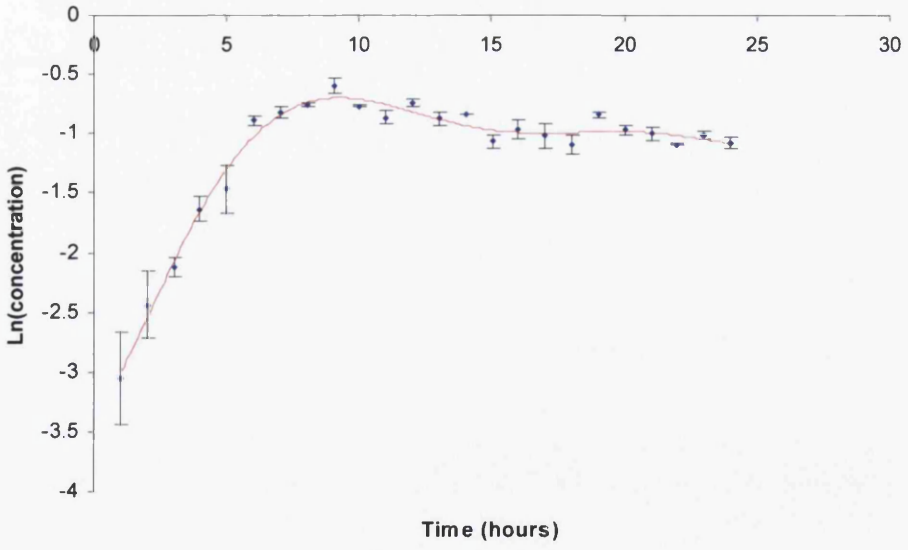

Figure 3-4: *Natural logarithm of concentration against time for anaerobically grown MR-1 cells. Errors given by* $d(\ln(x)) = d(x)/x$.

The straight line representing the exponential phase on the following graphs can be used to calculate a specific growth rate from its gradient.

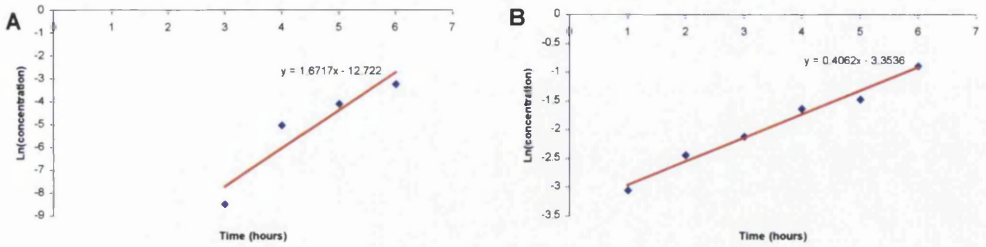

Figure 3-5: *The trendline and equation fit from Excel for the exponential growth phase, represented as a linear increase on the plot of ln(concentration) against time, for both aerobic (A) and anaerobic (B) cultures.*

The slope for the aerobic is 1.7 and for the anaerobic is 0.4 according to trendlines fitted to the data points for the exponential phase in Excel. Thus the specific growth rate for the aerobically grown cultures is just over 4 times that of the anaerobically grown cultures.

Table 3.2 summarises the data from the growth curves for both aerobically and anaerobically grown cells for comparison.

Growth medium	Aerobic	Anaerobic
Specific growth rate μ [hours^{-1}]	1.7	0.4
Doubling time [hours]	2.5	1
Duration of Lag Phase [hours]	3	<1
Duration of Exponential Phase [hours]	3	6

Table 3.2: *Quantitative data from growth curves showing comparison between cell populations grown in aerobic and anaerobic growth media.*

It is interesting however that there is no obvious lag time for the anaerobic culture, indicating that any lag time is less than 1 hour. Thus it seems that the aerobic bacteria adapt almost immediately to the anaerobic environment, which at first seems to suggest that they already have the ability to respire

without oxygen and are able to successfully reproduce in an oxygen free environment. However it can also be argued that they rapidly reproduce due to the need to create a generation of wholly anaerobically active cells straight away, without wasting any energy in the lag phase, to ensure the survival of the culture.

Work by Abboud et al has demonstrated that *S. oneidensis* cells grown aerobically at 22°C have a doubling time of 0.66 hours, compared with a doubling time of 67 hours for cells grown at 3°C[53]. The doubling time obtained at 30°C in this study is actually slower than that obtained by Abboud for 22°C, which suggests that the optimum temperature for growth is lower than 30°C. However, the doubling time for both the aerobically and anaerobically grown cells at 30°C are of similar magnitude to the referenced doubling time at 22°C and the low temperature doubling time is an order of magnitude greater.

Abboud et al also observed using TEM that the morphology of the cells was different when grown at low temperatures; cells formed long filaments up to 70μm in length (too large for their size to be evaluated from TEM images so confirmed with optical microscopy). Transferring the cold grown cells to a higher temperature resulted in their shape and size changing, becoming shorter and thinner with lengths of an average of 5.33μm and diameters of an average of 0.39μm after 100 hours at the higher temperature had elapsed.

3.1.1. Change in pH over time

During the 24 hour optical measurement study of the aerobically grown cells, a concurrent study was conducted measuring the pH of the growth media during the 24 hours after inoculation. This could not be done for the anaerobic media in the same way as the anaerobic media needed to remain

sealed. The following graph shows the change in pH in the hours after inoculation.

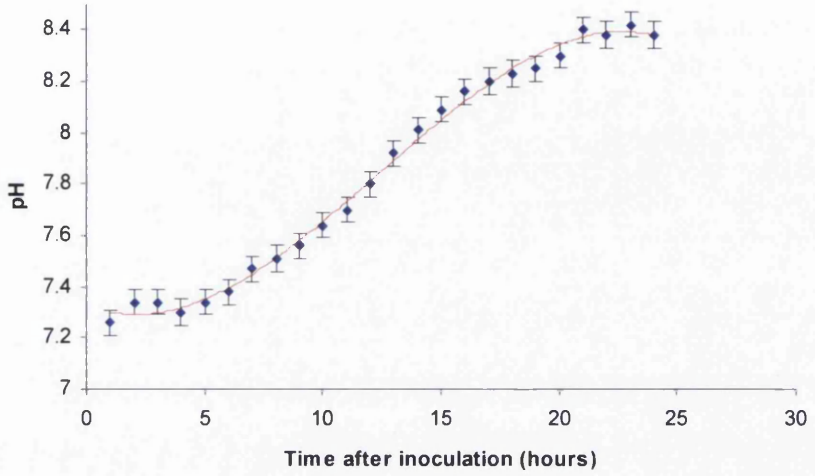

Figure 3-6: *Plot of pH of aerobic culture during growth against the time after inoculation in hours. The total change in pH is 1.1. Errors shown are 0.05pH based on pH meter limitations and a polynomial line of best fit is shown in red.*

The pH becomes more alkaline as time passes, from a pH of 7.3 to a pH of 8.4. There is a stalling of the increase up to hour 3, followed by a steady increase in pH from hour 4 to hour 16 after which the rate of increase slows, before stalling again after hour 21. Interestingly the change in pH continues after the end of the lag phase which is 6 hours after inoculation.

Previous work has shown that pH affects the roughness and nanomechanical properties of polystyrene surfaces incubated with cells from the *Shewanella* genus, *Shewanella putrefaciens* CIP 8040[145]. Comparing systems at pH 10 and pH 4 it was found that the lower, more acidic, pH resulted in a rougher surface and multiple adhesion signatures in the retract part of force spectra, suggesting the presence of polymeric substances.

There is nothing in the literature to date that outlines how or even if *S. oneidensis* MR-1 affects the pH of its environment, although there has been discussion of how ambient pH, as a control factor, affects the organism. Leaphart et al investigated changes in gene expression by *S.oneidensis* MR-1

in response to changes in environmental pH[146]. After being challenged with acid or alkaline environment for 60 minutes gave rise to changes in gene expression including genes involved in amino acid metabolism and cell membrane structure.

3.2. Cell size using High Performance Particle Sizer (HPPS)

In the paper by Venkateswaran which first defines *S. oneidensis* MR-1 as a new species, the size and shape of the cells of this organism were observed using TEM after staining with osmium chloride and found to be rod-like with a length of 2-3μm and a width of 0.4-0.7μm[41]. No measurement was made of anaerobically grown bacteria for comparison in Venkateswaran's study.

For the aerobically grown bacteria which had been washed with pure water and suspended in pure water there were two peaks of average size: the first at 2.7μm and the second at 1.6 μm. The first peak compares well with the measurement of the length of aerobic bacteria in Venkateswaran's paper. The second peak gives a value over twice as large as that given in Venkateswaran's TEM study for the cell diameter, and so cannot simply correspond to an average width of the cells.

A second experiment was conducted using unwashed cells straight from the culture flask. This gave an average size of 0.556 μm. It is possible that there was small cellular debris that would normally be removed through washing which contributed to this low average size, or that the medium in which the cells were suspended affected the size measurements.

The anaerobic bacteria in water showed only one peak, the average size from this was 0.720nm. However, as will be shown using AFM imaging in the next section the majority of anaerobically grown cells are longer in one direction, although the difference between width and length is less than for

aerobically grown bacteria. For this reason it is possible that the measured size is part-way between the length and width of the bacteria under observation.

3.3. ζ-potential study of Shewanella oneidensis MR-1

The isoelectric points for *S. oneidensis* MR-1 suspended in different concentrations of saline solution are shown in Table 3.3.

Concentration of NaCl (M)	LB aerobic	LB anaerobic	TS aerobic	TS anaerobic
Water	4.1	3.6	3.7	3.6
0.00001	4.2	4.6	3.5	4.1
0.0001	4.4	4.1	3.9	2.9
0.001	3.5	4.2	3.8	3.8
0.01	4.2	5.1	4.3	6.4
0.1	3.7	3.5	4.2	3.3

Table 3.3: *Isoelectric points (pH), where the zeta-potential is zero as calculated from graphs of zeta-potential against pH, are shown for each growth environment and concentration of NaCl.*

As can be seen from table 3.3.1, and even more clearly in the following graph (figure 3.3.1), the anaerobic samples show a greater range of values for the isoelectric points, indicating that the salt concentration affects the stability of anaerobic suspensions more strongly than the aerobic suspensions.

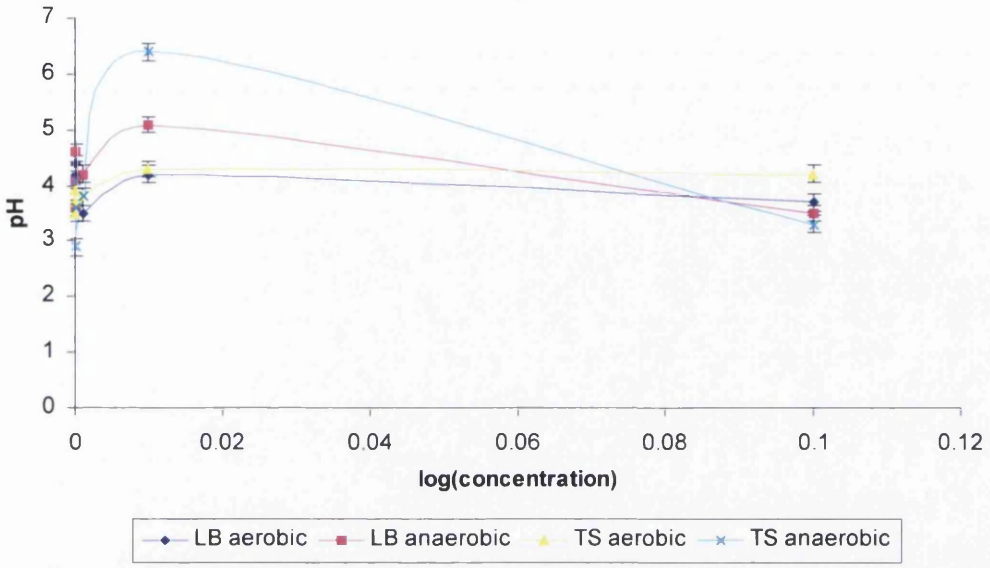

Figure 3-7: *pH against the base ten logarithm of NaCl concentration showing the Isoelectric pH points for samples from different growth media.*

There is also a greater variation in the samples grown in tryptone soy media rather than Luria Bertani media. Any difference between the two growth media indicates that environmental factors affect surface charge; however both growth media show less disparity under aerobic growth conditions.

Isoelectric points are a way of seeing at which pH particles are most likely to flocculate. However flocculation is still a possibility at all pH values where the zeta-potential is between +20mV and –20mV. Where the zeta-potential is above or below this range the particles are thought to be stable and will remain individual from one another and will not flocculate. Table 3.4 shows at what pH values the MR-1 cells are stable in suspension. MR-1 grown anaerobically in tryptone soy media shows the least stability whereas MR-1 grown anaerobically in Luria Bertani media shows the most stability.

Concentration NaCl (M)	Aerobic LB	Anaerobic LB	Aerobic TS	Anaerobic TS
Water	10	6	10.5	10
0.00001	2, 9+	6+	1.5	not stable
0.0001	2, 9+	6+	1.5,10.5	not stable
0.001	not stable	6+	2,6,10.5	not stable
0.01	2, 9+	6+	not stable	not stable
0.1	not stable	not stable	not stable	not stable

Table 3.4: *pH values at which zeta potential is stable are given for each type of growth media and each concentration of NaCl. A + after the pH value indicates all values studied which are higher than that value are also stable.*

The buffer pH necessarily affects the zeta potential of the cells, and it highlights further the differences between aerobic and anaerobic cells and also shows that changing growth media will change the surface chemistry of the cells. Most bacterial cells are neutrophiles and have mechanisms for maintaining internal neutral pH levels, with limitations on the external pH in which they can survive[1]. In the literature the effects of pH on *S. oneidensis* MR-1 have been observed in a few different ways. In one study cells exposed to acidic (pH 4) and alkaline (pH 10) environmental conditions for 30 and 60 minute periods showed no decrease in viability when plated out compared with that grown in pH 7 media with no exposure to other pH conditions, however transcriptome analysis of the different cells showed that gene regulation had been activated in the cells[146]. The exposure to pH 4 showed the greatest change in gene expression, and due to the large number of genes shown to be differentially expressed, the study concluded that the organism implements a diverse array of changes to respond to external pH conditions affecting transporters, amino acid consumption, central metabolism, and cell envelope composition.

In MFCs pH is a consideration in design of the chemical environment, and has been shown to affect the suitability of different bacterial strains for certain MFC environments. In work by Biffinger et al *S. oneidensis* MR-1 was found to be more suitable than *S. oneidensis* DSP10 for use in MFCs with

greater acidity[54]. The current produced by MFCs with each organism was compared under pH neutral or acidic (pH4-5) conditions and was shown to vary with pH, without a direct dependence on the size of the cell population, although that variable was also affected by pH. This paper demonstrates the insights into MFC design that can be directly uncovered simply by changing one environmental condition, in this case pH. Characterising the interaction of MR-1 cells with one another in suspension under varied pH and salt concentration provides a reference guide to suspension stability that can be used in the design of MFCs to encourage cells to stay in suspension or to flocculate, depending on what is desired.

The isoelectric point determined for cells showed no correlation with the age of the culture for the anaerobically grown cells, however for the aerobic cells the variation in isoelectric point was greater in the first few hours and became more consistent after 12 hours. In a study by Grasso et al ζ-potentials for *P. aeruginosa* were compared at different stages of growth and found to vary from –17.59mV in the logarithmic phase, -26.17mV in the stationary phase and –18.5mV in the decay phase[89]. All of these values are negative and at the limit of stability for the cells in suspension. The small variation in ζ-potential for *P. aeruginosa*, a gram-negative bacterium, suggests that a similarly small variation would be expected for *S. oneidensis* which is borne out by the minimal change over time of isoelectric point for *S. oneidensis*.

3.4. AFM imaging over time

In order to visualise the development of the bacteria under both aerobic and anaerobic conditions, AFM images were obtained at hourly intervals after a time, t = 0, when the new medium was inoculated. The aim of this study was

to find out what microbes in each of the defined growth phases looked like, and whether their morphology changed depending on the stage of growth. The anaerobic cells and aerobic cells of *S. oneidensis* MR-1 have a different morphology. In order to see the change in a culture of aerobic cells when transferred into anaerobic media, AFM images at intervals after anaerobic inoculation were taken. The variation in the cells as observed with AFM imaging is outlined for both aerobically and anaerobically grown cells over time in the next two sections.

3.4.1. Aerobically grown cells

As one might expect from the growth curves, for the first 4 hours there were few cells to be imaged. The surface areas scanned were often devoid of cells but many featured clusters of material spreading outwards from epicentres in an asymmetric snowflake like fashion, as shown in figure 3.8. These clusters do not feature in samples from 5 hours of growth onwards, this corresponds with a visible pellet only being noted on spinning down samples harvested after 5 hours from the time of inoculation. Extracellular material is referred to in several papers on AFM imaging of bacteria, including a study of how varying the washing process of *E. coli* affected the images obtained[147]. However there are no studies showing AFM imaging of liquid cultures in the early stages after inoculation from bacteria grown on solid medium, so there is little basis for comparison in the literature. It is likely that these clusters are down to components from the growth medium, such as salt crystals since there was no pellet visible on spinning down the harvested sample and hence the sample is a very dilute solution of the growth medium.

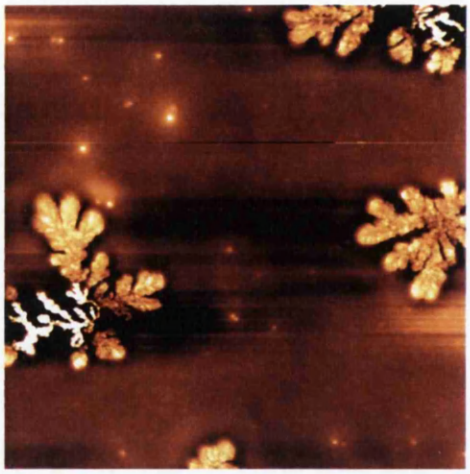

Figure 3-8: *30μm scan of sample taken from aerobic culture 1 hour after inoculation showing no cells and a number of clusters of material assumed to be salt crystals.*

At 6 hours after inoculation the surface shows a larger number of cells with unusually long cells that cross one another, as shown in figure 3.9. It is possible that some of these long cells are dividing into smaller cells which more closely match the size and shape expected from MR-1[41], but they appear to be continuous. Both the long and shorter cells are surrounded by extracellular material appearing as granules of various size. Flagella are also visible but prove difficult to assign to specific cells.

A. 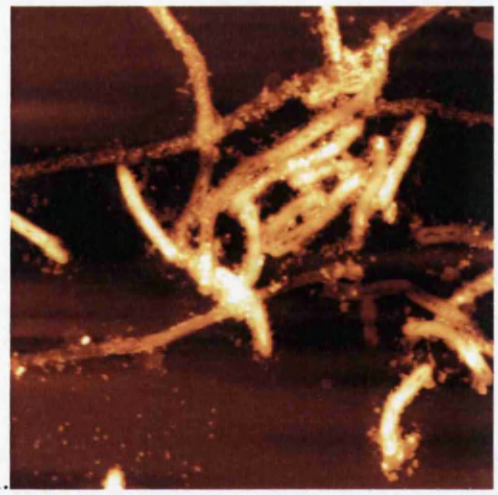 B. 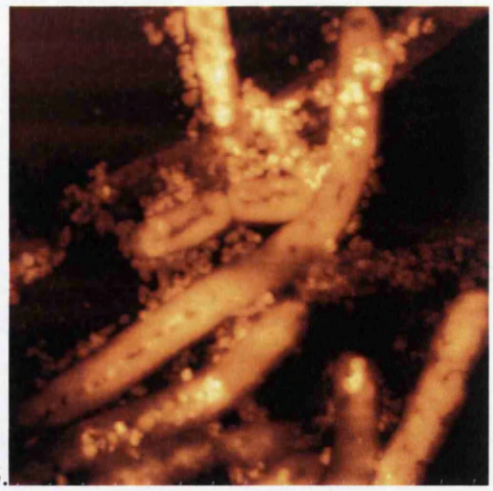

Figure 3-9: *Images of cells grown in liquid media 6 hours after inoculation from solid medium grown bacteria of scan size A. 30μm and B. 10μm. Extracellular material seen around cells. In the 10μm scan a flagellum can just be seen on left hand side in the top half of the image.*

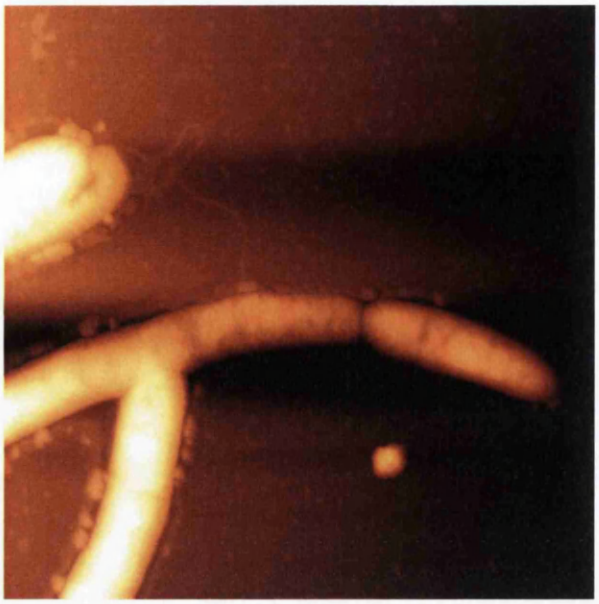

Figure 3-10: *Aerobically grown cells as seen at 7 hours. This 10 x 10μm AFM image shows a cell dividing at the end of a longer cell strand. Also visible are a flagellum and extra cellular material.*

The cells shown in figure 3.10 have similar extracellular material and appear to show a cell dividing away from the end of a longer cell strand. In the top left quarter of the image a flagellum can be seen. Extracellular material is visible around all the cells in the image.

Individual cells can be made out more clearly from 8 hours and after 10 hours the surface is predominantly covered by individual cells and pairs of dividing cells rather than the long chains or strands of cells.

In dividing pairs the two cells are the same length in the vast majority of cases, demonstrating that the division into two discrete cells only occurs when the cells are of suitable length. This can be seen in figure 3.11, where there are six discernible dividing pairs. The surfaces of some of the cells in this image appear mottled, indicating a variation in height over the surface, although there is no regular pattern. Other cells appear to have a channel of lower height in the centre along their length. It is possible that this is due to collapse of the cell caused by drying, as these images were taken in air.

Figure 3-11: *10 x 10μm AFM image of aerobic cells after 11 hours of growth showing multiple dividing pairs.*

From 11 to 15 hours of growth the cells are mostly individual and are found in clusters with some isolated. At 16 hours of growth surface structures become more visible on the cells.

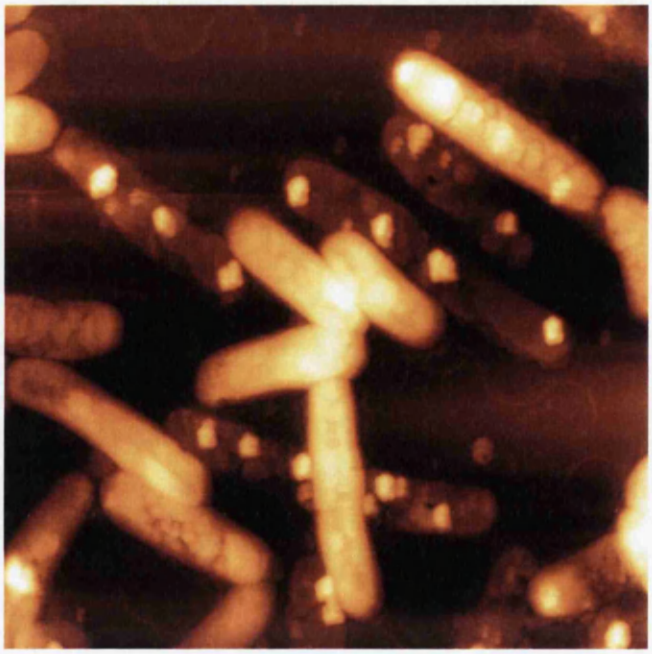

Figure 3-12: *10 x 10μm AFM image of aerobic cells after 17 hours of growth. Some cells maintain previously seen morphology but others show large surface features.*

Figure 3.12 shows aerobic cells after 17 hours growth. The cells maintain the long rodlike shape, flagella numbers have increased and so have the number of cells with relatively flat surfaces punctuated by globular clusters. In this image there are no clear dividing pairs.

After 17 hours the number of cells with the surface features like those in image 3.12 become more prevalent, however cells with surfaces like those in figure 3.11 are still present. Highly populated areas on the surface show cells constrained by available space.

3.4.2. Anaerobically grown cells

From images of the anaerobic culture it can be shown that groupings of cells and individual cells are present from hour 1, which is understandable since cells in liquid were injected directly into the anaerobic medium. The anaerobic growth curve showed no lag phase and therefore the cells are already multiplying after an hour post-inoculation. There is more debris outside of the cells in the anaerobic images for the first 3 hours, perhaps from cells damaged in the transfer from aerobic to anaerobic culture. However there are none of the snowflake-like clusters in any of the images for the anaerobically grown bacteria.

In the first 2 or 3 hours after inoculation the cells in the anaerobic culture appear to have less distinct edges than the aerobic cells. They are in clusters of 3 or more cells and there is some extracellular material visible. An image of a cluster of cells after 2 hours of growth is shown in figure 3.13.

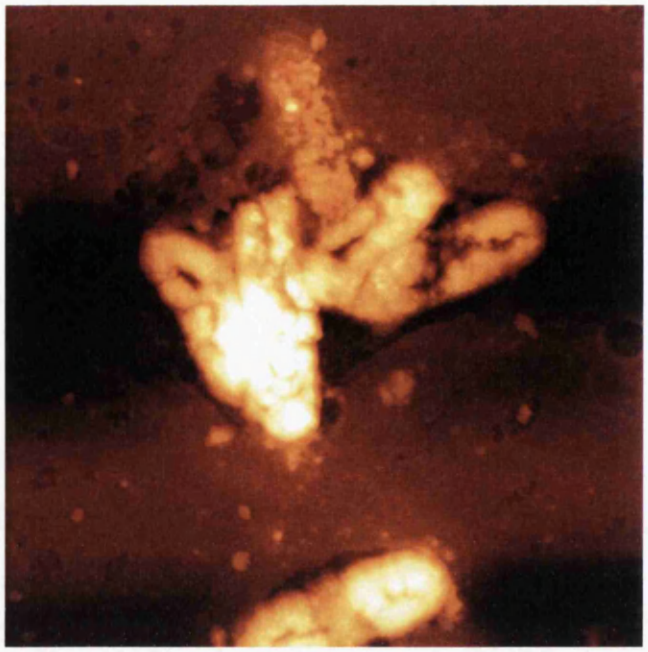

Figure 3-13: *Cells harvested from anaerobic culture 2 hours after inoculation from aerobic culture, in 10 x 10μm AFM image.*

In the images taken for the cells during the growth phase there appear to be dividing cells but the long chains of dividing cells as seen for the aerobically grown cells are not present. The surface becomes cleaner with individidual and small groupings of cells consistently from 5 hours onwards.

Figure 3-14: *Anaerobic cells 7 hours after inoculation. 10 x 10um AFM image.*

Figure 3.14 shows anaerobically grown cells after 7 hours of growth. The cells are more rounded and less rod-like than the aerobic cells. This is mainly because they are not as long as the aerobically grown cells. After 7 hours the cells remain similar in size and shape, however when the culture gets to 16 hours growth the same surface features as seen on the aerobic cells at 16 hours can be seen, as shown in figure 3.15.

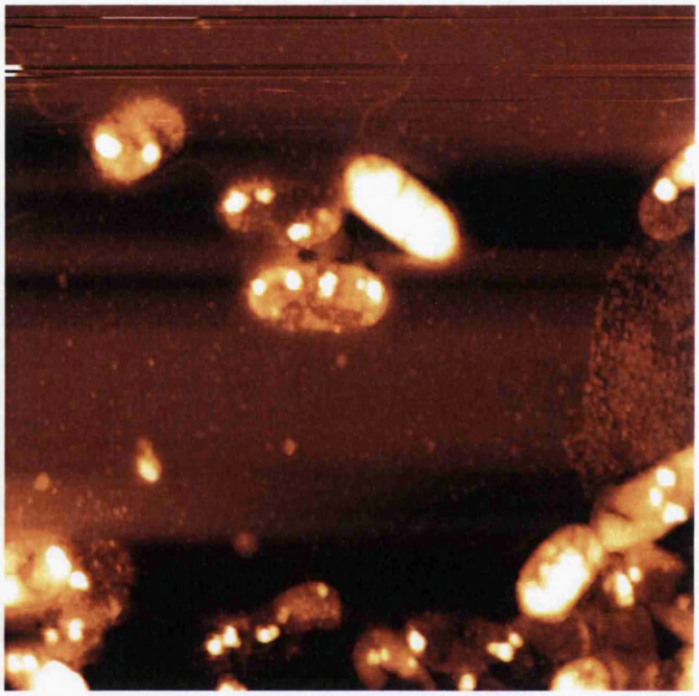

Figure 3-15: *10 x 10μm AFM image of anaerobic cells after 16 hours growth.*

It is possible that the flattened cells with the distinct surface protrusions are old or dead cells breaking down, and that the cells whose surface match those of cells from sooner after inoculation are the still living or newer generation of cells. This seems increasingly likely when it is considered that the numbers of cells that have less height overall and marked protrusions increase after 16 hours growth, becoming the overwhelming majority by 20 hours growth for the anaerobic cells.

The other possibility is that the surface protrusions are features of anaerobic cells, and that the cells from the aerobic culture displaying them were growing in an increasingly anoxic environment due to increasing population

(and hence less oxygen availability) and unequal distribution of oxygen in the shake flask, as discussed by Elias et al[52].

In work by Elias et al in 2008 the effects of different growth environments was studied by comparing the dissolved oxygen concentration, consumption rates, and proteome expression for cells grown in bioreactors with those grown in shake flasks[52]. The greater environmental control exercised over the bioreactor cultures led to less variability in measurements than seen in the shake flask cultures. Evidence was put forward to show that oxygen availability in the shake flasks was far from consistent, with proteins normally found in anaerobic cultures found to a greater extent in the shake flask cultures than in the bioreactor cultures. The variability of the shake flask (aerobic) cultures in terms of cell size and surface properties so far is in keeping with Elias et al's assertion that shake flasks are non-uniform growth environments in which variability is inevitable. The more homogenous anaerobic growth cultures by contrast show that adapting to their environment requires a more rigidly defined morphology and surface properties.

The morphological differences between *S. oneidensis* MR-1 cells grown with abundance of electron acceptors and those grown in the absence of electron acceptors have been demonstrated previously[51]. In this work redox heme proteins were identified as prevalent in protruding nanoscale structures when electron acceptors were absent, however addition of electron acceptors caused these structures to diminish.

Cytochromes OmcA and OmcB have been shown to be expressed on the outer membrane surface of *S. oneidensis* MR-1 cells by Myers and Myers[148]. In this particular study only anaerobically grown cells were investigated, with the presence of OmcA and OmcB on the outer membrane demonstrated via degradation by proteinase K. OmcA was shown to be the most

prominent of the two on the cell surface and the surface exposure of MtrB, a noncytochrome protein, was also noted.

In the early hours of the anaerobic culture however, most of the cells do not present the surface structures seen later in both cultures. It is possible that oxygenated media, extracted with the cells for injection into the anaerobic media, provided enough oxygen for the cells to continue metabolising aerobically initially. This might also account for there being virtually no lag time for the anaerobic growth curve as seen in section 3.1.

Global transcriptome analysis has also given insight into the effect of limiting oxygen in *S. oneidensis* MR-1 cultures. In work by McLean et al[149] chemostat cultures with a maintained level of dissolved oxygen formed aggregates when challenged with 0.68mM $CaCl_2$. These aggregates were stabilised by extracellular matrix material comprising DNA, protein, and glycoconjugates as observed by confocal microscopy using multiple stains, which bound to different molecules. However, when the oxygen levels dropped below detection the aggregates dispersed. Global transcriptome analysis of cells in this study showed that gene expression patterns consistent with biofilm formation was higher in the cells grown aerobically than with those in the oxygen limited culture. Perhaps counter-intuitively, cells from the oxygen-abundant culture also expressed genes thought to be involved in anaerobic electron transfer, McLean suggests that this is due to anoxic conditions within the interior of the cell aggregate.

What McLean's work, and others comparing transcriptome analysis of *S. oneidensis* MR-1 under different conditions, based on the original sequencing of the MR-1 genome[42], demonstrate is that environment determines the physicochemical composition of MR-1 cells. This alteration in gene expression in response to ambient conditions is demonstrated in the difference in cell size and shape, confirmed with HPPS particle sizing and

AFM imaging, and in the differences in surface charge as shown by the difference in ζ-potential, particularly in regard to the isoelectric points and stability.

3.4.3. Flagella

Flagella were visible on both aerobic and anaerobic images. The role of the flagellum is as a device for propulsion in motile cells. Clear AFM images of measurable flagella attached to cells can be difficult to obtain, due to the height difference between the cell and the flagellum. This difference means that although the data scale could be adjusted to display the surface of cells or the surface around the cells including flagella, adjusting the scale to view both simultaneously was problematic. In order to obtain better AFM topographical data about flagella then was more easily done by imaging them without their attached cells, by choosing areas containing only flagella from larger scan areas.

Figures 3.16 to 3.18 show the same 4.4μm by 4.4μm area in height, phase and amplitude. In the height image, figure 3.16, the surface features of the cells are harder to make out and the height difference affects the area surrounding the cells making the flagella harder to see. This is why it is interesting to compare the phase and amplitude images to see which features are preserved, less prominent, or more prominent in each set of data. The cells in these images are from an anaerobically grown culture at 5 hours of growth.

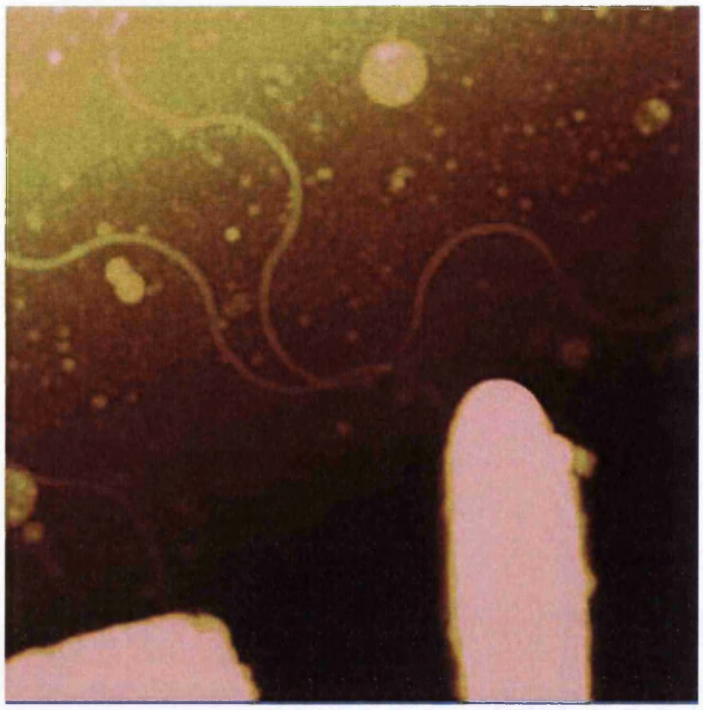

Figure 3-16: *AFM height image showing cells with flagella. Scan size 4.4 x 4.4μm.*

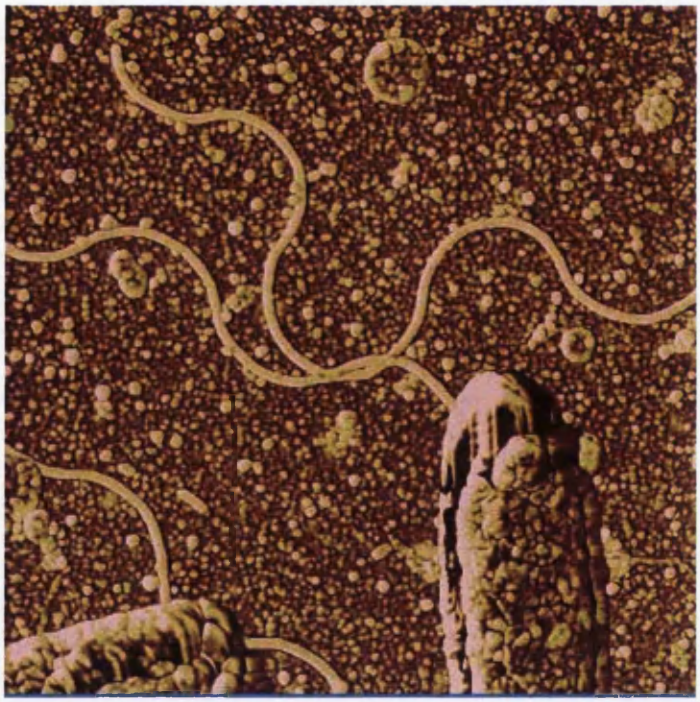

Figure 3-17: *AFM phase image showing cells and flagella, scan size 4.4 x 4.4μm.*

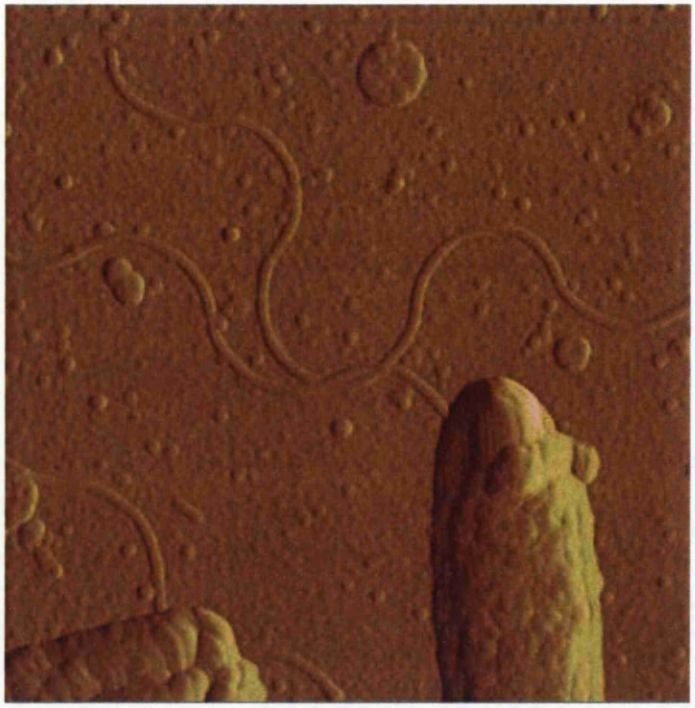

Figure 3-18: *AFM amplitude image showing cells and flagella, scan size is 4.4 x 4.4μm.*

The flagella here and in images from other cells at different ages of culture, for aerobic and anaerobic cells, were not shown to vary with these differences. The length of a flagellum was usually hard to measure as they lay curved on the surface, often tangled with others or under cells, and so from this study there is no reliable average length. A meaningful average length would be unlikely anyway as flagella may be damaged by the centrifugation used in washing cells when harvested.

The width or thickness of the flagella was easier to measure, and for both aerobic and anaerobic cells it was found to be approximately 74 ± 1nm. The image shown in figure 3.19 is a closer look at the flagella seen in figures 3.16 to 3.18.

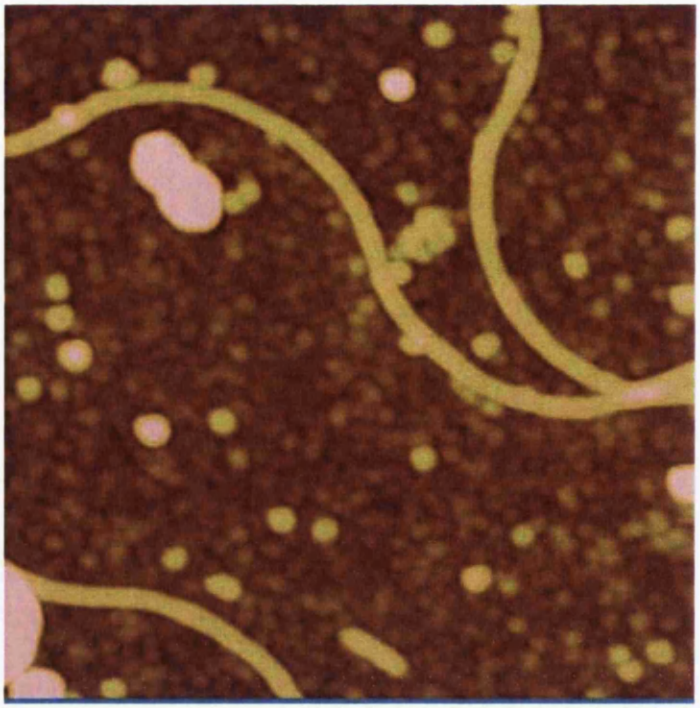

Figure 3-19: *2 x 2μm AFM height image showing three sections of flagella, area selected from larger area shown in figure 3.10.*

Work by Paulick et al in 2009 studied the driving mechanisms for the single polar flagellum of *S. oneidensis* MR-1 cells, showing that the organism is unique amongst its closest neighbours for having one flagellum with two possible stator systems to drive it depending on the environment[150]. The PomAB stator system is sodium-dependent, and the MotAB stator system is driven by the proton motive force, allowing MR-1 cells to take advantage of different ambient chemistry in the wild type. This is another example of the organisms highly opportunistic adaptability. The Paulick study does not explore differences in oxygen availability, although nutrient limited media is shown not to prevent cellular motility, nor does it describe the flagella themselves, since the main work of the paper is focussed on the stator systems and their genetic origin.

3.5. Chapter summary

Although there are differences in size and surface morphology between aerobic and anaerobically grown cells as demonstrated by comparing AFM images under identical preparation methods, the lack of any lag phase in the growth curves for anaerobically grown bacteria implies that the aerobic bacteria used to inoculate anaerobic cultures are capable of functioning as anaerobes immediately on removal of oxygen. Therefore the pathways used in alternative electron transfer, in this case using dissolved fumarate as the electron acceptor, are already present in aerobically grown cells. This effect may be exacerbated by the distribution of oxygen in the aerobic cultures being non-uniform, as discussed by Elias et al[52], leading to anaerobically functioning bacteria existing in the aerobic culture. This is in line with the transcriptome analysis findings by McLean et al[149] demonstrating that anaerobic-type bacteria are present in the centre of otherwise aerobically grown aggregates, and thus that differential oxygen levels in static or shaken cultures can lead to supposedly aerobic bacteria presenting with anaerobic cell metabolism.

The effect of pH on the surface charge on *S. oneidensis* MR-1 cells differs with salt concentration, and with the growth environment of the cells. The surface charge, as approximated by the ζ-potential, of anaerobically grown cells is more sensitive to salt concentration than that of aerobically grown cells, as shown by greater variation with changing salinity. ζ-potential as a measure of surface charge can be calculated by approximating cells as solid colloidal particles, although modelling them as soft particles with less defined boundaries is more correct.

4. Surface Plasmon Resonance characterisation of *Shewanella oneidensis* MR-1

The attachment of cells to a substrate can be monitored rapidly and reproducibly by SPR using a simple experimental set-up, as demonstrated by Jenkins et al in their 2005 paper comparing the adhesion of different strains of *Pseudomonas aeruginosa* to a plain gold surface[62]. This study used static SPR, as opposed to SPR under flow achieved using the BIAcore X system in this chapter, however the sensitivity of response to small mass changes allowed Jenkins et al to determine that the retractable pili expressed by the wild type *P. aeruginosa* cells allowed more cells to bind to the surface than mutant strains without pili or with non-retractable pili. In Jenkins' work the "early attachment kinetics" are mentioned and described to some extent qualitatively by discussing the maximum response, resonance angle of 600 for the wild type and 420, 300 for the two mutants, however association rates are not discussed. In previous work by Jenkins using static SPR cells of *P. aeruginosa* were killed using heat treatment, and these dead cells were found not to adhere to the sensor surfaces, unlike live cells in the same tests[63].

Uchida et al[151] used a BIAcore study to show that certain strains of *L. Acidophilus* recognise and bind with human colonic mucin (HCM) by injecting whole cells over HCM treated sensor chips. The results were discussed in terms of whether or not the cells bound to the chips and how much mass was bound to the surface, indicated by the net change in RU. Rate analysis was not applied to this study. The authors took care to point out that in the BIAcore the system detects changes in refractive index at distances of up to 0.3μm from the sensor surface, and that the dextran layer to which their HCM was bound was about 0.1μm thick, so that since the cells did not penetrate the dextran layer any change in response would only be due to cells bound close to the HCM molecules. Cells bound to other cells or

loosely attached at a distance greater than 0.3μm would not affect the response. Other papers suggest that aggregation of bacterial cells may have an effect on the regularity of response profiles in BIAcore sensorgrams[152], and although each result in the studies reported in this chapter was an average from 3 or more measurements there is the possibility of cellular aggregation affecting the results.

Rates of association and dissociation are a complicated issue for whole cell studies, and are sometimes by-passed in favour of comparisons of total response after injection. In her review paper, Otto describes the problems of describing whole cell binding data from SPR using rate constants[58]. Otto compares work by Kawashima et al in looking at binding of whole cells of oral streptococci to salivary components[75] with work by Oli et al concerning the specific binding of an adhesin on *S. mutans* cells and salivary agglutinin[69]. Oli's work finds changes in response that are ten times higher than Kawashima's which Otto suggests is due to the more specific nature of binding in Oli's experiment.

Oli et al state that they do not attempt to determine binding constants for the interaction due to the complexity of whole cell interaction, instead they use changes in response units for comparison between different cell mutants[69].

In the analysis of results in this chapter, the primary focus is on comparison of changes in total response after sample injection, bringing the level of quantitative analysis in line with published work such as that by Oli[69], Jenkins[63], Nobbs[68] and Uchida[153]. Further analysis was made of the kinetics of binding for the carbon coated sensor surfaces to demonstrate that rate constants can be used to examine the interactions even for undefined binding, so long as the rate constants are used as comparative values within the context of the study. This is in line with published work by Kawashima et al[75], as discussed in section 4.4.3. The successes and limitations of

analysing sensorgrams using BIAcore software model fitting to find these rate constants are also discussed in this chapter.

4.1. Initial BIAcore assay: poly-L-lysine functionalised surface

The poly-L-lysine functionalised surface was first used to determine a suitable regeneration solution for the surface after the addition of MR-1 cells, as described in the appendix. 1M NaOH was found to fit the requirements and was used to regenerate all the poly-L-lysine surfaces after cell injections by the injection of 10μL, or 30μL if the amount of cells on the surface was very large.

It was found that greater concentrations of bacteria in samples increased the net response, which was indicative of the mass attached to the surface after the sample injection had finished. Interestingly this increase was more apparent at the strongest salt concentrations. The highest difference in response due to concentration was at pH 7 for concentrations of 0.15M and 0.1M NaCl, for the weaker saline solutions the highest difference in response due to concentration was at pH 3 to 4.

Comparing the change in total response (in RU) with respect to pH for each saline solution, gives markedly different results for aerobically grown *S. oneidensis* MR-1, as shown in figure 4.1, and for the anaerobically grown bacteria, as shown in figure 4.2. It is worth pointing out that the highest average response for the anaerobic samples is almost twice as large as the highest for the aerobic samples at low pH values.

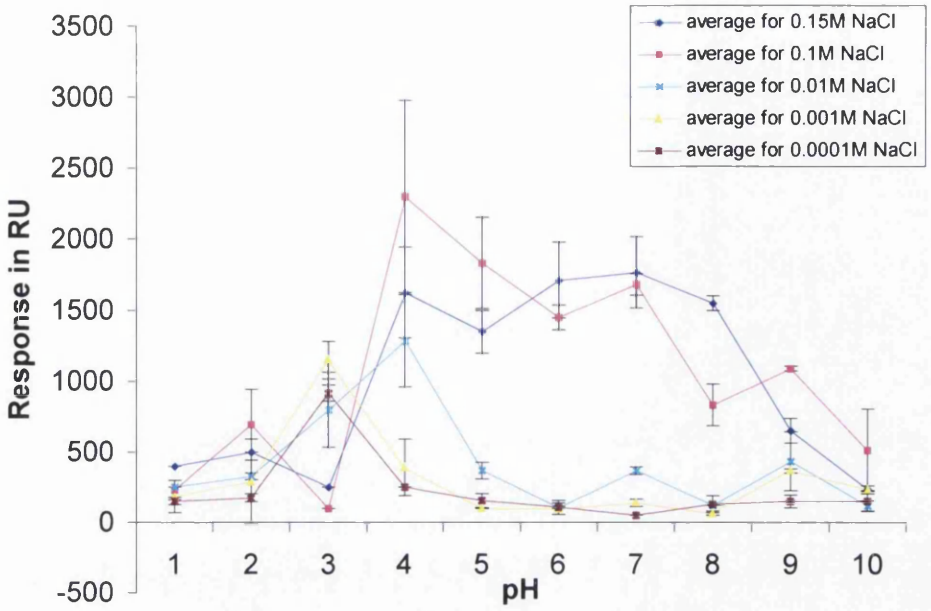

Figure 4-1: *Response in RU against pH for aerobically grown MR-1 cells, diluted by a factor of 5 in buffers of varying concentration of NaCl, using poly-L-lysine functionalised CM5 sensor chip. Errors shown are one standard deviation from the mean above and below the average.*

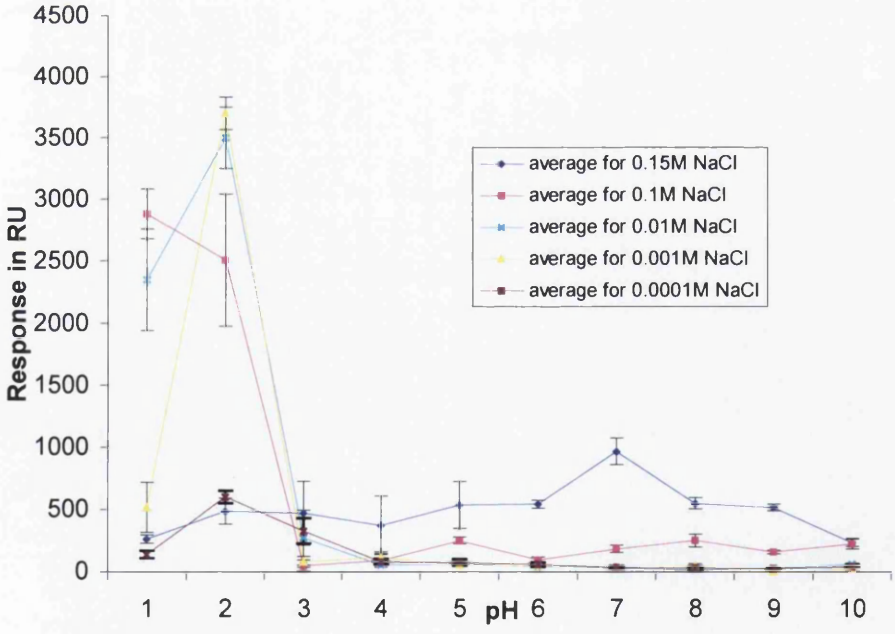

Figure 4-2: *Response in RU against pH for anaerobically grown MR-1 cells, diluted by a factor of 5 in buffers of varying concentration of NaCl as recorded on poly-L-lysine functionalised CM5 sensor chip. Errors shown are one standard deviation from the mean for each point.*

For the anaerobic there is a huge peak of response at pH 2 for NaCl concentration of 0.1M, 0.01M and 0.001M, and a smaller peak at the same pH for the lowest concentration. The strongest concentration, 0.15M NaCl, shows a distinct peak at pH 7.

The aerobic samples show a peak between pH 2 and 4 for all salinities. A second peak is apparent at pH 7 for 0.15M, 0.1M, and 0.01M solutions, and a third at pH 9 for 0.1M, 0.01M, and 0.001M solutions.

4.2. Age of culture assay

In this study a poly-L-lysine functionalised surface was used to compare the change in response due to injections of cells from the same culture medium over time. The age of the culture was measured as the time from inoculation. The study was undertaken for both aerobic and anaerobic cultures in order to compare the two. The change in response in RU is proportional to the amount of mass bound to the surface, and so a greater increase in RU from before the sample injection to after the injection means a greater mass bound to the surface. When comparing the aerobic and anaerobic samples taken over a 24 hour time period, as shown in figure 4.3, it is clear that the aerobic cells show a far greater variation than the anaerobic cells.

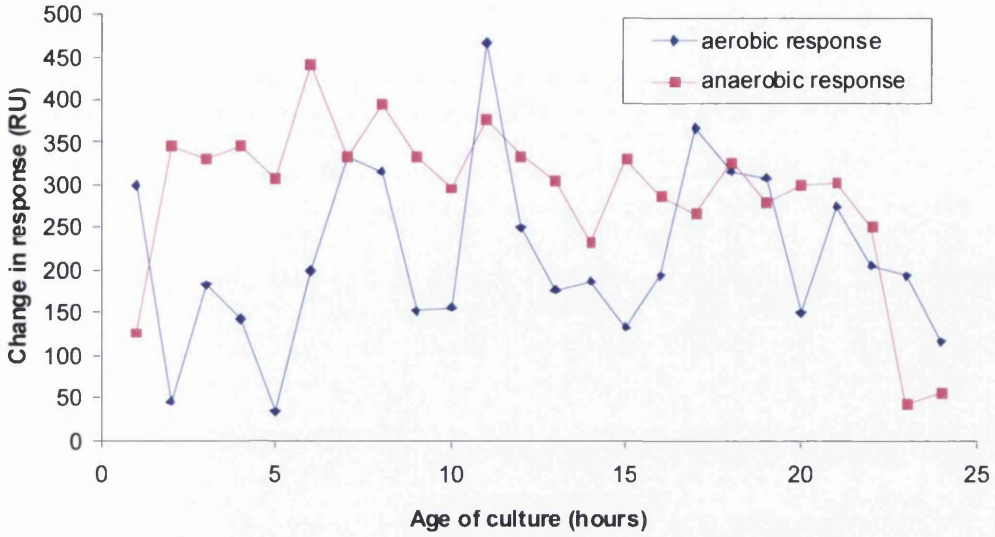

Figure 4-3: *Post-injection change in response (net change in response) in RU for cells from aerobic and anaerobic cultures over the age of the culture in hours.*

Looking at the aerobic and anaerobic studies separately, including errors of one standard deviation from the mean for each data point, this difference in variability is apparent in both the mean values and the variation (figures 4.4. and 4.5). Not only do the aerobic values vary more throughout the 24 hour time period but also the standard deviation from the mean also varies greatly, from less than 10% of the mean value (at t = 20 hours) to 155% of the mean value (t = 10 hours), with 11 data points having a standard error of over 50% of the value itself. The variability of results is the defining characteristic of the aerobic data for this study, with no trend discernable relating change in response with age of culture.

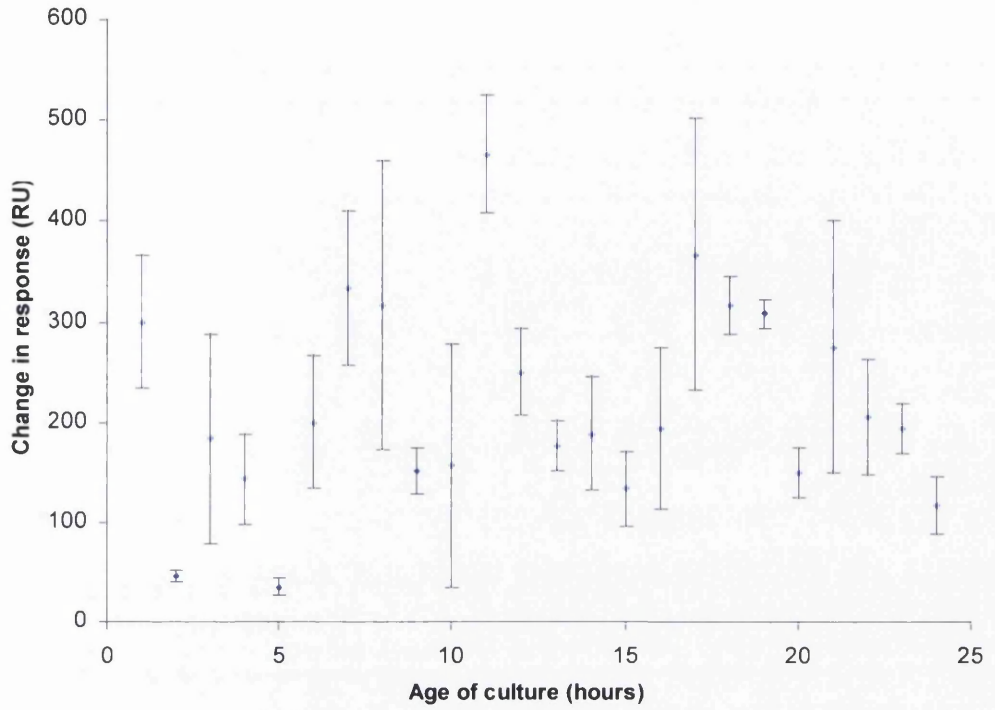

Figure 4-4: *Post injection response for samples of aerobically grown cells against age of culture with errors showing one standard deviation from the mean.*

When comparing the anaerobic study in figure 4.5 to the aerobic study in figure 4.4, there is clearly more regularity between results, and a lower average standard deviation. Only six values have a standard deviation of higher than 50% of the mean. In addition to this there is a trend which shows a jump in response from t = 1 hour to t = 2 hours, followed by a further increase around t = 6 hours, and then a gradual decrease until t = 22 hours, after which there is a sharp drop in response.

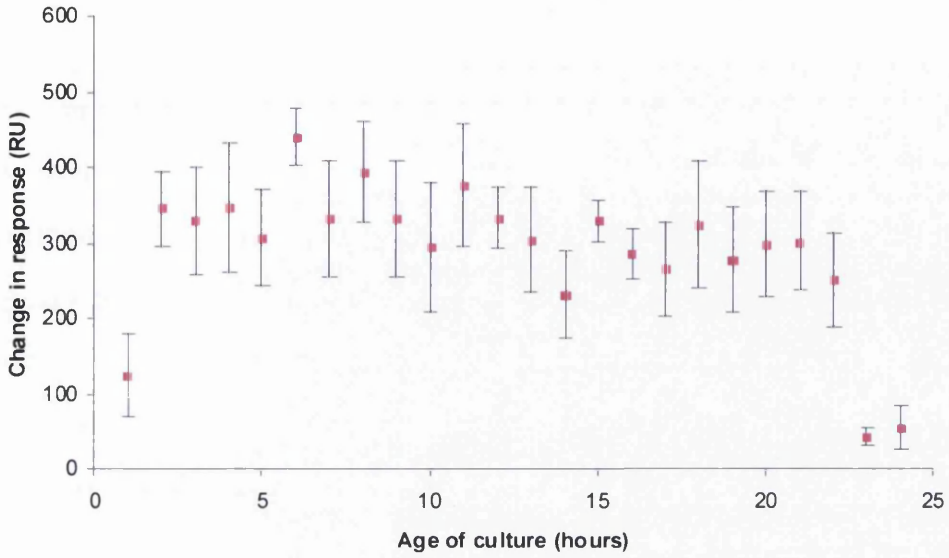

Figure 4-5: *Change in response after injection in RU for samples of anaerobically grown cells at different ages of culture with errors shown.*

The change in response after injection for the anaerobic samples is above 200RU after t = 2 hours and until t = 22 hours.

4.3. Carbon modified surface.

In order to approximate an electrode surface, sensor surfaces were coated with amorphous carbon. As a demonstration of this methodology this was sufficient, although future work in approximating electrodes with SPR sensors will require them to be coated with graphite to approximate graphite electrodes, or other materials specifically relevant to the process being investigated. The physical vapour deposition (PVD) approach was based on a similar approach in work by Lockett et al[154] rather than on the recommended surface immobilisation procedures embedded in the BIAcore control software. These programmed surface immobilisation procedures are based on coupling chemistries between organic and biological molecular species and have no established protocol for unusual surface preparation such as immobilising carbon. Instead the chip assembly kit (SIA Au kit)

available from BIAcore was used. In this kit the sensor surfaces are plain gold and are not yet mounted on the plastic frames used to handle the chips. In the same manner as Lockett et al, two plain sensor surfaces were coated with amorphous carbon using PVD to a thickness of 2nm and 10nm respectively. As a basis for comparison whole cell binding of *S. oneidensis* MR-1 to a plain gold sensor surface was also recorded.

In order to compare multiple injections of varying concentrations over the same sensor surface the resultant curves for each injection could be overlaid. The curves therefore needed to be normalised to starting at the same points in response (y-axis) and time (x-axis) so that they could be compared. This normalisation becomes more important when fitting curves for different concentrations simultaneously using the BIAcore software.

To adjust the curves in x and y for overlay comparison the following procedure was used.

Firstly the chosen sensorgram was selected, such as the one in Figure 4.6a. The first step, as for the sensorgrams in the previous sections, was to select and cut the parts of the sensorgram recorded during regeneration of the surface, as shown in Figure 4.6b. After this each curve is selected, cut, and re-pasted in a new colour so as to distinguish it from the other curves, as shown in Figure 4.6c. After this the curves are all normalised in time, x-axis, by selecting a starting point for the injection on each curve (Figure 4.6d). Once normalised in x, the curves can be normalised to the same starting response using the y-transform tool on the BIAEvaluation software, shown in Figure 4.6e. The baselines for all curves are highlighted at once and the average y-position calculated, which is then used as the starting point for all the curves. The final overlaid plot will look similar to Figure 4.6f.

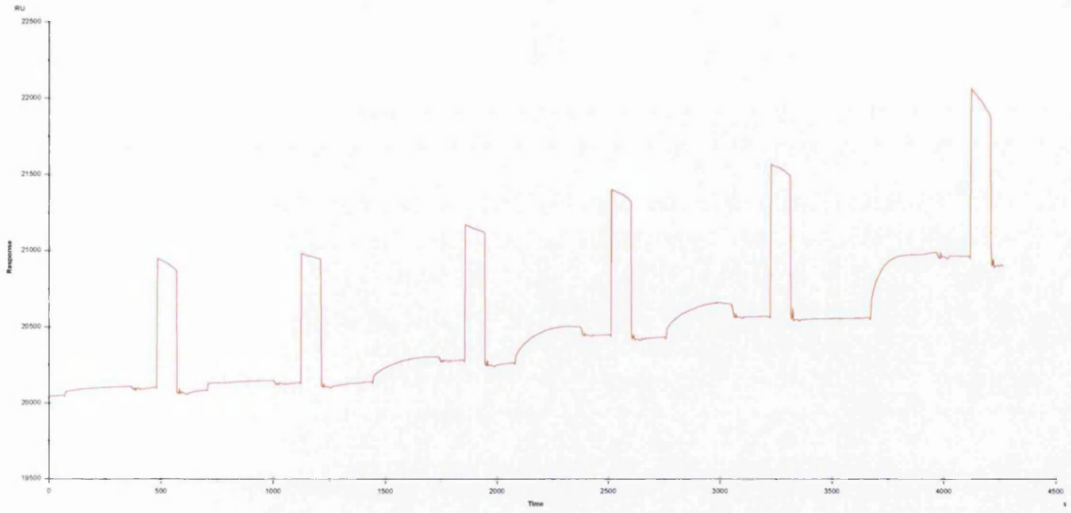

Figure 4-6a: *Sensorgram showing repeat injections over a surface increasing the concentration of the sample for each successive injection. The rectangular peaks represent regeneration of the surface. The sample used here is aerobically grown cells injected over the 2nm thick carbon sensor surface.*

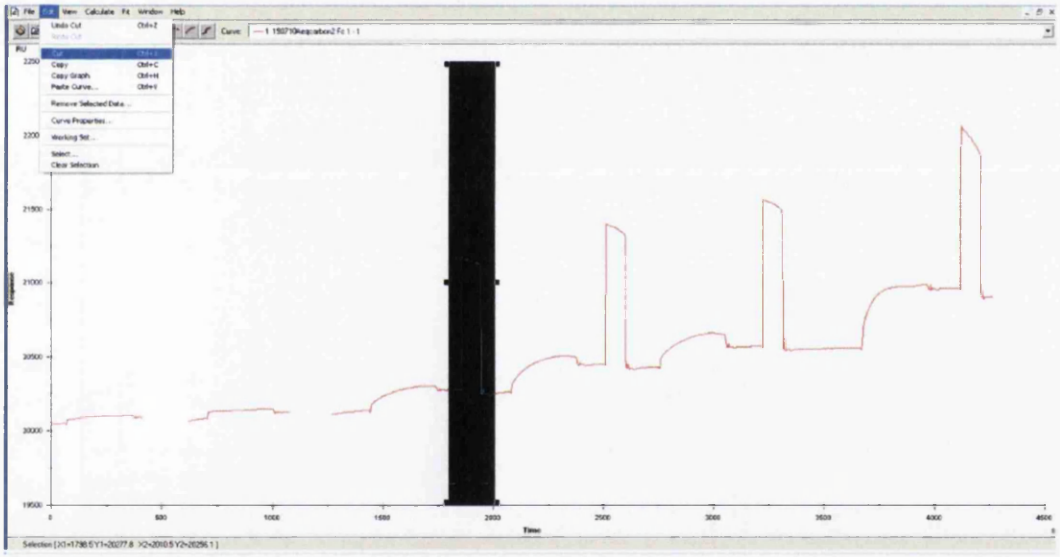

Figure 4.6b: *Highlighting and removal of regeneration signal from the sensorgram.*

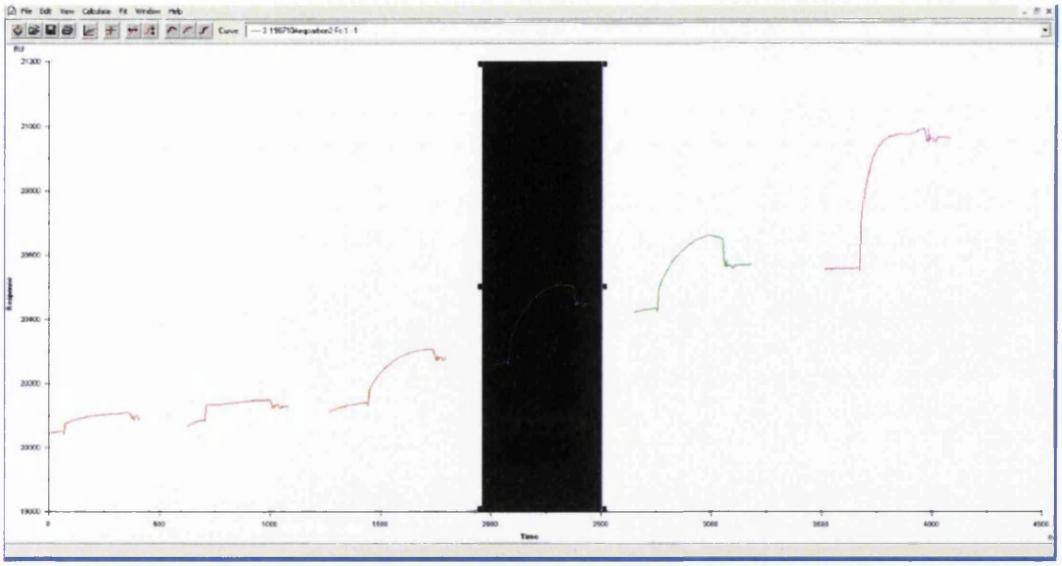

Figure 4.6c: *Selection and cutting of individual curves, followed by pasting in a new colour.*

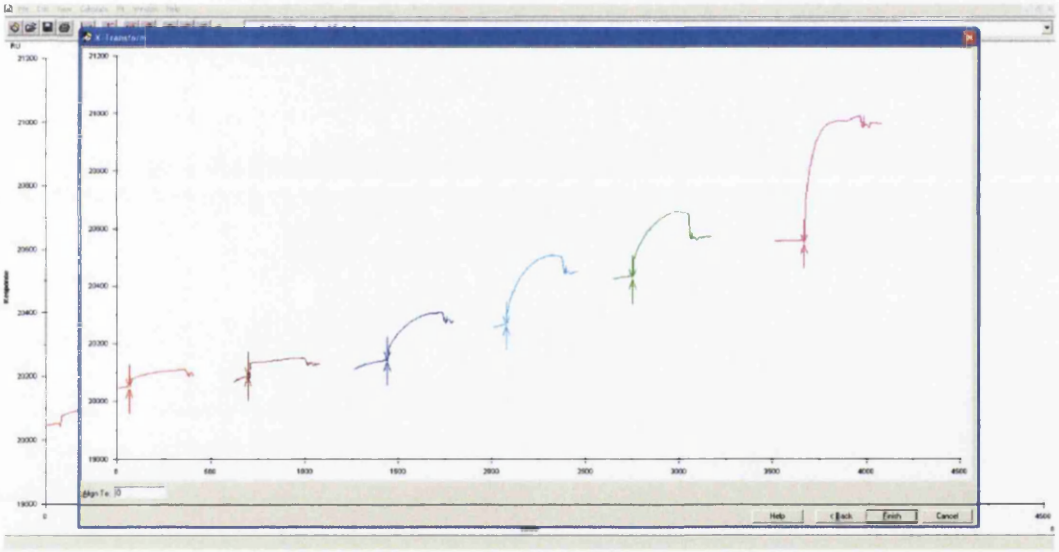

Figure 4.6d: *Crosshairs indicate starting point of injection on each curve, repositioning the crosshairs allows the user to change the position of this point. Once all are selected the curves are overlaid.*

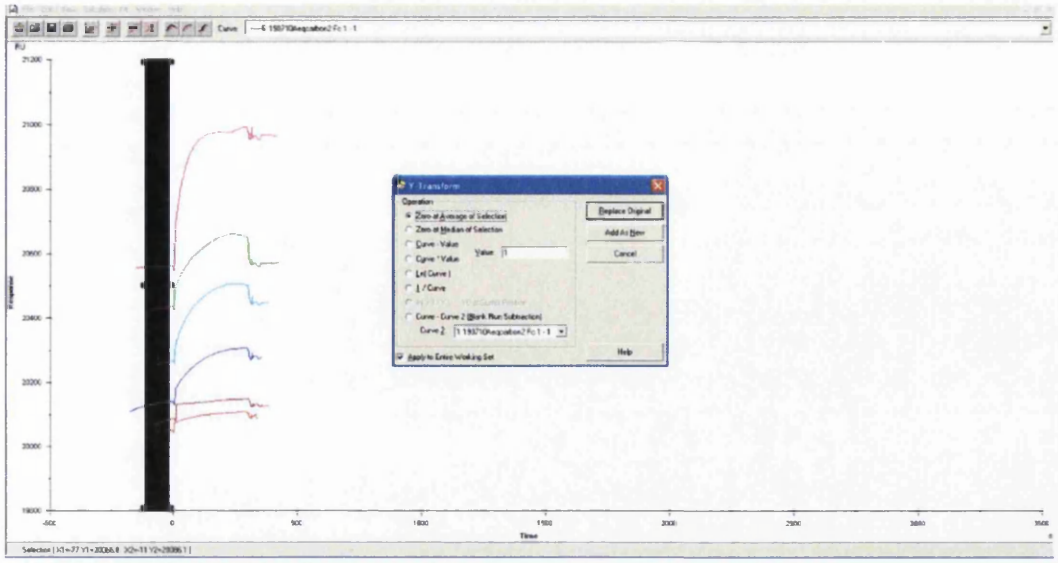

Figure 4.6e: *Y-axis normalisation: the baselines for all curves are highlighted and the y-position for all of them adjusted to the average.*

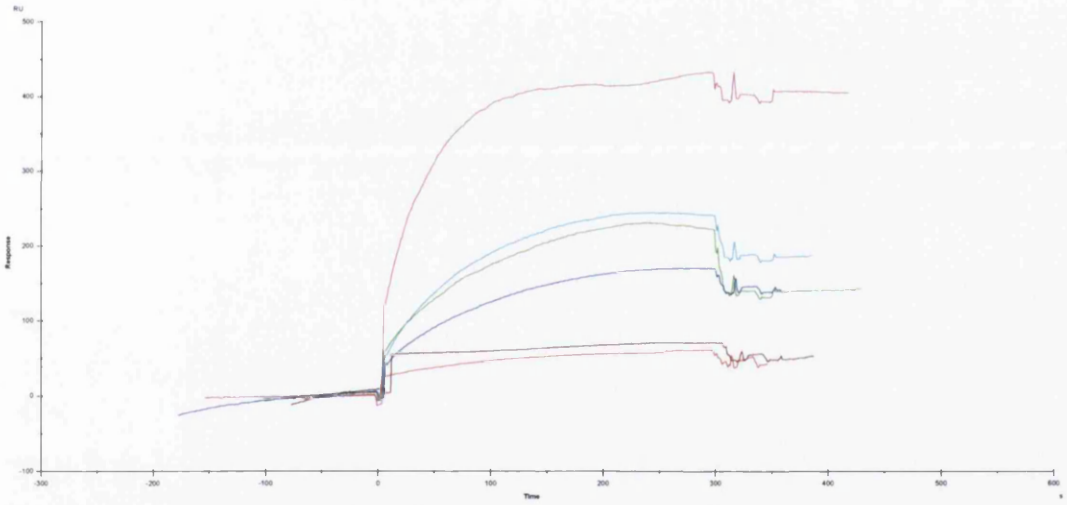

Figure 4.6f: *Resultant overlaid plot of curves taken at different concentrations.*

4.3.1. Plain gold sensor surface

Although the surfaces for the carbon-coated sensors were of uniform thickness, the binding of cells to a plain gold surface was briefly investigated for comparison. There is no reason to expect that the cells would not bind to the gold surface, however it is clear that the binding is different qualitatively from that of the cells to the carbon surfaces. The removal of cells from the

gold surface proved difficult, as the SDS solution used for the carbon-coated chips did not regenerate the surface consistently if at all, even though it had the best effect compared with the other recommended regeneration solutions that were tested: NaOH, EDTA, and ethanol, as described in the appendix.

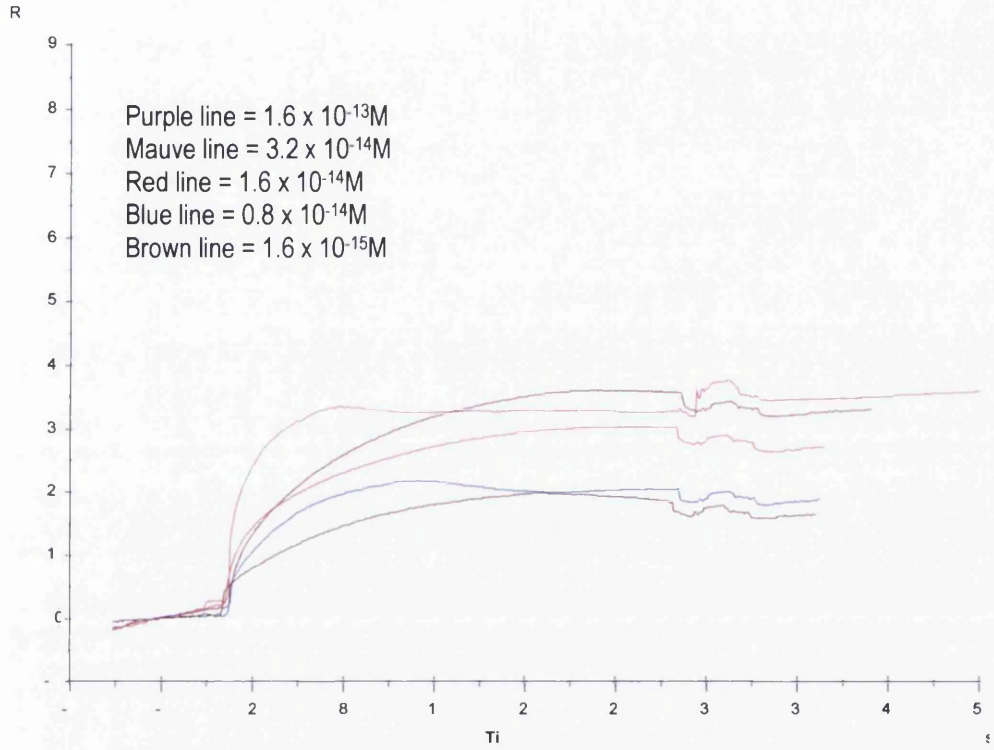

Figure 4-7: *Response against time for 100μL injections of aerobically grown cells over plain gold SPR sensor surface. The cells were injected at the same concentrations as for the carbon-coated sensor study.*

It is notable that the binding does not drop post injection, the cells are bound and do not dissociate once the injection is ended. This and the problems with regenerating the gold surface suggest that the cells may even bind more strongly to the gold surface, or to one another on the gold surface, than they do on the carbon-coated surface. The curves were fitted using the same model as for the carbon-coated surface. The fit was poorer for all concentrations than for the carbon-coated surface curves.

The interaction between the gold surface and the whole cells provides a comparison showing that the carbon-coated surface binding is distinct from, but not preferred to, the binding to the plain gold surface.

4.3.2. Carbon layers

In the work by Lockett et al, the aim of coating the sensor with amorphous carbon was to provide a substrate which would support DNA arrays, since arrays prepared on carbon-based substrates were known to be more stable than those on plain gold[154]. Amorphous carbon was used as it could be deposited at room temperature with no other changes to the sensor surface structure. The paper outlines that SPR measurements were taken to assess any effects on the sensor function due to the carbon layer, and it was found that although the carbon layer did not alter the gold film layer, a carbon layer of 7.5nm thickness (the thickness required for support of the DNA arrays) decreased the sensitivity of the sensor system by 42%, where sensitivity is defined as the maximum change in reflectivity as a function of the change in refractive index of buffer. The goal of the researchers in this case was to construct a surface with a DNA array in order to use SPR to measure binding to that DNA array.

In this study of whole cell binding, both aerobic and anaerobic cells were injected over the surfaces varying concentration of cells and the flow rate of the sample. In terms of simple net response after injection comparisons were drawn between aerobic and anaerobic cells, and between the two thicknesses of carbon.

The regeneration of the surface was the first problem. The BIAcore handbook suggests various possible regeneration solutions. Although 1M NaOH worked for the poly-L-lysine coated CM5 chips used in the previous experiments, it had no effect on the cells bound to the carbon. Other

recommended regeneration solutions were trialled (see appendix), to no avail. In the end sodium dodecyl sulphate solution (provided as part of the BIAcore maintenance protocol "desorb" to remove any bound biological material) proved to meet the requirements for regeneration for both aerobic and anaerobic cells on the carbon coated sensor chips.

In general, the lower the dilution (higher concentration) of the cells the greater the response measured, which is as expected. The response levels drop off rapidly from no dilution to a dilution factor of 100.

For the 10nm thick carbon sample the aerobic sample shows a faster drop in response than the anaerobic, with a response of around 230 RU at no dilution dropping to a response of 55RU at 5x dilution, with the lowest response being just over 10RU for 100x dilution.

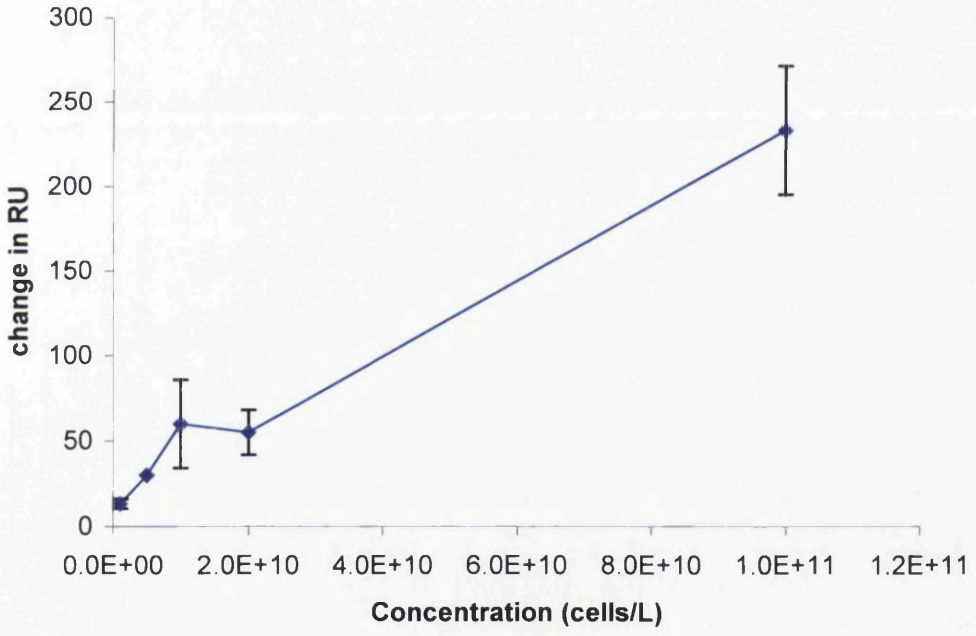

Figure 4-8: *Change in net RU against concentration of cell samples for aerobically grown cells in water using a sensor chip with a 10nm thick layer of amorphous carbon deposited onto a plain gold sensor surface.*

For the anaerobic sample however, the response has a maximum of 180RU decreasing to 140RU for 5x dilution and then decreasing more slowly to a low of 60RU for 100x dilution. The range of values for the change in

response for the anaerobic is 60-180RU, whereas for the aerobic it is 10-255RU.

Both sets of data show an increase in response from 5x dilution to 10x dilution, however as the error bars show, when the error is taken into account it cannot be said with great certainty that this is a feature of the concentration-response relationship, and an argument can still be made for the trend of decreasing concentration causing a decrease in response.

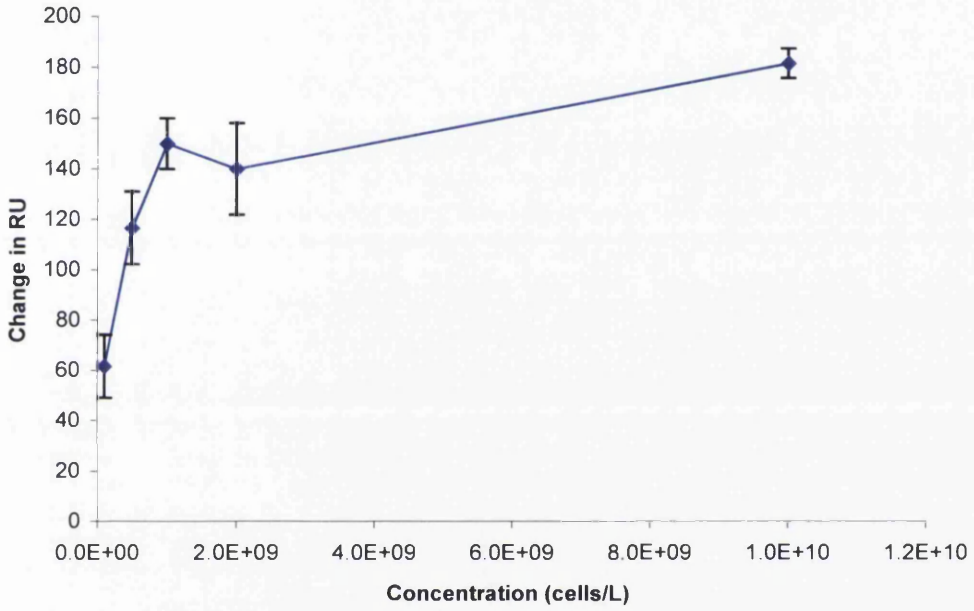

Figure 4-9: *Change in net RU against concentration for samples of anaerobically grown cells in water using a plain gold sensor chip prepared with 10nm thick layer of amorphous carbon.*

For the 2nm carbon surface the anaerobic cells have the same kind of response as for the 10nm surface, however the aerobic cells show a disparity with this pattern, with the maximum response being for the 10x dilution sample. The change in RU increases from no dilution to 5x dilution, to a maximum of 165RU for the 10x dilution, decreasing then down to 35RU for 100x dilution. By contrast the anaerobic samples go from a change in RU of 265 for no dilution, to 97RU for 5x dilution, then falling off more slowly to

40RU for the 100x dilution sample. The range of the anaerobic change in response is over one and a half times that of the aerobic change in response.

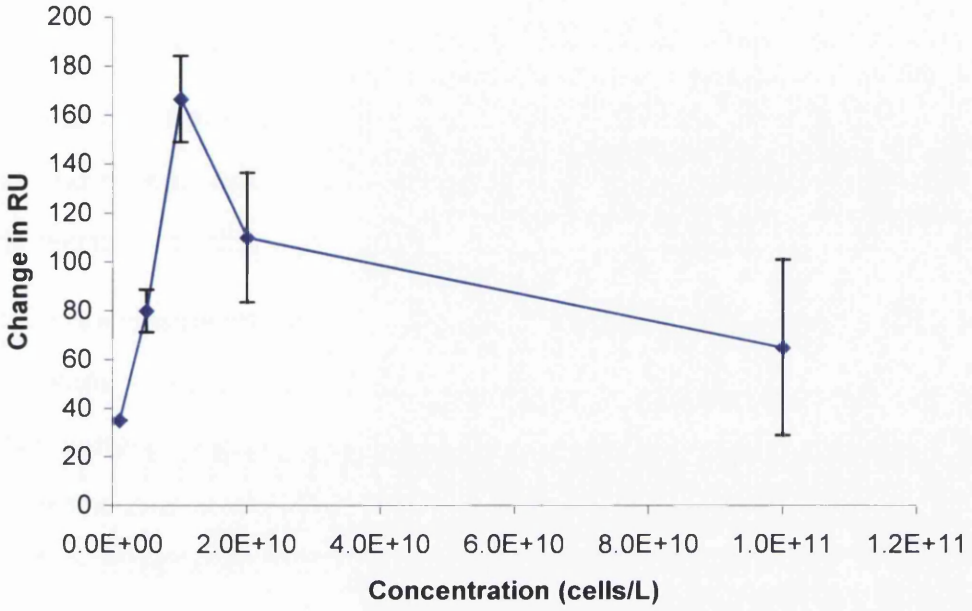

Figure 4-10: *Net change in RU for aerobically grown cells against concentration of cells in sample as measured on a plain gold sensor chip with a 2nm thick layer of amorphous carbon.*

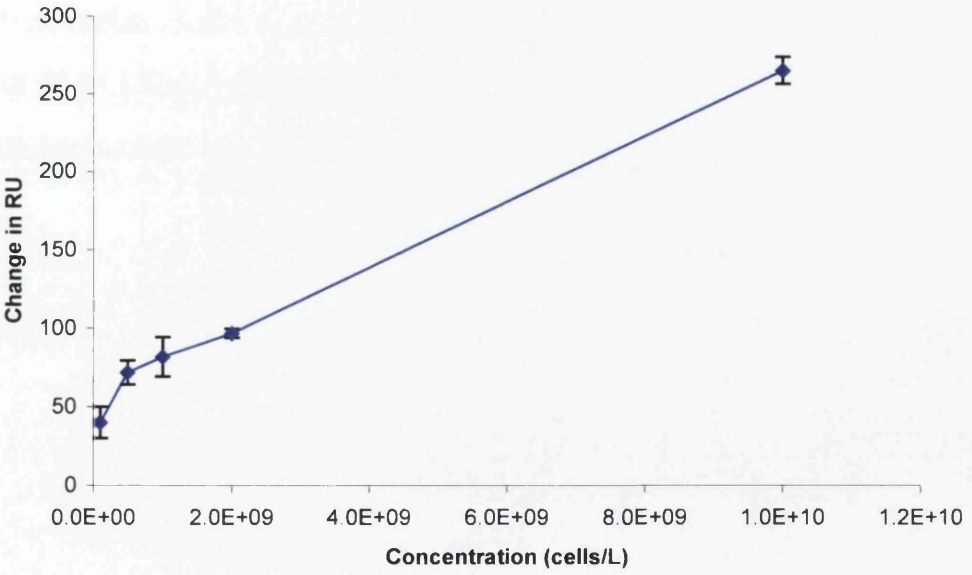

Figure 4-11: *Net change in RU for samples of anaerobically grown cells diluted in water and injected over 2nm thick layer of amorphous carbon prepared on plain gold sensor surface.*

As well as varying the concentration of the cells, the flow rate at which the sample was injected, and at which the running buffer was maintained, was varied from 3μL/min to 100μL/min. The net response left after the end of the injection was plotted against flow rate in order to compare the amount of cells bound (response) with respect to flow rate for each thickness of carbon layer and type of cells. The concentration of the cells was kept constant for each injection of cells.

Initially increasing the flow rate, from 5 to 10μL/min leads to an increase in the amount of cellular mass bound, for the aerobically grown cells on both carbon surfaces (figure 4.12 and figure 4.14) and for the anaerobically grown cells on the 2nm thick carbon surface (figure 4.15). The response for the first two flow rates is the same for the anaerobically grown cells on the 10nm thick surface (figure 4.13). As the flow rate increases to 30μL/min and then 50μL/min all cases show a decrease in response. Increasing the flow rate from 50μL/min to 100μL/min causes no change in response for either aerobic or anaerobic cells on the 10nm thick carbon surface. For the 2nm thick carbon surface there is an increase in response for the aerobic cell response from 50 to 100μL/min, and for the anaerobic on the same surface there is a decrease in response of a similar magnitude.

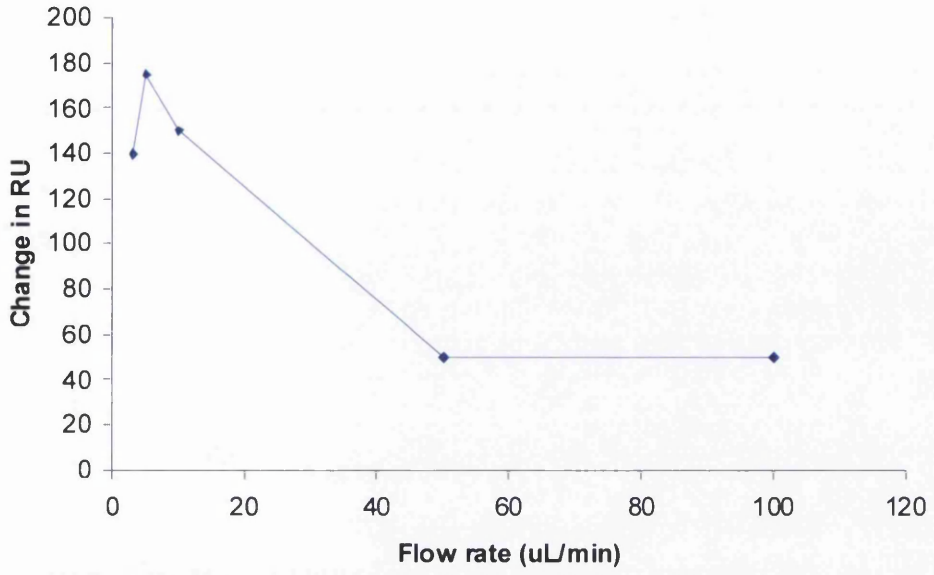

Figure 4-12: *Plot of response in RU against flow rate in μL/min for aerobically grown cells on a sensor with a 10nm thick carbon layer.*

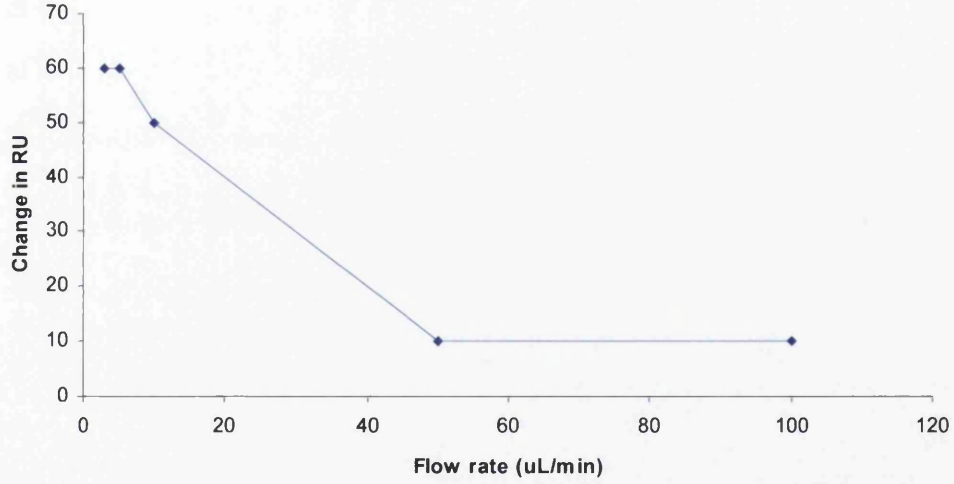

Figure 4-13: *Change in net response (RU) against flow rate (μL/min) for anaerobically grown cells on 10nm thick carbon coated surface.*

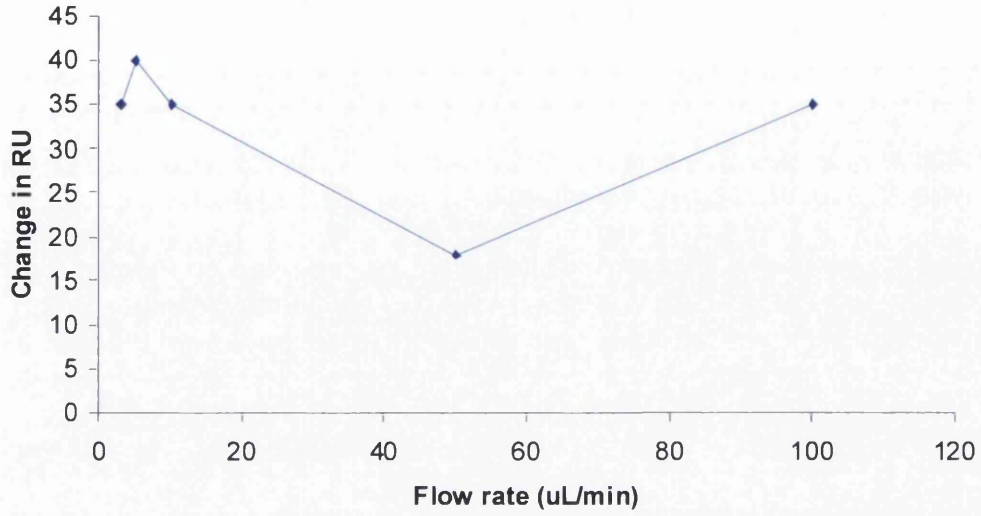

Figure 4-14: *Change in response in RU plotted against flow rate in μL/min for aerobically grown cells on the 2nm thick carbon layer sensor.*

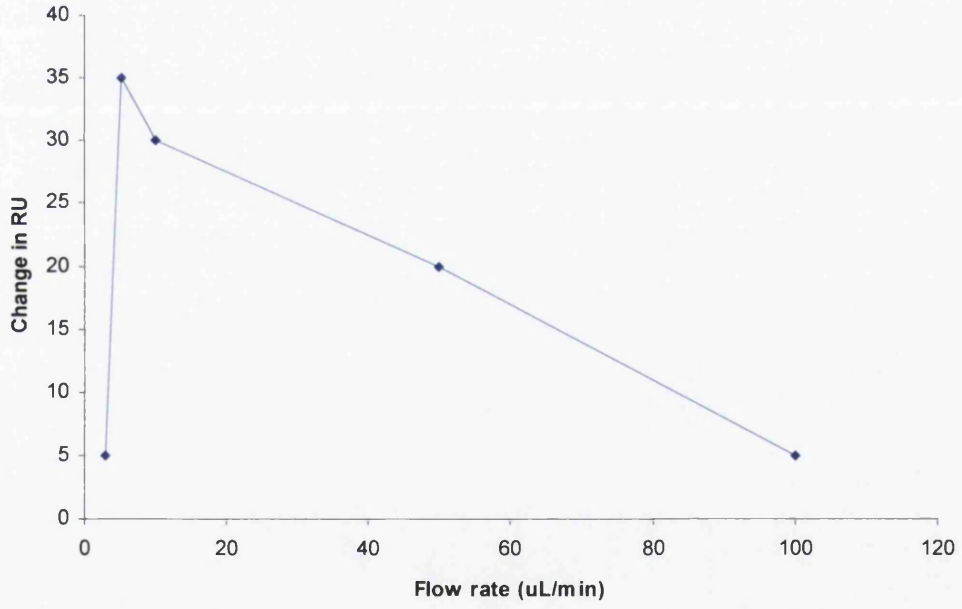

Figure 4-15: *Change in response from before to after injection for different flow rates using anaerobically grown cells and the 2nm carbon layer sensor.*

Unlike the other plots of net response against flow rate, the lowest flow rate increases net response in Figure 4.13. However the net response in RU is very low for all flow rates for the 2nm carbon layer sensor (maximum 40RU),

as shown in Figures 4.13 and 4.14 which means that any error in response levels will make a larger difference proportionally.

As well as the comparisons drawn above, by varying the flow rate for each combination of aerobic/anaerobic cells with the 2nm or 10nm thick carbon it can be seen that the binding rates are dependent on the flow rates, which indicates that the interaction is subject to mass transfer effects. This can affect the compatibility of binding models to the data, as will be discussed in the next section

4.3.3. Rate constants from BIAcore curves

The BIAcore Evaluation software allows the fitting of standard models to experimental data using the Marquardt-Levenberg algorithm which improves the fit of values for the model parameters by minimising the sum of the squared residuals, starting with initial values defined in each model.

$$S = \sum_{1}^{n} (r_f - r_x)^2 \qquad 4.1$$

In the above equation for the algorithm S is the sum of squared residuals, r_f is the fitted value at a given point and r_x is the experimental value at that point. Squaring the residuals ensures that deviations above and below the curve have equal weight in the fitting process.

The resultant values for the fit are based only on the mathematical process and it is for the user to interpret their relevance to the experimental reality. The simplest model for simultaneous fitting of k_a and k_d is a model describing 1:1 binding, based on the Langmuir isotherm for adsorption to a surface. The only input parameter required is the molar concentration of the analyte, A. The available binding sites are of a concentration B, which is zero when the response R is at R_{max}, that is to say when all the binding sites are

filled. When A binds with B a complex AB is formed (association), this complex can also decay back into separate components over time (dissociation). The rate equations for this simple 1:1 binding scenario are:

$$\frac{dB}{dt} = -(k_a \times A \times B) - (k_d \times AB) \qquad 4.2$$

$$\frac{dAB}{dt} = (k_a \times A \times B) - (k_d \times AB) \qquad 4.2$$

In this scheme k_a and k_d are the association and dissociation rate constants respectively. The total response is defined as AB+RI, where RI is the bulk refractive index contribution. The model gives rise to calculated parameters as well as fitted ones, including equilibrium affinity and dissociation constants K_A and K_D, the level of response for steady state binding R_{eq}, and the observed rate constant k_{obs} which is the slope of ln(dR/dt) against time t.

Other supplied models in the BIA Evaluation software include variants on the 1:1 binding model to take into account a drifting baseline or mass transfer effects, as well as models based around bivalent analytes, competing analyte reactions, and a system in which the complex AB can change conformation to form a new complex structure AB*.

The problem with fitting a model to the binding of cells to a surface is that the binding is not specific and it is also multi-valent. In using the pre-prepared models in the BIA Evaluation software the 1:1 with drifting baseline, and the 2-state (complex conformation change) model provided the best fits to the flow rate data when assessed separately. It is harder to get a good fit at the faster flow rates where the increase in response is very rapid and the duration of the injection is not very long.

The association constants of the aerobic cells on the 10nm carbon surface were very similar, as were most of those for the anaerobic cells although the association rate for the anaerobic cells at flow rate 50μL/min were an order of

magnitude higher than the others. The values of k_a as a function of flow rate are shown in figure 4.16. The consistency of the values of fitted parameters for both the aerobic samples suggests that the mass transfer effects are minimal, which was not expected. The anaerobic cells on the 2nm carbon layer show a steady increase in k_a with increasing flow rate.

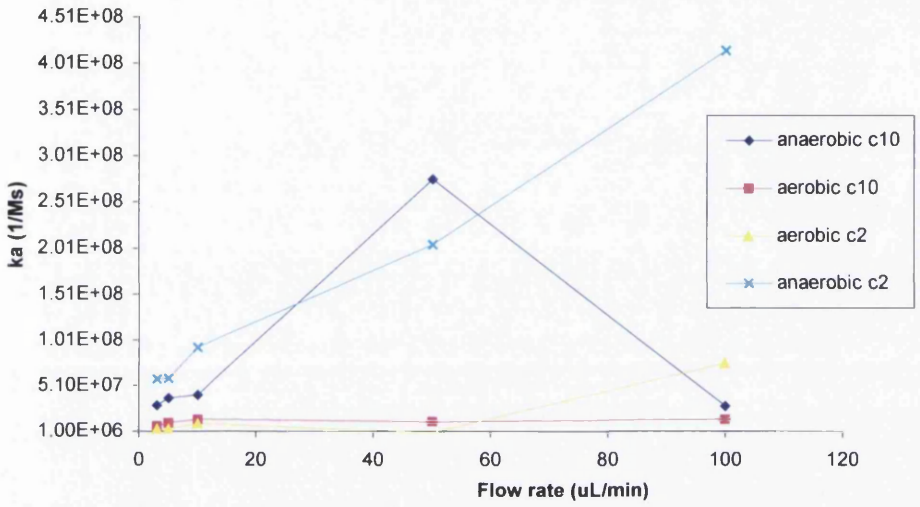

Figure 4-16: *Plot showing the association constant ka calculated using the 1:1 with drifting baseline model in the BIAcore Evaluation software for various flow rates for both aerobically and anaerobically grown cells on 10nm thick carbon (labelled c10) and 2nm thick (labelled c2) carbon sensor surfaces respectively.*

The maximum amount that can be injected into the system in one injection is 100μL, and so this maximum volume was the amount injected for each different concentration with the aim of achieving equilibrium during the injection at a flow rate of 20μL/min. The resulting sensorgrams could then be compared at equilibrium. The sensorgrams for each concentration for aerobic cells are shown overlaid onto one graph in figure 4.16 for the 10nm thick carbon coated sensor and in figure 4.17 for the 2nm thick carbon coated sensor.

In figure 4.16 the highest concentration of cells gives rise to the highest response, shown in purple on the figure. The shape of this curve is more rounded than those of the lower concentrations which show a levelling off

very soon after injection, although the height at which the curves reach some kind of equilibrium is greater as the concentration increases.

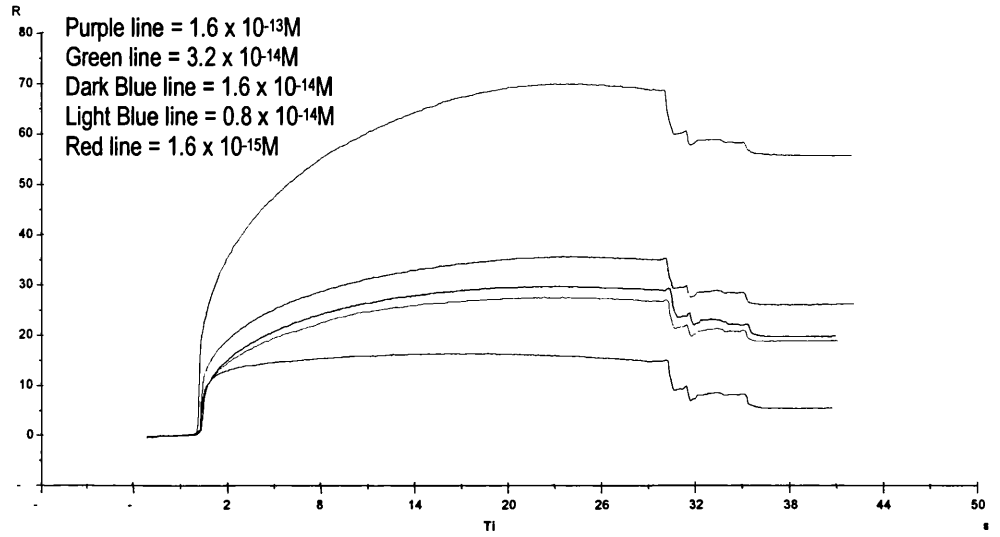

Figure 4-17: *Overlaid plots of different concentrations of aerobic cells binding to the 10nm thick carbon surface. The net response is higher for the highest concentration (purple line), decreasing with concentration. However, the curve shape for the different concentrations is also different.*

In order to fit parameters to the data in figure 4.16 simultaneously in order to obtain rate constants for the sample, rather than individually fitting rate constants to each curve, the 1:1 binding model with drifting baseline was adjusted by changing R_{max} from a globally fitted parameter to a locally fitted one. This is because the R_{max} for each curve is going to be different due to the variance in concentration. The fit was found to be better for the lower concentration curves, with the difference at the end of injection for the highest concentration curve being the most obvious disparity between fitted curve and experimental curve, as shown in Figure 4.18.

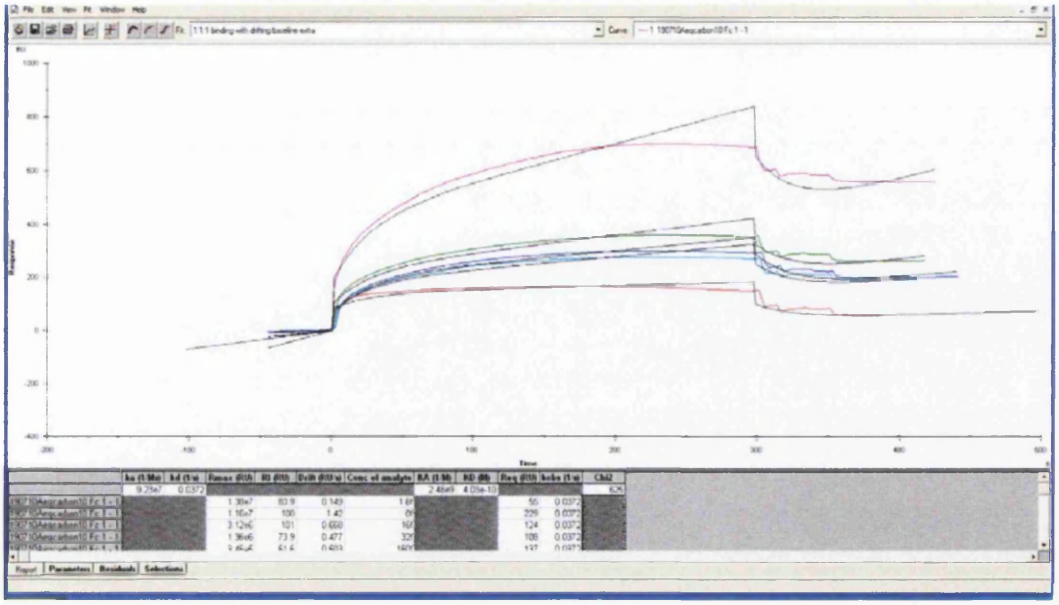

Figure 4-18: *Simultaneous ka and kd fit to curves for the same sample at varying concentrations using 1:1 binding with drifting baseline.*

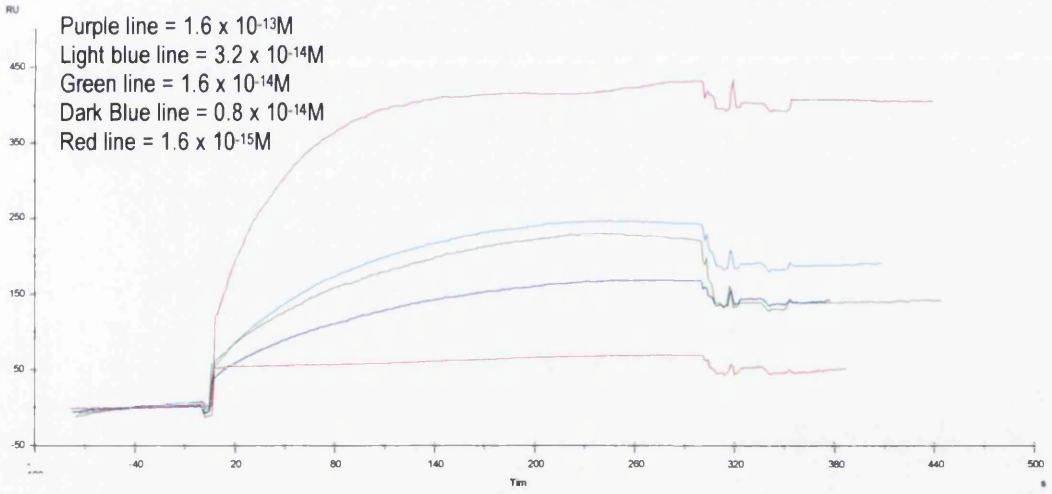

Figure 4-19: *Response against time for various concentrations of aerobic cells on the 2nm carbon sensor surface.*

Fitting parameters simultaneously to the aerobic cells on the 2nm carbon surface was conducted in the same way as for those on the 10nm thick carbon surface, despite the differences in the curves. Interestingly, the maximum response is higher for the thicker carbon layer, which can be seen just by looking at the scale of the y-axis on figure 4.19 compared with figure

4.18. The curves on the 2nm carbon surface show a marked change from rapid binding on injection (line rises vertically) to a steadily decreasing amount of new binding over time (curved part of lines). This is in contrast with the shape of the curves for aerobic cells taken on the 10nm thick carbon layer.

The two sets of curves for the anaerobic cells on 10nm and 2nm thick carbon (figures 4.10 and 4.21 respectively) also show differences in shape compared to one another although the difference in maximum response is smaller than for the aerobic cells. Changing the concentration has a greater effect on the binding of anaerobic cells to the 2nm carbon layer than to the 10nm carbon layer and there is very little drop in response after injection for the thinner layer suggesting that the anaerobic cells detected during injection are prevalently binding to the surface, rather than simply near it.

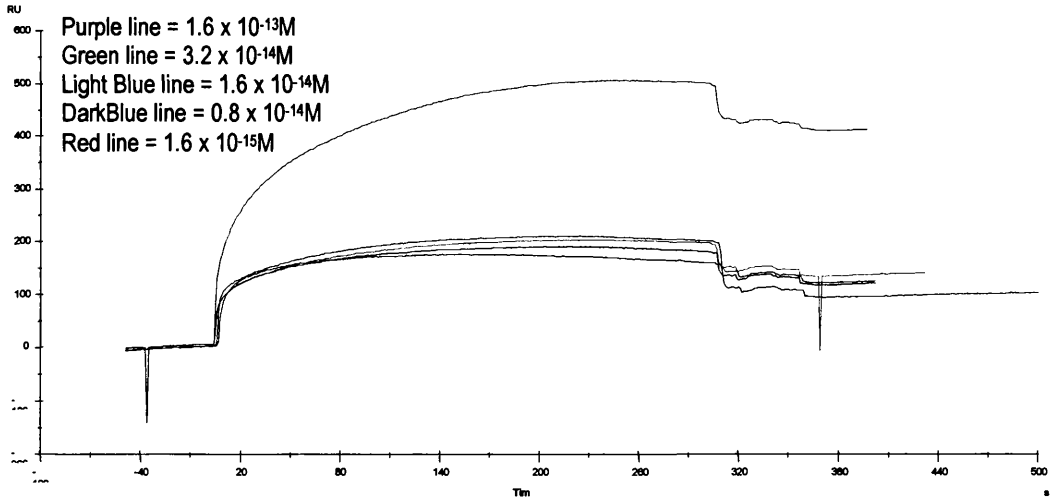

Figure 4-20: *SPR response against time for injections of increasing concentrations of anaerobic cells over a sensor chip with a 10nm thick layer of carbon. All concentrations show a similar level of response except for the strongest concentration, the non-diluted cell solution, which shows a much greater level of response.*

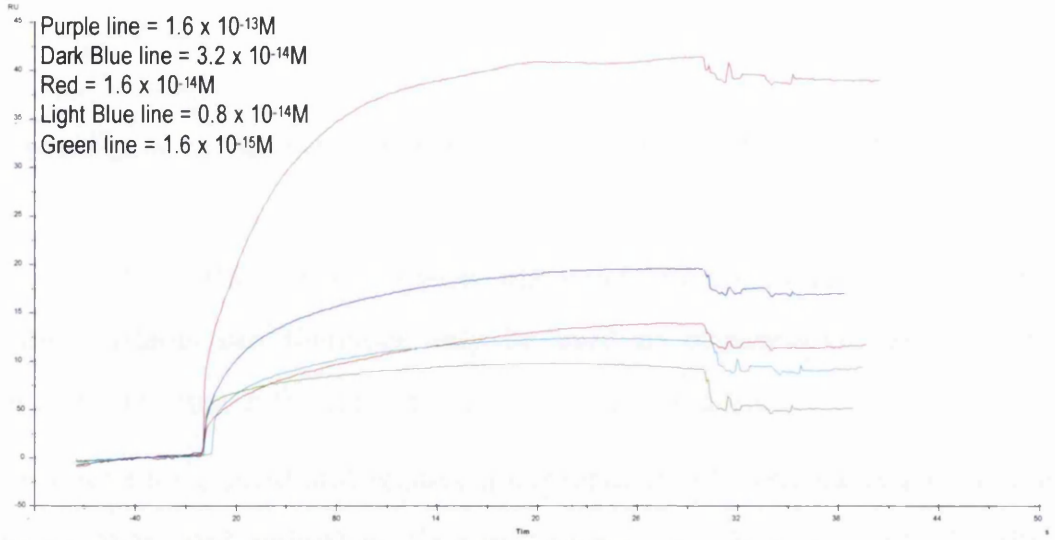

Figure 4-21: *Response against time for varying concentrations of anaerobically grown cells using the 2nm thick carbon layer sensor chip. The lower concentrations are not grouped so closely as for the 10nm carbon layer chip. The maximum response level for the highest concentration is similar, however the curve for the 2nm carbon layer chip is less smooth than that for the 10nm carbon layer chip. This is the same for the aerobic cells.*

The association and dissociation rate constants as well as the equilibrium association and dissociation constants were calculated for each set of data. As expected from the shape of the curves, the parameters calculated for both of the sample sets with anaerobic cells are very close to one another. The aerobically grown cells have a lower k_a on the 2nm carbon layer than on the 10nm carbon layer, however they have a similar k_d.

	10nm carbon layer		2nm carbon layer	
Parameter	Aerobic	Anaerobic	Aerobic	Anaerobic
k_a ($M^{-1}s^{-1}$)	$9.23x10^7$	$3.29x10^8$	$2.86x10^7$	$2.67x10^8$
k_d (s^{-1})	0.0372	0.0456	0.0346	0.0432
K_A (M^{-1})	$2.48x10^9$	$7.22x10^9$	$8.28x10^8$	$6.18x10^9$
K_D (M)	$4.03x10^{-10}$	$1.38x10^{-10}$	$1.21x10^{-9}$	$1.62x10^{-10}$

Table 4.1: *Fitted and calculated association and dissociation rates for cells grown aerobically and anaerobically as measured when binding to a plain gold BIAcore sensor with 10nm and 2nm coatings of amorphous carbon.*

The rate constant data provides a comparative measure describing the experimental curves numerically. However in the case of whole cells caution

must be exercised in apportioning significance to these parameters. The BIAcore system itself offers no way of understanding what cell constituents are binding to the surface unless an assay is conducted using different isolated cell surface components to confirm binding. The cell surface has a variety of molecular surface species that will interact with the substrate. The rate constants can therefore only be used as comparative values or to evaluate binding in the context of the cell-chip interaction.

This need for context and relative interpretation of kinetic parameters is the reason that many published BIAcore studies using whole cells only describe yes/no-binding assays, and do not investigate the rate constants involved. Even in studies of non-cellular material the kinetic analysis is sometimes neglected, for example in work by Takeuchi et al[64] which examines the binding of mucin to various polymers, the quantitative analysis simply comprised of comparison between percentage RU decrease after the injection of different adhesive polymers to remove mucin from the sensor surface. The rate constants are more directly applicable to specific monovalent binding however some kinetic analysis of the binding mechanism is still achievable and provides another method of comparison for different samples and substrates.

Even when kinetic analysis is undertaken it is presented with the caveat that these are the rate constants for an over-simplification of the binding process. Medina et al calculated "apparent rate constants" for the binding of antibody anti-*E. coli* 0157:H7 to pre-immobilised *E. coli* cells[76]. The rate constants were calculated at equilibrium and used to compare the effects of 3 different pHs on the binding of the cells to the surface during sensor chip preparation.

However, rate constants for whole cells have been calculated in work on oral streptococci by Kawashima et al[75]. In this study *S. mutans, S. sanguis* and *S. mitis* were injected over sensors functionalised with human salivary

components. The overall change in response for *S. mutans* binding to the salivary components was found to be approximately 106RU, a value of the same order as the changes in response found for *S. oneidensis* MR-1 on the carbon and plain gold surfaces and the poly-L-lysine surface, although at higher concentrations MR-1 showed net changes compared with that reported by Kawashima. However, *S. mutans* binding to BSA and mIgG was found to give lower changes in response of only 72RU and 45RU respectively, the latter being close to the lower end of net responses found with *S. oneidensis* MR-1 on the carbon surfaces. In comparison *E. coli* binding to galabiose surfaces studied by Salminen et al were found to cause maximum changes in response of 60 to 140RU[152], binding of wild type *S. gordonii* to salivary agglutinin reached a maximum change in response of around 200RU in work by Nobbs et al[68], and Uchida et al found changes of 350RU for *L. crispatus* cells binding to biotinyl polymer surfaces[153].

In order to calculate k_{on}, Kawashima determined the gradient of the graph of response against optical density, which was related to bacterial concentration, defining k_{on} as the increase in RU per single bacteria. For the bacteria *S. mutans*, *S. sanguis*, and *S. mitis* k_{on} was calculated to be 2.4×10^{-11}, 4.1×10^{-11} and 1.3×10^{-11} RU/cell respectively. The same parameter calculated for aerobic and anaerobic *S. oneidensis* MR-1 for each thickness of carbon is shown in table 4.2. The values of k_{on} were calculated using a line of best fit to find gradients for the graphs showing change in response against concentration in section 4.3.2. The fit was very good for the aerobic cells on the 10nm carbon layer, and for the anaerobic cells on the 2nm carbon layer but those for the other two cases were not so well fitted. The last data point (lowest concentration) was omitted from the fit for the aerobic cells on the 10nm thick carbon layer in order to get a usable fit.

	10nm carbon layer		2nm carbon layer	
Parameter	Aerobic	Anaerobic	Aerobic	Anaerobic
k_{on} (RU/cell)	$2x10^{-9}$	$8x10^{-9}$	$4x10^{-10}$	$2x10^{-8}$

Table 4.2: *Values of k_{on} calculated for aerobic and anaerobic cells on 10nm and 2nm thick carbon layers.*

The values of k_{on} for *S. oneidensis* MR-1 attaching to the 10nm carbon coated surface are two orders of magnitude greater than those for the oral streptococci attaching to salivary components in Kawashima's study. Those for the 2nm thick layer are also larger than those for the oral streptococci, by three orders of magnitude for the anaerobic, but for only one for the aerobic. As well as demonstrating a greater difference in k_{on} for the thinner carbon layer, this also suggests that the binding of *S. oneidensis* MR-1 to carbon is qualitatively and quantitatively different to that of *S. mutans, S. sanguis* and *S. mitis* to salivary components, with a greater change in response per cell. This difference is not surprising when considering the differences between the cells, streptococci are gram-positive for example, whereas MR-1 is gram-negative, but the two scenarios also differ in terms of substrate and so cannot be directly compared.

Kawashima uses the BIAcore evaluation software to determine k_{off}, which is described as kd and shown for *S. oneidensis* MR-1 in table 4.1. For *S. mutans, S. sanguis* and *S. mitis* k_{off} values are 0.0029, 0.0047, and 0.0035s^{-1}. The values recorded in table 4.1 are 0.0372, 0.0456, 0.0346, and 0.0432s^{-1} for aerobic and anaerobic cells with the 10nm and aerobic and anaerobic cells with the 2nm thick carbon layers respectively. The values for *S. oneidensis* are an order of magnitude higher for this dissociation constant as well.

Finally, Kawashima explores the ratio of kon to koff, with values of $8.2x10^{-9}$, $7.2x10^{-9}$ and 3.8x10-9 (RU s)/cell for *S. mutans, S. sanguis* and *S. mitis* respectively. The results of the same calculation for the *S. oneidensis* MR-1 cells under study in this chapter are given in table 4.3.

	10nm carbon layer		2nm carbon layer	
Parameter	Aerobic	Anaerobic	Aerobic	Anaerobic
k_{on}/k_{off}(RUs/cell)	$5x10^{-8}$	$2x10^{-7}$	$1x10^{-8}$	$5x10^{-7}$

Table 4.3: *Values of k_{on}/k_{off} for aerobically and anaerobically grown cells on sensor surfaces coated with a 10nm and 2nm carbon layer.*

Once again these values are larger than those found by Kawashima for the oral streptococcal strains binding to salivary components. It is more interesting, however, to see that the two aerobic results are of the same order of magnitude, whilst the two anaerobic results are one order of magnitude larger, showing a pattern not seen when looking at k_{on} and k_{off} separately.

4.4. Chapter summary

In this chapter there are two key areas of investigation that have been explored. The first is the continued examination of the differences between aerobically and anaerobically grown *S. oneidensis* MR-1. The second is the development of a method for measuring in real time the binding under specified flow of whole cells to inorganic surfaces.

Regarding the differences between aerobic and anaerobic MR-1, the BIAcore based assays have further outlined the physical and chemical variability of aerobically grown cells, contrasted with the relative uniformity of anaerobically grown cells. It can be inferred from this that the restrictions of the anaerobic growth environment require cells to conform to the anaerobic regime in order to survive, whilst aerobic cells are more varied. The aerobic cells, although grown in a shake flask, may not have equal access to oxygen[52] and therefore some of them may be more anaerobically active than others.

The use of amorphous carbon to approximate an inorganic surface using the BIAcore to detect binding is interesting, as it leaves the question of what

other material could be used in this way? The next step in further investigation of electrodes would be to use graphite. Beyond that there is the possibility of using metals, for example those which are susceptible to microbially aggravated (or inhibited) corrosion. Although binding can be assessed using other techniques, SPR requires minimal sample preparation for cells, does not require cells to be labelled, and also during the injection SPR is sensitive to mass near the surface, not just that which binds completely and remains after the injection. The potential for layering analytes including cells is also there to look at different interactions, which may not be possible with other methods.

5. Force Study characterisation of *Shewanella oneidensis* MR-1

Force spectroscopy has been used to study the mechanical properties of fixed and living cells[155, 156]. As discussed in the introduction, the shape of the approach and retract curves that constitute the force spectrum reflects the nature of the interaction between the probe and the surface. In this chapter the interactions between two different types of colloid probe and cells grown aerobically and anaerobically, each probed in water at pH 7 and in a weak salt solution at a pH corresponding to the relevant isoelectric point determined in Chapter 3, are compared. The key elements of interaction under study are the snap-in force when the probe approaches the surface, the adhesion force when the probe is retracted from the surface, and the indentation of the cell surface from which the Young's modulus of the cell can be calculated.

To study indentation requires using the piezo movement and the cantilever deflection measured on a soft sample as well as on a hard surface (usually glass) for a reference curve[104]. The point at which the tip is in contact with the surface is considered to be at a tip height of zero. Should the tip continue to move into the surface after this point it is considered to be indenting the sample. The indentation depth is therefore calculated as the tip height (which will be less than zero) minus the cantilever deflection for the sample, minus the deflection at the same height on the reference curve. Once indentation is calculated the Young's modulus can be worked out by relating the indentation to the modulus according to established models, such as Hertz. Although there is precedence in the literature for using the Hertz model to interpret indenting force spectra on bacterial cells, there are arguments for the use of variant models, and as ever such models must be interpreted in relation to the physical reality of the force interactions. In 2005

Butt et al published "Force measurements with the atomic force microscope: technique, interpretation and applications"[157]. This work is a comprehensive summary of the underlying theory involved in force spectroscopy as well as reviewing experimental approaches.

The Hertz model is used in many studies of bacterial cells, although cells do not meet the original criteria for the model since it assumes a homogenous deformable flat surface and a rigid indenter. Despite this, Hertz is a useful approximation if the probe used is much stiffer than the sample and so it is often used in comparative studies, and has become the default model in much of the literature. Hertz also assumes that the effect of adhesion forces is negligible, and is not suitable for modelling interactions where adhesion forces are large. For a spherical probe Butt[157] gives the following equation in summary of the model:

$$F = \frac{2E\sqrt{R}}{3(1-\nu^2)}\delta^{3/2} \qquad 5.1$$

Where E is the Young's modulus, R is the radius of the spherical probe, δ is the indentation, and ν is the Poisson's ratio, assumed to be a value usually between 0.3 and 0.5, with the latter being more commonly used for cells[157]. The Hertz model has been developed for other geometries such as a parabolic tip or a conical tip, and much of the literature will term these alternate versions as part of the Sneddon approach. Other authors refer to any of these models simply as Hertzian.

For a parabolic indenter[103, 114, 158] with R as the radius of curvature:

$$F = \frac{4E\sqrt{R}}{3(1-\nu^2)}\delta^{3/2} \qquad 5.2$$

For a conical indenter[158] with a half opening angle α:

$$F = \frac{2\tan\alpha}{\pi(1-\nu^2)} E\delta^2 \qquad 5.3$$

All Hertzian models assume that the any adhesion forces are negligible in comparison with the maximum loading force. When there are large adhesion forces it is necessary to use a model that encompasses the effect of adhesion, such as JKR theory. JKR is applied to scenarios with softer samples, large probes and large adhesion[157].

Interactions between *S. oneidensis* MR-1 and a mineral have been observed through probing a mineral surface with a cell-coated probe by Lower et al, publishing their findings in 2001[48], and in a later paper by Lower where the *S. oneidensis* MR-1 results were compared with analogous results for *E. coli* K12[47]. The mineral used in these studies was goethite, a naturally occurring iron oxide-hydroxide with the formula FeO(OH). The presence of the Fe(III) ion in goethite was the reason for using this mineral, as these studies had the aim of demonstrating that MR-1 would recognise the Fe(III) ion and adapt its metabolism to suit electron transfer pathways resulting in the reduction of Fe(III) to Fe(II). When comparing the interaction between the goethite and a probe functionalised with cells of MR-1 it was found that forces of adhesion were stronger between the mineral and cells in an anaerobic environment. Lower's conclusions were that when the oxygen pathway is removed the electron transfer from cell to mineral is the main pathway and the cells develop greater affinity for the mineral. The interaction between the *E. coli* cells and goethite were described by Lower as non-specific, compared with a specific bond between *S. oneidensis* and goethite.

5.1. Plain tip

In order to gain insight into possible problems with force spectra in liquid using cell samples an initial study was conducted using a plain silicon contact tip (Park Scientific, model ULCT-NTHW, Park Systems, Leatherhead, Surrey). The cantilever was thermally tuned in air to determine the spring constant, using the force spectroscopy calibration tool in the JPK operating software. A force spectrum was taken on a clean glass cover slip securely fixed to a glass slide and the spring constant calculated. This calibration was required whenever the chip was replaced or moved as its position on the holder affects the values obtained.

For the following results the sensitivity was 60.05nm/V and k=0.21N/m. From these values the deflection was converted from volts (V) to newtons (N), and thus the resulting curves showed data in terms of force, rather than deflection, against distance.

With the plain tip it was possible to image the surface clearly before proceeding with the force spectra. Thus the force spectra targeted specific sites on the surface. The sample investigated was a suspension of aerobically grown cells, harvested at 20 hours growth, and air dried onto a clean glass coverslip overnight, imaged in pure water. In a 25μm area there were about 20 whole cells, of which 4 were solitary or just barely touching other cells.

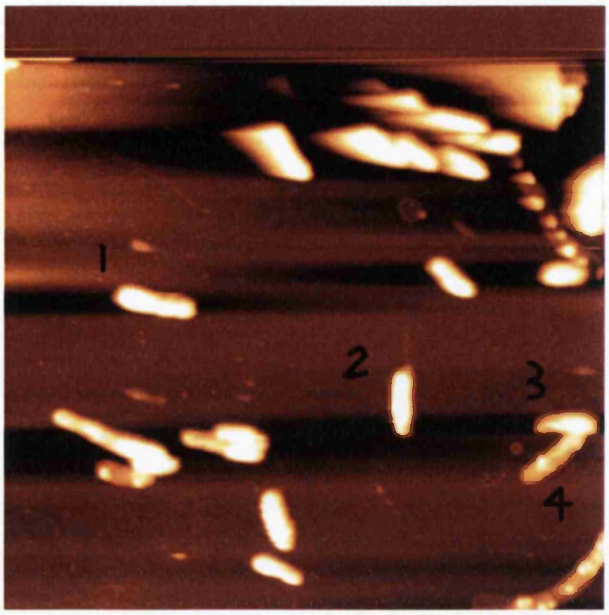

Figure 5-1: *25μm by 25μm AFM image using plain tip to image aerobic cells in water. The tip came away from the surface for the lines at the top of the image, which was a problem when imaging in liquid. The cells in this image that were probed using force spectroscopy are numbered 1 to 4.*

On this sample, on a part of the surface away from any cells, there was no snap-in force. On retract there was a maximum attractive force of 15nN. The approach and retract curves matched in the contact regime. Although this site appeared to be on a "clean" part of the sample surface it is possible that extracellular material was present there causing adhesion on retraction.

Curves taken on cells showed a difference between the approach and retract curves in the contact regime: a "loading-unloading hysteresis"[157] implying some deformation of the cells. Figure 5.2 shows an example of this hysteresis. In this plot of force against distance there is no force on the approach until the contact regime, followed by a linear increase in force. However on retraction from the surface the decrease in force is not linear, and as the curve moves past the contact point it does not return to the baseline force of the approach curve.

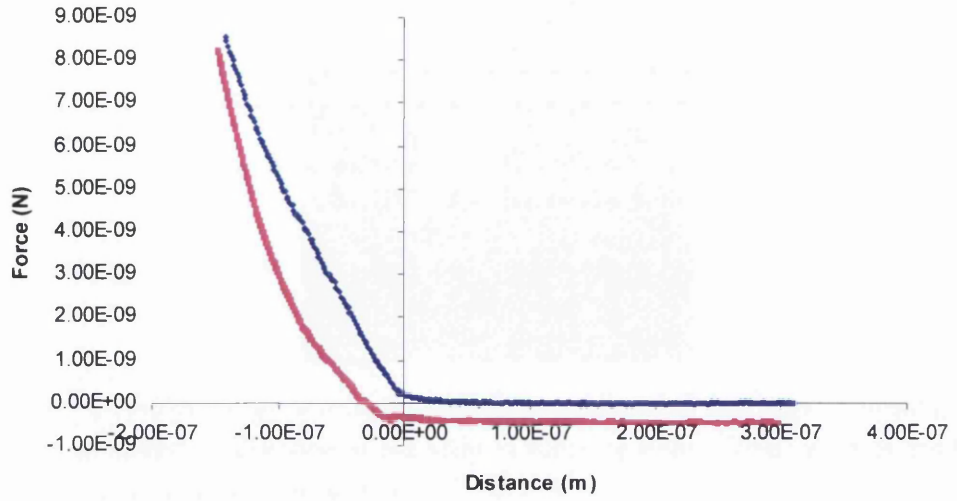

Figure 5-2: *Plot of data points for interaction with loading force of 7nN showing loading-unloading hysteresis between approach (dark blue) and retract (purple) phases of interaction. Plot generated in Excel using raw data exported from JPK Nanowizard software.*

The adhesive force for a load force of 1nN was 0.1nN, an order of magnitude less than the adhesive force on cell-free parts of the surface; there was no snap-in force for any of the cells. Successive curves were taken increasing the force up to 11nN, in general showing a decrease in adhesive force and an increase in difference between the approach and retract curves. This suggests that repeated force spectra of increasing load force on the same site deformed the surface, damaging or removing the source of the adhesive force. In one extreme case a particular cell was re-imaged after unusual force data in which the force spectra taken at the centre of the cell were found to match exactly with the reference from a cell-free site, and it was found to have been removed during the force study, leaving an outline of material behind, as shown in figure 5.3 below. This dislodging of the cell was certainly due to the action of the AFM tip.

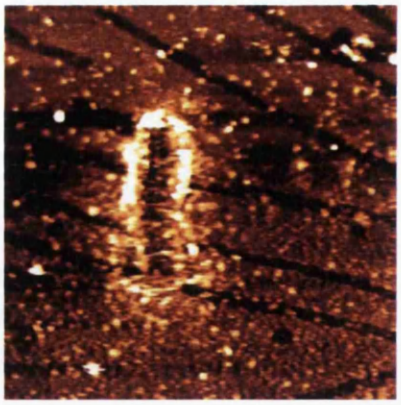

Figure 5-3: *AFM image of cell site after force spectra, cell has been removed leaving outline of material. The size of the scan is 6μm by 6μm. This cell was visible in figure 5.1 marked as cell number 2.*

5.1.1. Young's modulus

The Young's modulus for the plain tip probe was calculated for comparison with the values measured for the iron oxide and graphite probes, in sections 5.4 and 5.5.2 respectively. For the plain tip the Hertz model for a conical indenter was used, calculating the Young's modulus from a plot of the force against the indentation to the power of δ^2.

The modulus was calculated for the aerobic cells in water only, and was found to be 25.4 ± 3.3 kPa for the one cell site investigated. This initial value was obtained in order to have a baseline figure with which to compare the mineral probe results.

5.2. Iron oxide colloid probe

When using the iron oxide probe or the graphite probe imaging of the surface prior to conducting force spectroscopy was difficult. The resultant images, such as those in Figure 5.4 below, showed no discernable details of individual cells on the surface, although there were sites on the surface that were clearly higher topographically due to groupings of cells, as expected

from looking at the images taken with sharp tips described in chapter 3. This problem was due to the radius of curvature of the probes with respect to the size of surface features (e.g. probes of 5μm diameter compared with cells of 1-3μm in width/length) and required the resulting force data to be carefully considered to identify curves on cells as distinct from those on the background.

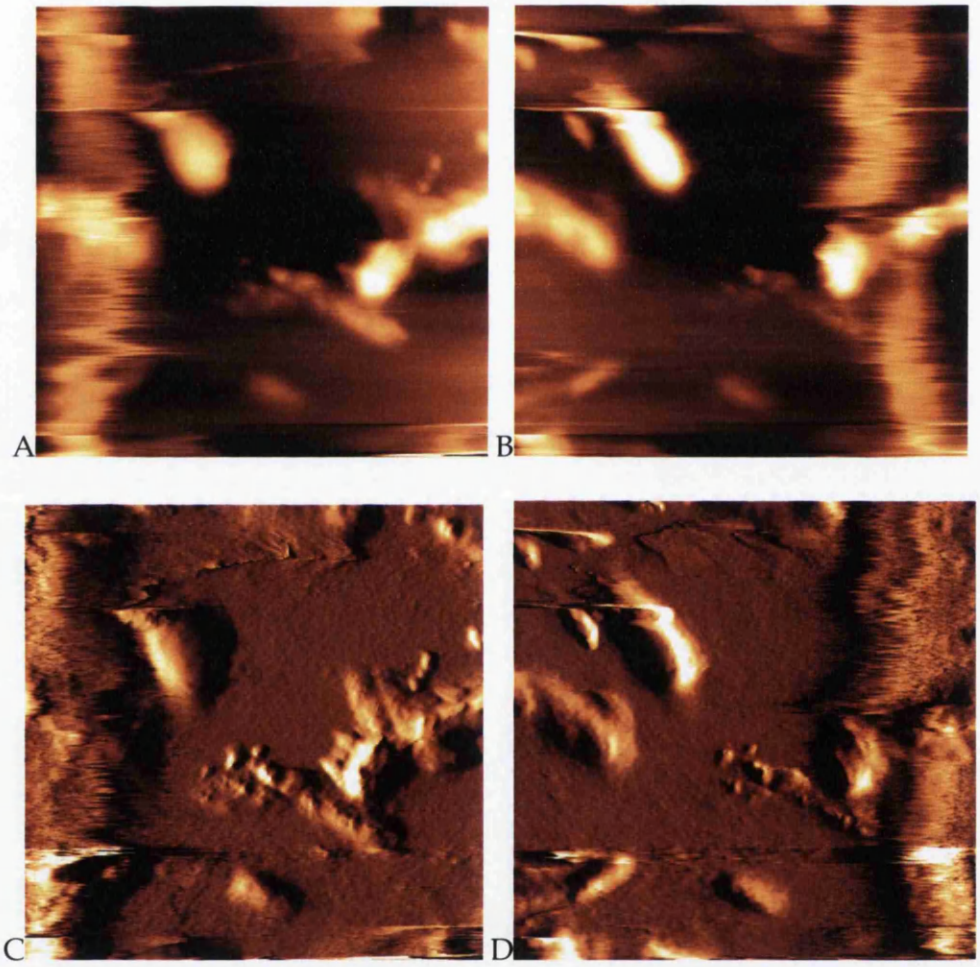

Figure 5-4: *10μm by 10μm scan of surface using iron oxide probe images generated using trace (A) and retrace (B) data. Groups of cells are discernible as raised areas however comparison of trace and retrace shows artefact (right hand side of A, left hand side of B) as distinct from cell groups. Comparison of trace and retrace as well as error signal images(C and D) were used to differentiate between such artefacts and areas of raised topography, assumed to be cells. In these images the cells are anaerobically grown and the liquid is water.*

Figures 5.5 and 5.6 below show force spectra for aerobically grown cells in water and salt solution respectively, as acquired using an iron oxide probe. The contact point is harder to determine for the curve taken in water, suggesting a soft contact with the cell on approach.

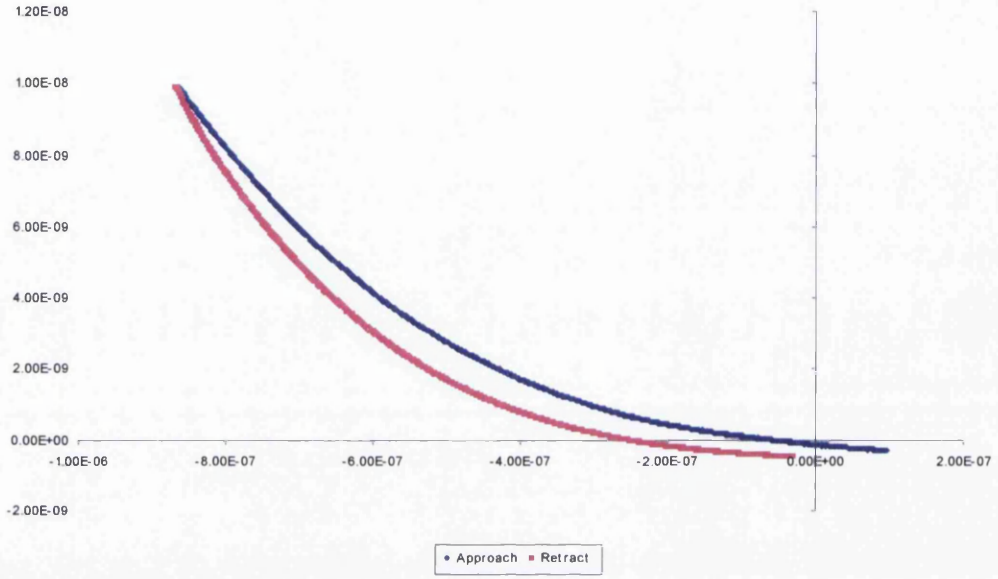

Figure 5-5: *Force spectrum for aerobically grown cells probed in water at pH 7 by an iron oxide probe.*

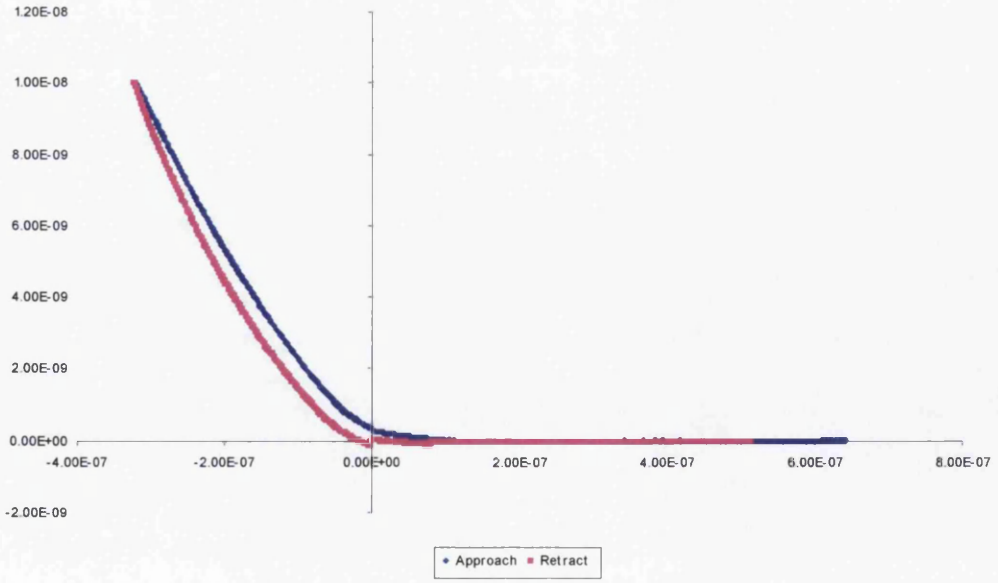

Figure 5-6: *Force spectrum obtained using an iron oxide probe with aerobically grown cells in low salt solution at pH 3.5.*

The next two figures show spectra for the anaerobically grown cells taken using an iron oxide probe. The spectrum for the cells in water shows a jagged retract profile typical of multiple adhesion forces being overcome. The forces in this spectrum and others from the same site on the sample are larger than for any other on this sample, and yet not the same as spectra taken on glass, which have one large adhesion event. The average adhesion to cell sites for this sample is lower than measured from this spectrum however adhesion to this sample is the highest for all the sample-environment combinations, as discussed in the next section. The force spectrum for the anaerobically grown cells in the salt solution is very similar to that taken in water, although with less adhesion and a repulsive effect when nearing the contact point on the approach curve.

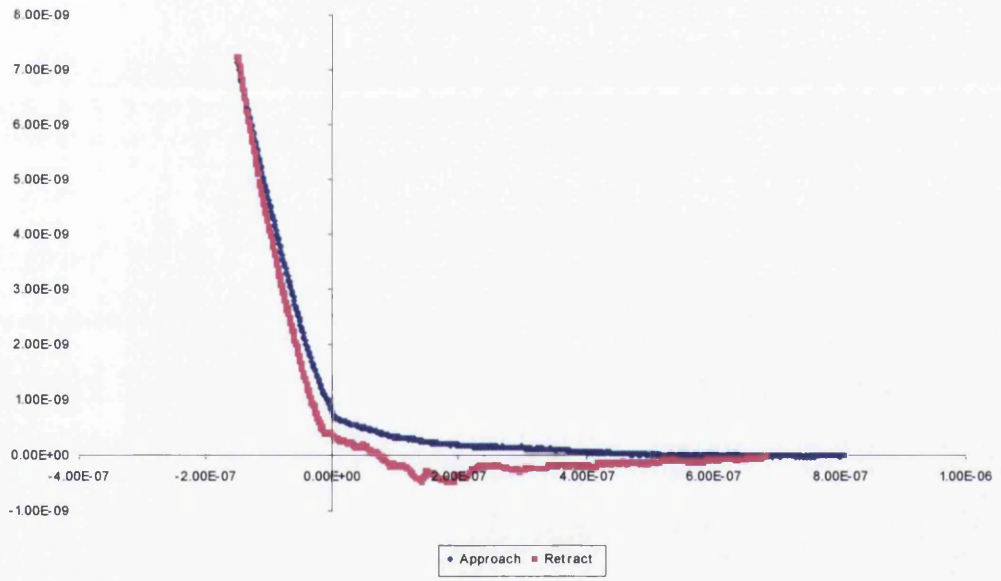

Figure 5-7: *Force spectrum obtained for anaerobically grown cells in water at pH 7 using an iron oxide probe*

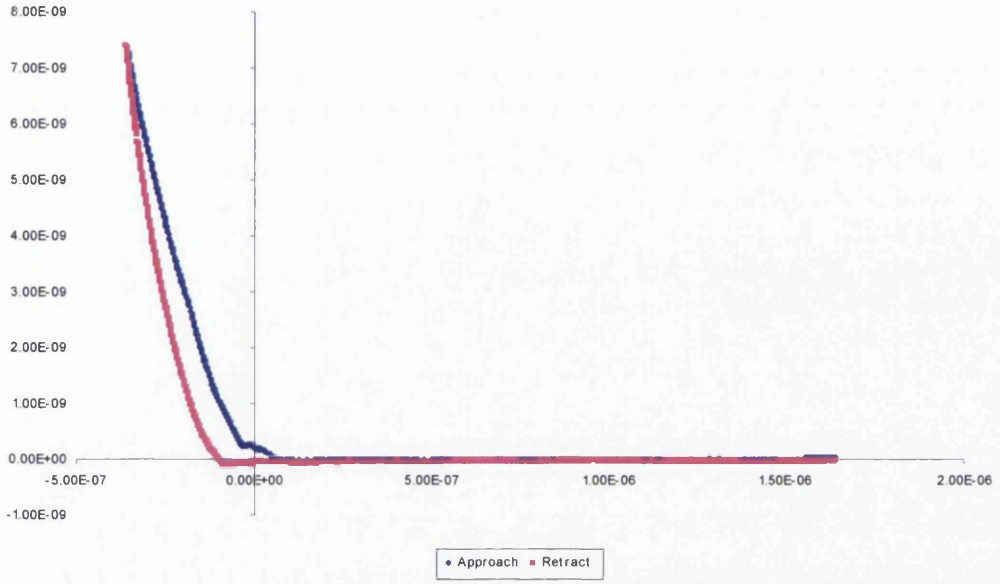

Figure 5-8: *Force spectrum for anaerobically grown cells in salt solution at pH 4 obtained with an iron oxide probe.*

5.3. Adhesion

When studying the force curves using the JPK Data Processing software it is possible to reposition the curve by adjusting the baseline force on the approach to zero, and to alter the x-offset such that the contact point is at zero distance, after converting the deflection to force and the height to distance. Once this initial preparation has been done the JPK Data Processing has an option for finding the lowest point on a selected part of the curve, either approach or retract, allowing measurement of any snap-in force on the approach and any adhesion force on retract. The software can also calculate the area between the retract curve and the zero force baseline. This area represents the work of adhesion and is an energy measurement in Joules. Where a classic adhesion profile is seen this can be useful in comparing the energies involved.

The iron oxide probe generated the following adhesion and surface energy, with different sample-environment combinations, as outlined in Table 5.1.

The errors shown in this table are one standard deviation from the mean and are in most cases very large in comparison with the mean values.

	Surface Energy (J)	Force of adhesion (pN)
Aerobic cells in water at pH 7	$5.5 \pm 7.0 \times 10^{-17}$	0.23 ± 0.21
Aerobic cells in 10^{-4}M NaCl at pH 3.5	$4.5 \pm 4.0 \times 10^{-17}$	0.15 ± 0.06
Anaerobic cells in water at pH 7	$1.2 \pm 0.95 \times 10^{-17}$	0.34 ± 0.24
Anaerobic cells in 10^{-4}M NaCl at pH 4	$2.2 \pm 2.7 \times 10^{-17}$	0.15 ± 0.14

Table 5.1: *Surface energy and adhesion force values obtained using JPK data processing software for aerobically and anaerobically grown cells in water and low salt solution using the same iron oxide probe with a diameter of 5μm.*

The adhesion forces are of the order of 0.1pN for all sample-environment combinations. The surface energies are also all on the same scale, however the energies for both experiments using aerobically grown cells are higher than those using anaerobically grown cells. The adhesion force is higher when the force spectra are obtained in water than in the salt solution, which is consistent with findings from van der Mei[159] and Dufrene[160].

Building on earlier work by the group that was principally authored by van der Mei, Dufrene et al investigated the effect of salt concentration on probe-microbe interaction[160]. In experiments with two different strains of *Streptococcus salivarius* it was found that probes approaching strain HB, which has a fibrillated surface, in water experienced a long-range repulsion at around 100nm from the surface. The range of this repulsion decreased to around 10nm in a solution of 0.1M KCl. For strain HBC12, which has a plain non-fibrillated surface, the ranges of repulsion in water and 0.1M KCl were 20nm and 10nm respectively. From this evidence the researchers concluded that the increased salt solution caused a "collapse of fibrillar mass" for strain HB, allowing the probe to approach without repulsion. The largest adhesion

force using bacteria in this study was found between the probe and the fibrillated strain in water, at 0.9 ± 0.4nN. The extension and related adhesion of surface fibrils or polymers is the suggested reason for HB in water having the highest adhesion. In contrast with *S. salivarius* HB, *S. oneidensis* MR-1 is not fibrillated, however surface polymers on the MR-1 surface may similarly extend further in water than in salt, causing greater adhesion on retraction of the probe from the surface. The adhesion for MR-1 is far less than that for HB, on the scale of pN rather than nN, however since the adhesion is also higher for anaerobically grown cells in water than in salt, it can be posited that surface molecules on both types of cell are better able to adhere to the probe in water, due to greater extension from the cell surface.

This aligns with similar effects on long cell-surface polymers which were found with *Pseudomonas putida* by Abu-lail and Camesano in 2003[142]. In low salt solution a large brush layer of 440nm extended from the surface of the cells, increasing salt concentration compressed this layer and in 1M KCl it extended only 120nm from the cell surface. However in this study the force of adhesion increased with the increase in salt concentration and decrease in brush layer extension, suggesting that for *P. putida* the cell surface is more adherent when the probe can get closer to it without the obstacle of an extended brush layer.

5.4. Young's modulus

In order to model the indentation the Hertz model adapted for a spherical indenter was used. The contact part of the curve on approach was used to generate a plot of the force against the indentation to the power of 3/2. The slope of this line was used to calculate a single value for the Young's modulus of the sample at a particular site and an average value was taken

for all of the estimated cell sites probed. This was done both in water at neutral pH and in 0.1mM NaCl with the pH adjusted to that of the isoelectric point for each sample.

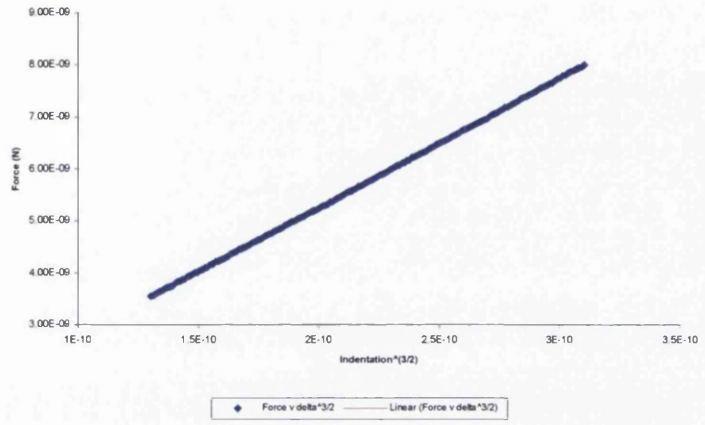

Figure 5-9: *Indentation region of curve plotted as force against* $\delta^{3/2}$ *for aerobically grown cells in water with a linear trend-line fitted. From the equation for the trend-line the Young's modulus E can be calculated.*

For initial comparison between the aerobically and anaerobically grown cells in water at neutral pH, and then in salt solution at adjusted pH, a maximum loading force of 10nN was used. After this initial study the loading force used for each sample/environment combination was increased by increments of 10nN. A maximum loading force for generating usable force spectra was found for each sample. Loading forces above this maximum gave rise to incoherent spectra.

For the aerobically grown cells in water an average Young's modulus of 11.0 ± 2.8 kPa was calculated. In contrast anaerobically grown cells in water demonstrated a Young's modulus of 35.5 ± 4.2 kPa, and a maximum loading force of 88nN. The anaerobically grown cell force spectra showed snap-in forces of a maximum of 1.3nN, but with the majority of spectra showing snap-in force 0.2nN or smaller.

In the pH adjusted salt solution, with a pH to match the isoelectric points as found in chapter 3, the Young's moduli for the aerobically grown cells was

higher than that for the anaerobically grown cells, the reverse of the situation in water. The Young's modulus for the aerobically grown cells in the pH adjusted salt solution was 25.3 ± 7.7 kPa. The measured Young's modulus for the anaerobically grown cells decreased from that measured in water to 0.35 ± 0.06 kPa, a hundred times smaller.

In comparing adhesion for the two types of cells and the two different environments for each of them, both aerobically and anaerobically grown cells showed lower adhesion in salt solution than in water. Conversely, aerobically grown cells were stiffer in salt than water whilst for the anaerobic cells the reverse was seen.

	Maximum load force (nN)	E (kPa)
Aerobic cells in water at pH 7	70	11.0 ± 2.8
Aerobic cells in 10^{-4}M NaCl at pH 3.5	76	25.3 ± 7.7
Anaerobic cells in water at pH 7	76	35.3 ± 4.2
Anaerobic cells in 10^{-4}M NaCl at pH 4	88	0.35 ± 0.06

Table 5.2: *Maximum load force and Young's modulus values for each sample as measured with the same iron oxide probe, iron oxide particle of diameter 5μm.*

5.5. *Graphite colloid probe*

As with the iron oxide probe, the graphite probe was not good for imaging the surface or distinct cells, so the force spectra taken were considered carefully in comparison to force spectra taken on a plain surface. The indentation was modelled using Hertz for a spherical indenter, as for the iron oxide probe.

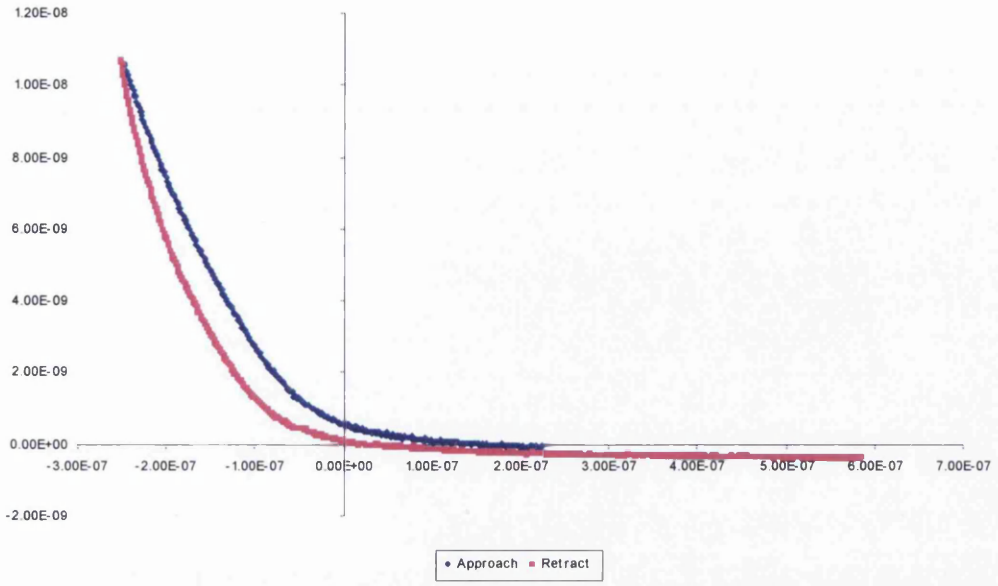

Figure 5-10: *Force curve obtained for aerobically grown cells in water at pH 7 using a graphite probe.*

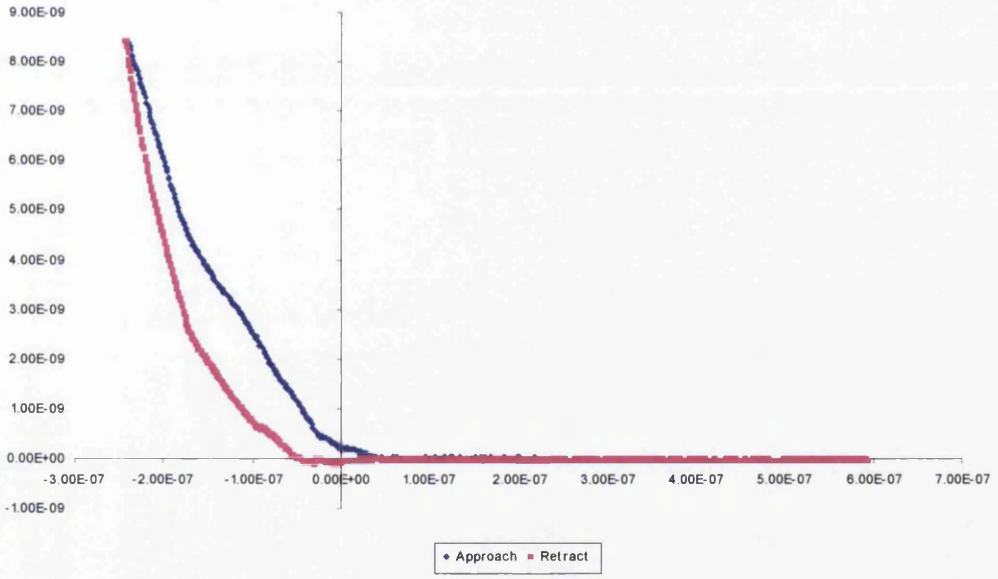

Figure 5-11: *Force spectrum for aerobically grown cells in salt solution at ph 3 obtained using a graphite probe.*

As can be seen in figures 5.10 and 5.11 showing force curves using aerobically grown cells, the contact regime for the cells in salt solution is less linear. There is no snap-in force for either curve, both curves show a difference between approach and retract and both return to the baseline force

on retraction from the surface. The curve in salt solution appears to show more adhesion however when averages using values for all the curves taken in each environment were calculated it was found that adhesion forces were of a similar magnitude and variation for both environments, as will be described in the next section.

In figures 5.12 and 5.13 force spectra for anaerobically grown cells in water and salt solution respectively are shown. The force spectrum for these cells in water shows repulsion as the probe approaches the contact point, which drops beyond a certain range. This means that there is a clear difference between the approach and retract curves, which is not seen on the spectrum for the anaerobically grown cells in the salt solution. There is no adhesion on the spectrum shown in water compared with a small adhesion shown in the salt solution, however when the averages are taken this difference disappears, as discussed in the next section.

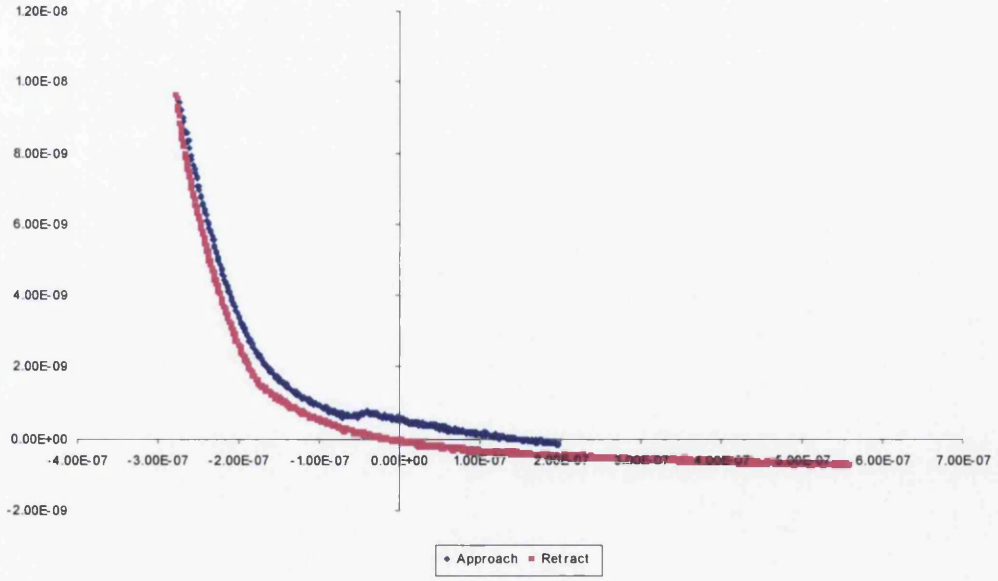

Figure 5-12: *Force spectrum obtained for anaerobically grown cells in water at pH 7 using a graphite probe.*

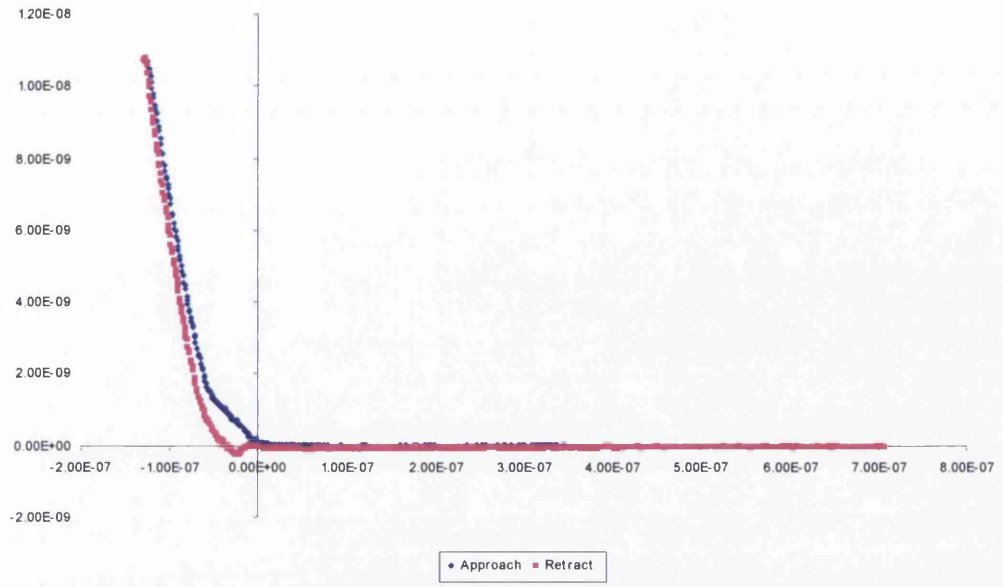

Figure 5-13: *Force spectrum obtained using a graphite probe for anaerobically grown cells in low salt solution at pH 4*

The disparity between baselines for approach and retract does affect the measured surface energy for the anaerobically grown cells in water however, as it stands out as the largest measured energy with the largest variation. This is seen in table 5.3.

5.5.1. Adhesion

The force of adhesion with the graphite probe was in all cases lower than the equivalent with the iron oxide probe, by a factor of ten. The surface energy was higher for the anaerobically grown cells than for the aerobically grown cells, but it was also less consistent with the error (one standard deviation from the mean) for the anaerobically grown cells in water being larger than the mean value itself.

	Surface Energy (J)	Force of adhesion (pN)
Aerobic cells in water at pH 7	$6.7 \pm 1.3 \times 10^{-17}$	0.26 ± 0.09
Aerobic cells in 10^{-4}M NaCl at pH 3.5	$3.3 \pm 0.6 \times 10^{-17}$	0.23 ± 0.08
Anaerobic cells in water at pH 7	$12.4 \pm 17.1 \times 10^{-17}$	0.18 ± 0.06
Anaerobic cells in 10^{-4}M NaCl at pH 4	$4.7 \pm 2.4 \times 10^{-17}$	0.16 ± 0.09

Table 5.3: *Surface energy and adhesion force values obtained using JPK data processing software for aerobically and anaerobically grown cells in water and low salt solution from force spectra obtained using the same graphite probe, made with a graphite particle of diameter 5μm.*

For the graphite probe the aerobically grown cells showed similar adhesion in both environments, as did the anaerobically grown cells, showing that the type of cell was more of a factor in the differences in interaction than the chemical environment for the graphite probe. This differs from what was found with the iron oxide probe

5.5.2. Young's modulus

The Young's modulus as measured by the graphite probe varied from the Young's modulus as measured by the iron oxide probe, and was also more variable. The average Young's modulus for aerobically grown cells in water was 26.7 ± 15.6 kPa, larger than the equivalent value for the iron oxide probe. The maximum loading force was around 76nN, slightly lower than that for the iron oxide probe. For anaerobically grown cells the average Young's modulus was 50.7 ± 24.6 kPa and the maximum loading force was 105nN.

In the pH adjusted salt solution the measured Young's moduli for the two types of cell are much higher. For aerobically grown cells the Young's modulus is 79.3 ± 23.9 kPa, which is around 3 times larger than that measured in water. The Young's modulus measured for the anaerobically grown cells is 116.2 ± 16.5 kPa, which is over twice that measured in water

and also has the lowest proportional error of any of the measured Young's moduli.

	Maximum load force (nN)	E (kPa)
Aerobic cells in water at pH 7	76	26.7 ± 15.6
Aerobic cells in 10^{-4}M NaCl at pH 3.5	77	79.3 ± 23.9
Anaerobic cells in water at pH 7	106	50.7 ± 24.6
Anaerobic cells in 10^{-4}M NaCl at pH 4	106	116.2 ± 16.5

Table 5.4: *Maximum load force and Young's modulus values for each sample as measured using the same graphite probe of diameter 5μm.*

Graphite is a softer material than iron oxide. Iron oxide crystals are known to have Young's moduli between 215 and 350GPa, although when considering a volume of powdered iron oxide the modulus is demonstrably lower [161]. By contrast the Young's modulus of manufactured forms of graphite is around 28-31GPa[162], varying depending on the form of the graphite. The difference between the Young's modulus for graphite and the range of Young's modulus for cells should be large enough for the Hertz model to be applicable. If the softness of graphite were a problem for the probe at all, it would be due to repeated force spectra taken on the plain glass surface, which is harder than the graphite, probe itself.

5.6. Chapter summary

The values for Young's modulus of the cells and near-cell surface are for the most part in the expected region of 10 to 100kPa for cells[157]. The Young's modulus for glass is in the region of 65GPa[163] and although this value will vary for different types of glass the relative softness of the biological surfaces is apparent by six orders of magnitude when comparing Young's modulus

values with that of the substrate, and in comparison with the Young's moduli of the probes used.

The pH and salt concentration of the buffer affects the recorded force-distance spectra. This is to be expected as the chemical environment changes any double layer effects and may also affect the conformation of cellular surface components, as described by van der Mei[159], Dufrene[160], and Abu-lail and Camesano[142].

Adhesion forces were ten times higher for the iron oxide probe than for the graphite probe, which adds further evidence to Lower et al's assertion that *S. oneidensis* MR-1 forms a specific bond with iron minerals due to recognition of the presence of Fe(III)[47, 48]. Their finding that adhesion to the iron oxide-hydroxide goethite was greater under anaerobic conditions than under aerobic conditions is also borne out here as the adhesion force for the anaerobically grown cells is higher than that for the aerobically grown cells. However since the force spectra in this thesis were conducted in an aerobic environment this effect may have been diminished. Lower et al used a cell-coated probe in contact with a mineral substrate, in a reverse of the experiments conducted for this thesis, demonstrating the versatility of AFM force studies and also demonstrating that the findings about *S. oneidensis* MR-1 are consistent even using different approaches in AFM.

6. Conclusions

This investigation for the explores in detail the effect of ionic strength and growth environment on *S. oneidensis* MR-1, particularly with regard to its microbe-microbe and microbe-surface interaction. Novel experimental methods that use a commercially available SPR system are used to investigate microbe-substrate interaction where the substrate approximates MFC electrodes. For the first time comparison of interactions between cells grown aerobically and anaerobically and probes of different material are made as measured by force spectroscopy. The aim of providing a comprehensive microbial profile for MR-1 as set out in the aims and objectives is achieved, as is the aim of providing information useful in the design of biosensors and MFCs. The development of novel methodology for investigating whole cell interaction with SPR sensor surfaces approximating device components is an added achievement of this research.

There are questions raised in this study that would be the starting point for further work and these are discussed later in this chapter with reference to the literature and the potential use of other existing techniques, as well as the further development of methods used in this research.

6.1. Key outcomes of research

6.1.1. Characterisation of MR-1

The oxygenated environment is a more successful environment for MR-1 than the anaerobic environment, in terms of longevity, due to the second phase of growth after 20 hours which is present for aerobic but not for anaerobic cells, and maximum concentration. Although these results point to the limitation of growth in the anaerobic environment, it can be argued that

the anaerobic environment is more successful in that there is no lag phase, compared with a 3 hour lag phase for the aerobic culture, and in that the doubling time for the anaerobic cells is 1 hour, less than the 2.5 hours for the aerobic cells. In conclusion, whilst the population will be larger and survive longer under aerobic conditions, anaerobic conditions will result in more rapid growth. The lack of lag phase for the anaerobic system suggests that aerobically grown cells are able to function and reproduce as anaerobes as soon as is necessary. It is possible that the decreased doubling time is due to shorter lifetimes for individual cells requiring them to reproduce earlier, as the methods used did not distinguish between living and dead cells.

The growth of aerobic and anaerobic cells is therefore shown to have inherent differences, demonstrating the adaptation to ambient conditions of which *S. oneidensis* is known to be capable. This is further supported by the AFM imaging of cells harvested at different stages of growth. The images of aerobic cells in long chains which cannot be distinguished as doubling pairs compared with obvious doubling pairs of anaerobic cells in the growth phase shows that the two types of cell look very different when reproducing (for example comparing Figure 3.10 with Figure 3.14).

This study is the first to investigate surface charge of MR-1 through ζ-potential and the first to compare the effect of salt concentration of aerobically and anaerobically grown cells respectively. The organism was found to form stable suspensions at certain pH values, in most cases at pH 2 or lower and pH 6 or higher. Measured isoelectric points, all between pH 3 and pH 6, changed with salt concentration, with this change being greater for anaerobically grown cells than aerobically grown cells, suggesting that their surface chemistry is more strongly affected by the chemical environment. The organism has been reported in the literature to be halotolerant, perhaps due to seawater origins before adaptation to the environment of Lake

Oneida[41]. However, no zeta potential investigation of *S. oneidensis* MR-1 has been carried out before and so there was no information about the effect of salt concentration on the surface charge of MR-1 microbes before this study.

Variability in binding to a poly-L-lysine coated SPR sensor surface was greater for the aerobically grown cells than for the anaerobically grown cells, as can be seen when comparing Figure 4.1 with Figure 4.2. The variability in size and shape over time for the aerobically grown cells using AFM imaging in combination with the SPR data is evidence for the heterogeneity of aerobically grown cells, compared with the anaerobically grown cells which showed less variation in size and shape according to the AFM images in Chapter 3, and less variation in binding over time to the poly-L-lysine functionalised SPR sensor chip as can be seen when comparing Figure 4.4 with Figure 4.5.

Novel work was carried out using probes of different materials, iron oxide which is a mineral *S. oneidensis* MR-1 has shown "directed affinity" for, according to previous research[48], and graphite which is commonly used for MFC electrodes[164], to investigate interactions between these materials and cells grown aerobically and anaerobically. Adhesion forces measured using the iron oxide probe showed a greater difference between samples in water and samples in pH adjusted salt solution, 0.08pN for the aerobic and 0.19pN for the anaerobic cells, than those measured using the graphite probe, which showed differences of 0.03pN for the aerobic and 0.2pN for the anaerobic. Thus the adhesion of cells to the graphite probe is more consistent than the adhesion of cells to the iron oxide probe as regards ambient conditions, and the errors in the measured adhesion are lower in proportion to the adhesion values for the graphite probe than for the iron oxide probe. This relates to Lower et al's findings[47] that MR-1 shows stronger adhesion

to goethite than another gram negative bacteria, *E. coli*, the reason being that MR-1 reduces iron as part of anaerobic respiration and therefore responds to its presence with increased adhesion force compared to adhesion force to other materials and compared to adhesion by non-metal reducing bacteria. The largest adhesion force was measured for anaerobic cells in water at pH 7 using the iron oxide probe as 0.34 ± 0.24pN, however the error associated with this value is proportionally large, indicating the inconsistency of adhesion values for this sample-probe combination.

Further to the adhesion measurements, the indentation of cell surfaces by probes was measured and used to calculate Young's modulus, E, for both aerobic and anaerobic cells. For the iron oxide probe the average value of E measured for the cells suspended in 10^{-4}M NaCl at pH 3.5 (E = 25kPa) was 14kPa higher than for the cells in water at pH 7 (E = 11kPa). For the anaerobic cells measured with the iron oxide probe the average value of E for cells in 10^{-4}M NaCl at pH 4 was ten times smaller (0.35kPa compare with 35kPa) than that for cells in water at pH 7. For the iron oxide probe the anaerobic cells in salt solution at the isoelectric point were the softest by an order of magnitude (0.35kPa). The graphite probe data matches the trend for the aerobic cells, with E being 52kPa larger for the salt solution at pH 3.5 than for water (79kPa and 27kPa respectively), but shows the reverse of that seen for the iron oxide probe for the anaerobic cells, for which E is 66kPa larger for the pH adjusted salt solution (E = 116kPa) than for the water sample (50kPa). For the graphite probe the anaerobic cells in salt solution at the isoelectric point were the stiffest by an order of magnitude (116kPa). The ionic strength of the solution will affect the configuration of molecular species on the cell surface as well as the cell wall itself and this is the origin of the difference between E measured in water at neutral pH and E measured in salt solution at an adjusted pH.

A recurring observation throughout this research has been the heterogeneity of aerobically grown cells compared with the relative homogeneity of anaerobically grown cells. This was observed with AFM imaging, in the ζ-potential measurements and in the SPR studies using poly-L-lysine. This suggests that cells living in the anoxic environment must maintain a specific morphology and surface chemistry that facilitates electron transfer to the replacement electron acceptor, whereas cells growing in an oxygen rich environment are able to grow larger and more varied as electron accepting oxygen is abundant and therefore respiration is not limited.

The experimental findings of this research are specific to the organism *S. oneidensis* MR-1 but the theory based on these findings can be expanded to include characterisation of gram-negative bacteria, dissimilatory metal reducers and facultative anaerobes in general using MR-1 as a model organism.

6.1.2. Experimental Design

Investigating via SPR the adhesion of whole cells to a PVD coated sensor surface was a further development of work using carbon-coated sensors to look at bio-molecule adhesion by Lockett et al[154], extending Lockett's idea into hitherto uncharted territory. The possibilities for further research presented by successful application of this experimental design are many and varied: in Chapter 1 the interactions of cells with inorganic surfaces such as microbially activated corrosion are briefly outlined, coating sensor surfaces with nanometre thick layers of metal could allow the use of SPR to investigate the adhesion of microbes to metal under various buffer conditions in order to understand better the environmental causes of corrosion for example. Applications for the coatings of medical implants that

need to be resistant to the formation of microbial biofilms can also be envisioned. Comparative binding assays involving different strains or even genetically modified strains of bacteria, already undertaken using BIAcore systems with conventional surface preparation, could also be conducted on PVD coated sensors.

The limitation for this kind of investigation however, is the non-specificity of the binding due to the various binding possibilities on the surface of most bacteria. Use of simple binding models can only give comparative rather than absolute data, and must be applied consistently for the resultant rate constant values to have any meaning. In the comparative studies in this research aerobically grown cells were shown to have association rates of the order of $10^7 M^{-1}s^{-1}$ on both the 2nm and 10nm thick carbon surface, with the association rates for the anaerobically grown cells being an order of magnitude greater.The dissociation cases were of the same magnitude for both aerobic and anaerobic on both surfaces. Using the k_{on} parameter as described by Kawashima et al it was interesting to see that the aerobic and anaerobic values of kon from the 10nm carbon layer data were similar, $2x10^{-9}$ and $8x10^{-9}$ RU/cell respectively, whereas those from the 2nm carbon layer differ by 2 orders of magnitude: $4x10^{-10}$ RU/cell for the aerobically grown and $2x10^{-8}$ RU/cell for the anaerobically grown cells. This may indicate that the 2nm carbon layer is not as complete as the 10nm carbon layer, allowing cells to interact with and bind to the gold surface beneath. Alternatively, since the depth of the carbon layer is shown by Lockett et al to affect the sensitivity of the SPR system the difference between the aerobic and anaerobic binding may not be as strongly measured by the sensor surface with the thicker carbon layer. Further studies would be required to discover which of these explanations is correct.

6.2. *Applications and wider context*

Microbial fuel cells and biosensors are dependent on the interface between biological components and inorganic circuitry. In this research the nature of interaction of whole *S. oneidensis* MR-1 cells with graphite and amorphous carbon approximated the interaction of such cells to MFC electrodes. Adhesion of cells to graphite was compared, using force spectroscopy, to adhesion of cells to iron oxide, which as a common naturally occurring near-surface mineral is reduced by MR-1 in oxygen limited environments. The salt concentration and pH of the solution in which the MFC is maintained can be used to alter the level of binding of cells to electrodes as demonstrated in the poly-L-lysine SPR assay.

The interaction of whole cells with surfaces mimicking electrodes of different composition could be investigated using the new experimental method outlined in the latter part of Chapter 4.

Microbial fuel cells are important as they have the potential to fulfil energy requirements for low power, autonomous, devices. The development of multi-organism MFCs offers the opportunity to develop such devices that take advantage of the optimum combination of microbes using different fuels and different electron pathways to give continuous power. Research into such poly-species MFCs has already shown that microbial populations will adjust to the environment of the MFC system establishing a natural order of successful organisms[35], showing preference for those which self-mediate electron transfer.

The introduction to Logan's 2008 book, Microbial Fuel Cells, outlines his vision for the development of MFCs, believing that they will be developed initially as a method of reclaiming energy from wastewater[18]. Having initially stated that "requirements for making MFC's economically viable as a method for energy production are demanding", Logan makes the case that as

domestic, animal and food processing wastewaters in his native USA contain an estimated 17GW in the form of biodegradable organic matter, recovering this energy would be enough to make the water infrastructure of the USA self sufficient. He envisions that this goal is an achievable milestone in the development of MFCs and is a strong incentive for further MFC research.

Research into wastewater treatment using microbial fuel cells has been an ongoing concern since studies in the late 1990's by Kim et al[15, 165]. Successes have included the development of mediator-less MFCs[30]. Now armed with greater knowledge of the surface molecules[166-168] and electron transfer pathways[46, 169, 170] which has been developed in the intervening years, and the effect of environment on cell-cell and cell-surface interaction of a commonly used MFC organism along with novel methodology for investigating cell-electrode interaction developed in this thesis, further research into MFCs can be targeted for specific situations and take advantage of specific features of *S. oneidensis* MR-1. If energy can be recovered from wastewater using MFCs such that the drain on energy resources to treat wastewater is mitigated, this will pave the way for novel alternative energy sources such as MFCs and related biomass conversion methods to be taken seriously in the wider realm of energy production.

In the immediate future innovative approaches to energy production are needed to meet rising global demands and to concurrently tackle the problems of increased carbon dioxide levels in the atmosphere by reducing the global reliance on fossil fuels. Although production of current from MFCs in laboratory environments is on the scale of mA there is potential for scaling up the technology, and in the future as fossil fuels become scarcer and the effects of climate change become more apparent, all possible safe, renewable energy sources will have their part to play.

6.3. *Future work*

Of the many directions in which future work could be taken, the priorities are:

- Application of the effect of environmental conditions on the MR-1 bacteria to the design of MFCs using this bacterium.
- Use of the BIAcore SPR system to investigate whole cell binding to PVD coated surfaces approximating practical cell-surface interactions.
- Force spectroscopy of living cells under various process relevant environmental conditions.

In 2008 Biffinger et al examined the influence of pH on MFC output, using two different strains of *S. oneidensis*: DSP10 and MR-1[54]. MFC systems were maintained at pH 5, 6 and 7 for each strain. Further work could use Biffinger's methodology to measure current and power density for MFC systems optimised for cellular adhesion to electrodes, or for those optimised for stable suspension of cells in order to examine the effects of posited mediators excreted from cells such as flavins, described as mediating extracellular electron transfer in a 2008 study by Marsili et al[44].

Since *S. oneidensis* can transfer electrons extracellularly via direct contact and self-expressed chemical mediation, the chemical environment can be adjusted so that these cells adhere or remain planktonic, with the MFC continuing to produce a current. Therefore design of MFCs using more than one organism could be constructed such that the other organisms' requirement to be in electrode contact is met whilst *S. oneidensis* continues to be active in current production.

Many MFCs use graphite fibre brush electrodes at the anode, which have high specific surface area and porosity compared with other forms of graphite or carbon-based electrodes such as carbon cloth[18].

Approximating a fibre brush electrode in SPR would be complicated by the limits of detection away from the surface, as would any approximation of such an electrode surface with force spectroscopy. Both methods allow researchers only to assess the interaction on a very small scale, at the scale of a point on the surface of one fibre rather than at the scale of a whole graphite brush anode.

Research into binding interaction using the PVD coated SPR sensor for whole cells could be developed for MFC research by using graphite rather than amorphous carbon to more closely match the anode properties. The problem with non-specific binding inherent to whole cell studies such as this would suggest that isolated molecules from the cell surface, such as surface cytochromes, could be injected over the PVD coated surface in order to identify the active surface molecules involved in binding. This kind of study would be closer to the original use of BIAcore and other SPR equipment for specific one-on-one binding. The influence of pH and salt concentration in running buffers and sample solutions could be investigated further in this way.

Alternatively, whole cells of mutant *S. oneidensis* species designed to be deficient or artifically abundant in specific OM molecules could be used in comparison with the wild type MR-1 in the SPR study. Such a comparative strain of the bacteria could also be used for comparison throughout all the studies in this research from growth monitoring to ζ-potential as well as forces spectroscopy.

Research into the growth of *S. oneidensis* MR-1 has shown the effect of temperature on growth, and the effect of pH on gene expression, and with the growth curves and quantitative growth data in this thesis as a starting point the effect of pH and salinity on cell culture growth could be used to find the limits of survivability for MR-1 in diverse environments. This in

turn would provide information about the limitations on chemical environment for working MFCs using this organism, as well as the sustainability of MFCs. The need for continuous energy supply from MFCs will require an understanding of how the microbial community will progress in the different phases of growth and how a stable, living, culture can be maintained over time.

Further AFM research could include single molecule force spectroscopy experiments designed to measure adhesion of a sharp AFM tip to OM molecules on cells imaged by such a tip. This set up would require high resolution AFM in liquid. In contrast a colloid probe coated with isolated OM molecules could be used to measure adhesion between an estimated number of molecules and a substrate such as graphite or iron oxide.

S. oneidensis MR-1 presents a vital model organism for MFCs, as well as biosensors using gram-negative metal-reducing bacteria. Applicable areas of research using this organism include genomic studies, bioremediative studies, biosensors, MFCs, generic microbe-inorganic interface studies, isolation and characterisation of surface molecules, and electron transfer pathway identification. Insight into the metabolic function and the cellular interface of MR-1 allows understanding of the evolutionary adaptation of microbes for the environments they encounter and the strategies they develop for variation in environment. The "design" of microbial machinery used by individual cells for survival provides precedent for man-made design on similar scales as well as ready made nano-devices for use in biotechnology applications. From energy production, as described previously, to medical applications either encouraging or removing biofilms, as well as corrosion and other effects of microbial action, a fundamental understanding of the lives of bacteria such as MR-1 is essential as science

hurtles towards a world where technology is ever smaller and more complex and its application ever more wide-reaching.

7. References

1. Madigan, M.T., et al, *Brock Biology of Microorganisms*. 12th ed: Pearson Education.
2. Barthlott, W., Neinhuis, C., *Purity of the sacred lotus, or escape from contamination in biological surfaces.* Planta, 1997. **202**: p. 1-8.
3. Goodsell, D.S., *Bionanotechnology: Lessons From Nature*. 2004: Wiley-Liss.
4. Svitel, J., et al, *Gluconobacter in biosensors: applications of whole cells and enzymes isolated from gluconobacter and acetobacter to biosensor construction.* Biotechnology Letters, 2006. **28**: p. 2003-2010.
5. Darder, M., Aranda, P., Ruiz-Hitzky, E., *Bionanocomposites: A new concept of ecological, bioinspired, and functional hybrid materials.* Advanced Materials, 2007. **19**: p. 1309-1319.
6. Du, Z., Li, H., Gu, T., *A state of the art review on microbial fuel cells: a promising technology for wastewater treatment and bioenergy.* Biotechnology Advances, 2007. **25**: p. 464-482.
7. Macleay, I., Harris, K., Annut, A., *Digest of UK Energy Statistics 2010,* D.o.E.a.C. Change, Editor. 2010, National Statistics: London.
8. Legras, J.-L., Merdinoglu, D., Cornuet, J-M., Karst, F., *Bread, beer and wine: Saccharomyces cerevisiae diversity reflects human history.* Molecular Ecology, 2007. **16**: p. 2091-2102.
9. McKane, L., Kandel, J., *Microbiology: essentials and applications.*: McGrawHill Companies.
10. Mitchell, J.G., Kogure, K., *Bacterial motility: links to the environment and a driving force for microbial physics.* FEMS Microbial Ecology, 2005. **55**: p. 3-16.
11. Ghuysen, J.M., Hakenbeck, R., *Bacterial Cell Wall*. New Comprehensive Biochemistry. Vol. 27. 1994, Amsterdam: Elsevier.
12. Beveridge, T.J., Graham, L. L., *Surface layers of bacteria.* Microbiological Reviews, 1991. **55**(4): p. 684-705.
13. Lodish, H., Berk, A., Kaiser, C. A., Krieger, M., Scott, M. P., Bretscher, A., Ploegh, H., *Molecular Cell Biology*. 6th Edition ed. 2008, New York: W. H. Freeman and Company.
14. Gralnick, J.A., Newman, D. K. , *Extracellular respiration.* Molecular Microbiology, 2007. **65**(1): p. 1-11.

15. Kim, B.H., et al, *Electrochemical activity of an Fe(III)-reducing bacterium, Shewanella putrefaciens IR-1, in the presence of alternative electron acceptors.* Biotechnology Techniques, 1999. **13**: p. 475-478.

16. Shi, L., et al, *Respiration of metal (hydr)oxides by Shewanella and Geobacter: a key role for multi-haem c-type cytochromes.* Molecular Microbiology, 2007. **65**(1): p. 12-20.

17. Bond, D.R., *Electrode-reducing microorganisms that harvest energy from marine sediments.* Science, 2002. **295**: p. 483-484.

18. Logan, B.E., *Microbial Fuel Cells*: WileyBlackwell.

19. Mandal, D., et al, *The use of microorganisms for the formation of metal nanoparticles and their application.* Applied Microbiology and Biotechnology, 2006. **69**: p. 485-492.

20. Kowshik, M., et al, *Microbial synthesis of semiconductor CdS nanoparticles, their characterization, and their use in the fabrication of an ideal diode.* Biotechnology and bioengineering, 2002. **78**(5): p. 583-588.

21. Gericke, M., Pinches, A., *Biological synthesis of metal nanoparticles.* Hydrometallurgy, 2006. **83**: p. 132-140.

22. Kumar, N., Curtis, W., Hahm, J., *Laterally aligned, multiwalled carbon nanotube growth using Magnetospirillium magnetotacticum.* Applied Physics Letters, 2005. **86**: p. 173101-173103.

23. Mansfeld, F., *The interaction of bacteria and metals.* Electrochimica acta, 2007. **50**: p. 7670-7680.

24. Wall, J.D., Krumholz, L. R., *Uranium Reduction.* Annual Review of Microbiology, 2006. **60**: p. 149-166.

25. Schneider, R.P., et al, *Contamination levels and preliminary assessment of the technical feasibility of employing natural attenuation in 5 priority areas of Presidente Bernardes Refinery in Cubatao, Sao Paulo, Brazil.* Environmental Monitoring and Assessment, 2006. **116**: p. 21-52.

26. Batzias, F.A., Siontorou, C. G., *A knowledge-based approach to environmental biomonitoring.* Environmental Monitoring and Assessment, 2006. **123**: p. 167-197.

27. Lovley, D.R., *Bug juice: harvesting electricity with microorganisms.* Nature Reviews Microbiology, 2006. **4**: p. 497-508.

28. Lewis, K., *Symposium on Bioelectrochemistry of Microorganisms IV Biochemical Fuel Cells.* Bacteriological Reviews, 1966. **30**(1): p. 101-113.

29. Debabov, V.G., *Electricity from microorganisms.* Microbiology, 2008. **77**(2): p. 123-131.

30. Kim, H.J., et al, *A mediator-less microbial fuel cell using a metal reducing bacterium, Shewanella putrefaciens.* Enzyme and Microbial Technology, 2002. **30**: p. 145-152.

31. Bond, D.R., Lovley, D. R., *Electricity production by Geobacter sulfurreducens attached to electrodes.* Applied and Environmental Microbiology, 2003. **69**(3): p. 1548-1555.

32. Holmes, D.E., et al, *Microarray and genetic analysis of electron transfer to electrodes in Geobacter sulfurreducens.* Environmental Microbiology, 2006. **8**(10): p. 1805-1815.

33. Reguera, G., et al, *Biofilm and nanowire production leads to increased current in Geobacter sulfurreducens fuel cells.* Applied and Environmental Microbiology, 2006. **72**(11): p. 7345-7348.

34. Moon, H., Chang, I. S., Kim, B. H., *Continuous electricity production from artificial wastewater using a mediator-less microbial fuel cell.* Bioresource Technology, 2006. **97**: p. 621-627.

35. Rabaey, K., *Biofuel cells select for microbial consortia that self-mediate electron transfer.* Applied and Environmental Microbiology, 2004. **70**(9): p. 5373-5382.

36. Rismani-Yazdi, H., Carver, S. M., Christy, A. D., Tuovinen, O. H., *Cathodic limitations in microbial fuel cells: an overview.* Journal of Power Sources, 2008. **180**: p. 683-694.

37. Kim, B.H., Chang, I. S., Gadd, G. M., *Challenges in microbial fuel cell development and operation.* Applied Microbiology and Biotechnology, 2007. **76**: p. 485-494.

38. Larsen, L.H., Revsbech, N. P., Binnerup, S. J., *A microsensor for nitrate based on immobilized denitrifying bacteria.* Applied and Environmental Microbiology, 1996. **62**(4): p. 1248-1251.

39. Mrazek, J., Spormann, A. M., Karlin, S., *Genomic comparisons amongst γ-proteobacteria.* Environmental Microbiology, 2006. **8**(2): p. 273-288.

40. Meshulam-Simon, G., et al, *Hydrogen metabolism in Shewanella oneidensis MR-1.* Applied and Environmental Microbiology, 2007. **73**(4): p. 1153-1165.

41. Venkateswaran, K., et al, *Polyphasic taxonomy of the genus Shewanella and description of Shewanella oneidensis sp. nov.* International Journal of Systematic Bacteriology, 1999. **49**: p. 705-724.

42. Heidelberg, J.F., et al, *Genome sequence of the dissimilatory metal ion-reducing bacterium Shewanella oneidensis.* Nature Biotechnology, 2002. **20**(11): p. 1118-1123.

43. Newman, D.K., Kolter, D. R., *A role for excreted quinones in extracellular electron transfer.* Nature, 2000. **405**: p. 94-97.

44. Marsili, E., et al, *Shewanella secretes flavins that mediate extracellular electron transfer.* Proceedings of the National Academy of Sciences USA, 2008. **105**(10): p. 3968-3973.

45. Reguera, G., et al, *Extracellular electron transfer via microbial nanowires.* Nature, 2005. **435**(7045): p. 1098-1101.

46. Gorby, Y.A., et al, *Electrically conductive bacterial nanowires produced by Shewanella oneidensis strain MR-1 and other microorganisms.* Proceedings of the National Academy of Sciences USA, 2006. **103**: p. 11358-11363.

47. Lower, S.K., *Directed natural forces of affinity between a bacterium and mineral.* American Journal of Science, 2005. **305**: p. 752-765.

48. Lower, S.K., Hoachella, M. F., Beveridge, T. J., *Bacterial recognition of mineral services: nanoscale interactions between Shewanella and alpha-FeOOH.* Science, 2001. **292**: p. 1360-1363.

49. Lower, B.H., Hochella, M. F., Lower, S. K, *Putative mineral-specific proteins synthesized by a metal reducing bacterium.* American Journal of Science, 2005. **305**: p. 687-710.

50. Lies, D.P., et al, *Shewanella oneidensis MR-1 uses overlapping pathways for iron reduction at a distance and by direct contact under conditions relevant for biofilms.* Applied and Environmental Microbiology, 2005. **71**(8): p. 4414-4426.

51. Biju, V., et al, *Combined spectroscopic and topographic characterization of nanoscale domains and their distributions of a redox protein on bacterial cell surfaces.* Langmuir, 2007. **23**(1333-1338).

52. Elias, D.A., et al, *The influence of cultivation methods on Shewanella oneidensis physiology and proteome expression.* Archive of Microbiology, 2008. **189**: p. 313-324.

53. Abboud, R., et al, *Low-temperature growth of Shewanella oneidensis MR-1.* Applied and Environmental Microbiology, 2005. **71**(2): p. 811-816.

54. Biffinger, J.C., et al, *The influence of acidity on microbial fuel cells containing Shewanella oneidensis.* Biosensors and Bioelectronics, 2008. **24**: p. 900-905.

55. Timp, G., *Nanotechnology.* 1999: Springer.

56. Turbadar, T., *Complete absorption of light by thin metal films.* Proceedings of the Physical Society, 1959. **73**: p. 40-44.

57. *BIAcore Technology Note 1: Surface Plasmon Resonance.* 2001, BIAcore AB.

58. Otto, K., *Biophysical approaches to study the dynamic process of bacterial adhesion.* Research in Microbiology, 2008. **159**: p. 415-422.

59. Innes, R.A., Sambles, J. R., *Optical characterisation of gold using surfaces plasmon-polaritons.* Journal of Physics F: Metal Physics, 1987. **17**: p. 277-287.

60. Karlsson, R., *Real-time competitive kinetic analysis of interactions between low-molecular-weight ligands in solution and surface-immobilized receptors.* Analytical Biochemistry, 1994. **221**: p. 142-151.

61. Flanagan, M.T., Pantell, R. H., *Surface Plasmon Resonance and Immunosensors.* Electronics Letters, 1084. **20**(23): p. 968-970.

62. Jenkins, A.T.A., et al, *Surface plasmon resonance shows that type IV pili are important in surface attachment by Pseudomonas aeruginosa.* Journal of the Royal Society Interface, 2005. **2**: p. 255-259.

63. Jenkins, A.T.A., et al, *Study of the attachment of Pseudomonas aeruginosa on gold and modified gold surfaces using surface plasmon resonance.* Biotechnology Progress, 2004. **20**: p. 1233-1236.

64. Takeuchi, H., et al, *Novel mucoadhesion tests for polymers and polymer-coated particles to design optimal mucoadhesive drug delivery systems.* Advanced Drug Delivery Reviews, 2005. **57**: p. 1583-1594.

65. Waswa, J.W., Debroy, C., Irudayaraj, J., *Rapid detection of Salmonella enteriditis and Eschericia coli using surface plasmon resonance sensor.* Journal of Food Process Engineering, 2006. **29**: p. 373-385.

66. Fivash, M., Towler, E. M., Fisher, R. J., , *BIAcore for macromolecular interaction.* Current Opinion in Biotechnology, 1998. **9**: p. 97-101.

67. BIAcore, *Kinetic and Affinity Analysis using BIA Level 1 Course Documentation*: BIAcore AB.

68. Nobbs, A.H., et al, *Consequences of a sortase A mutation in Streptococcus gordonii.* Microbiology, 2007. **153**: p. 4088-4097.

69. Oli, M.W., Mcarthur, W. P., Brady, J., *A whole cell BIAcore assay to evaluate P1-mediated adherence of Streptococcus mutans to human salivary agglutinin and inhibition by specific antibodies.* Journal of Microbiological Methods, 2006. **65**: p. 503-511.

70. Karlsson, R., Michaelsson, A., Mattsson, L., *Kinetic analysis of monoclonal antibody-antigen interactions with a new biosensor based analytical system.* Journal of Immunological Methods, 1991. **145**: p. 229-240.

71. Gill, A., et al, *Analysis of kinetic data of antibody-antigen interaction from an optical biosensor by exponential curve fitting.* Journal of Biotechnology, 1996. **48**: p. 117-127.

72. Nieba, L., Krebber, A., Pluckthun, A., *Competition BIAcore for measuring true affinities: large differences from values determined from binding kinetics.* Analytical Biochemistry, 1996. **234**: p. 155-165.

73. O'Shanessy, D.J., Winzor, D. J., *Interpretation of deviations from pseudo-first-order kinetic behaviour in the characterization of ligand binding by biosensor technology.* Analytical Biochemistry, 1996. **236**: p. 275-283.

74. Parsons, I.D., et al, *Probing the molecular mechanism of action of co-repressor in the E. coli methionine repressor-operator complex using surface plasmon resonance (SPR).* Nucleic Acids Research, 1995. **23**(2): p. 211-216.

75. Kawashima, M., et al, *Real-time interaction of oral streptococci with human salivary components.* Oral Microbiology Immunology, 2003. **18**: p. 220-225.

76. Medina, M.B., van Houten, L., Cooke, P. H., Tu, S. I., *Real-time analysis of antibody binding interactions with immobilized E. coli O157:H7 cells using the BIAcore.* Biotechnology Techniques, 1997. **11**(3): p. 173-136.

77. Leonard, P., Hearty, S., Quinn, J., O'Kennedy, R., *A generic approach for the detection of whole Listeria monocytogenes cells in contaminated samples using surface plasmon resonance.* Biosensors and Bioelectronics, 2004. **19**: p. 1331-1335.

78. Quinn, J.G., et al, *Development and Application of Surface Plasmon Resonance-Based Biosensors for the Detection of Cell–Ligand Interactions.* Analytical Biochemistry, 2000. **281**(2): p. 135-143.

79. Hunter, R.J., *Introduction to Modern Colloid Science.* Oxford Science Publications. 1993, Oxford: Oxford University Press.

80. Wilson, M., Kannangara, K., Smith, G., Simmons, M., Raguse, B., *Nanotechnology: Basic Science and Emerging Technologies.* 2002: Chapman & Hall/CRC.

81. Shaw, D.J., *Colloid and Surface Chemistry.* 4th ed. 1992, Oxford: Butterworth-Heinemann Ltd.

82. *Zeta potential measurement using laser Doppler electrophoresis (LDE).* 2010 [cited September 2010]; Available from:

http://www.malvern.com/LabEng/technology/zeta_potential/zeta_potential_LDE.htm.

83. Wilson, W.W., Wade, M. M., Holman, S. C., Champlin, F. R., *Status of methods for determining bacterial cell surface properties based on zeta potential methods.* Journal of Microbiological Methods, 2001. **43**: p. 153-164.

84. Hunter, R.J., *Zeta Potential in Colloid Science.* Colloid Science: A Series of Monographs., ed. R.H. Ottewille, Rowell, R. L. 1981, London: Academic Press Inc. Ltd.

85. Dague, E., et al, *Probing surface structures of Shewanella spp. by microelectrophoresis.* Biophysical Journal, 2006. **90**: p. 2612-2621.

86. van Loosdrecht, M.C.M., et al, *Electrophoretic mobility and hydrophobicity as a measure to predict the initial steps of bacterial adhesion.* Applied and Environmental Microbiology, 1987. **53**(8): p. 1898-1901.

87. Satou, J., et al, *Streptococcal adherence on various restorative materials.* Journal of Dental Research, 1987. **67**(3): p. 588-591.

88. Vanhaecke, E., et all, *Kinetics of Pseudomonas aeruginosa adhesion to 304 and 316-L stainless steel: role of cell surface hydrophobicity.* Applied and Environmental Microbiology, 1990. **56**(3): p. 788-795.

89. Grasso, D., Smets, B. F., Strevett, K. A., Machinist, B. D., *Impact of physiological state on surface thermodynamics and adhesion of Pseudomonas aeruginosa.* Environmental Science and Technology, 1996. **30**: p. 3604-3608.

90. Wiesendanger, R., *Scanning-probe-based science and technology.* Proceedings of the National Academy of Sciences USA, 1997. **94**: p. 12749-12750.

91. Binnig, G., Rohrer, H., *Scanning tunneling microscopy - from birth to adolescence.* Reviews of Modern Physics, 1987. **59**(3): p. 615-629.

92. Binnig, G., Quate, C. F., Gerber, C., *Atomic Force Microscope.* Physical Review Letters, 1986. **56**(9): p. 930.

93. Marti, O., Drake, B., Hansma, P. K., *Atomic force microscopy of liquid-covered surfaces: atomic resolution images.* Applied Physics Letters, 1987. **51**(7): p. 484-486.

94. Dufrene, Y.F., et al, *Direct probing of the surface ultrastructure and molecular interactions of dormant and germinating spores of Phanerochaete chrysosporium.* Journal of Bacteriology, 1999. **181**(17): p. 5350-5354.

95. Scheuring, S., Sturgis, J. N., *Atomic force microscopy of the bacterial photosynthetic apparatus: plain pictures of an elaborate machine.* Photosynthesis Research, 2009. **102**: p. 197-211.

96. Dupres, V., Alsteens, D., Pauwels, K., Dufrene, Y. F., *In vivo imaging of S-layer nanoarrays on Corynebacterium glutamicum.* Langmuir, 2009. **25**(17): p. 9653-9655.

97. *A Practical Guide to SPM.* 2005 [cited September 2010]; Available from:

http://www.veeco.com/pdfs/library/SPM_Guide_0829_05_166.pdf.

98. Magonov, S., Whangbo, M-H., *Surface Analysis with STM and AFM.* 1996, Weinheim and New York: VCH Publishers Inc and VCH Verlagsgesellschaft mbH.

99. Morris, V.M., Kirby, A. R., Gunning, A. P., *Atomic Force Microscopy for Biologists.* 2004, London: Imperial College Press.

100. Wiesendanger, R., *Scanning Probe Microscopy and Spectroscopy: Methods and Applications.* 1994, Cambridge: Cambridge University Press.

101. Poole, C.P., Owens, F. J., *Introduction to Nanotechnology.* 2003: Wiley.

102. Bowen, W.R., Doneva, T., Hilal, N., Wright, C. J., *Atomic force microscopy: images and interactions.* Microscopy and Analysis, 2001. **81**: p. 5-7.

103. Heinz, W.F., Hoh, J. H., *Spatially resolved force spectroscopy of biological surfaces using the atomic force microscope.* Nanotechnology, 1999. **17**: p. 143-150.

104. Vinckier, A., Semenza, G., *Measuring elasticity of biological materials by atomic force microscopy.* FEBS Letters, 1998. **430**: p. 12-16.

105. Vadillo-Rodriguez, V., Beveridge, T., Dutcher, J. R., *Surface viscoelasticity of individual gram-negative bacterial cells measured using atomic force microscopy.* Journal of Bacteriology, 2008. **190**(12): p. 4225-4232.

106. Butt, H.J., *Measuring electrostatic, van der Waals, and hydration forces in electrolyte solutions with an atomic force microscope.* Biophysical Journal, 1991. **60**: p. 1438-1444.

107. Muller, D.J., Engel, A., *The height of biomolecules measured with the atomic force microscope depends on the electrostatic interactions.* Biophysical Journal, 1997. **73**: p. 1633-1644.

108. Sheng, X., Ting, Y. P., Pehkonen, S. O. , *Force measurements of bacterial adhesion on metals using a cell probe atomic force microscope.* Journal of Colloid and Interface Science, 2007. **310**: p. 661-669.

109. Wojcikiewicz, E.P., Zhang, X., Moy, V. T., *Force and compliance measurements on living cells using atomic force microscopy.* Biological Procedures Online, 2004. **6**(1): p. 1-9.

110. Bolshakova, A.V., Kiselyova, O. I., Yaminsky, I. V., *Microbial surfaces investigated using Atomic Force Microscopy.* Biotechnology Progress, 2004. **20**: p. 1615-1622.

111. Arnoldi, M., Fritz, M., Bauerlein, E., et al, *Bacterial turgor pressure can be measured by atomic force microscopy.* Physical Review E, 2000. **62**(1): p. 1034-1044.

112. Xu, W., et al, *Modeling and measuring the elastic properties of an archael surface, the sheath of Methanospirillm hungatei, and the implication for methane production.* Journal of Bacteriology, 1996. **178**(11): p. 3106-3112.

113. Touhami, A., Nysten, B., Dufrene, Y., *Nanoscale mapping of the elasticity of microbial cells by atomic force microscopy.* Langmuir, 2003. **19**: p. 4539-4543.

114. A-Hassan, E., et al, *Relative microelastic mapping of living cells by atomic force microscopy.* Biophysical Journal, 1998. **74**: p. 1564-1578.

115. Heuberger, M., Dietler, G., Schlapback, L., *Mapping the local Young's modulus by analysis of the elastic deformation.* Nanotechnology, 1994. **5**: p. 12-23.

116. Sirghi, L., Ponti, J., Broggi, F., Rossi, F., *Probing elasticity and adhesion of live cells by atomic force microscopy indentation* European Biophysics Journal, 2008. **37**: p. 935-945.

117. Allison, D.P., Hinterdofer, P., Han, W., *Biomolecular force measurements and the atomic force microscope.* Current Opinion in Biotechnology, 2002. **13**: p. 47-51.

118. Wright, C.J., Shah, M. K., Powell, L. C., Armstrong, I., *Application of AFM from microbial cell to biofilm.* Scanning, 2010. **32**: p. 134-149.

119. Kasas, S., Gotzos, V., Celio, M. R., *Observation of living cells using the atomic force microscope.* Biophysical Journal, 1993. **64**: p. 539-544.

120. Kasas, S., Ikai, A., *A method for anchoring round shaped cells for atomic force microscope imaging.* Biophysical Journal, 1995. **68**: p. 1678-1680.

121. Ahimou, F., Touhami, A., Dufrene, Y. F., *Real-time imaging of the surface topography of living yeast cells by atomic force microscopy.* Yeast, 2003. **20**: p. 25-30.

122. Micic, M., et al, *Correlated atomic force microscopy and fluorescence lifetime imaging of live bacterial cells.* Colloids and Surfaces B: Biointerfaces., 2004. **34**: p. 205-212.

123. Schaer-Zammaretti, P., Ubbink, J., *Imaging of lactic acid bacteria with AFM - elasticity and adhesion maps and their relationship to biological and structural data.* Ultramicroscopy, 2003. **97**: p. 199-208.

124. Doktycz, M.J., et al, *AFM imaging of bacteria in liquid media immobilized on gelatin coated mica surfaces.* Ultramicroscopy, 2003. **97**: p. 209-216.

125. Soon, R.L., et al, *Atomic force microscopy investigation of the morphology and topography of colistin-heteroresistant Acinetobacter baumannii strains as a function of growth phase and in response to colistin treatment.* Antimicrobial agents and chemotherapy, 2009. **53**(12): p. 4979-4986.

126. Pompl, R., et al, *The effect of low-temperature plasma on bacteria as observed by repeated AFM imaging.* New Journal of Physics, 2009. **11**: p. 115023.

127. McEwen, G.D., Wu, Y., Zhou, A., *Probing nanostructures of bacterial extracellular polymeric substances versus culture time by raman microspectroscopy and atomic force microscopy.* Biopolymers, 2009. **93**(2): p. 171-177.

128. Chalmeau, J., et al, *Contribution to the elucidation of the structure of the bacterial flagellum nano-motor through AFM imaging of the M-Ring.* Ultramicroscopy, 2009. **109**: p. 845-853.

129. Arnoldi, M., Kacher, C. M., Bauerlein, E., et al, *Elastic properties of the cell wall of Magnetospirillum gryphiswaldense investigated by atomic force microscopy.* Applied Physics A, 1998. **66**: p. S613-S617.

130. Lower, S.K., Tadanier, C. J., Hochella, M. F.,, *Measuring interfacial and adhesive between bacteria and mineral surfaces with biological force microscopy.* Geochimica et Cosmica Acta, 2000. **64**(18): p. 3133-3139.

131. Ahimou, F., Denis, F. A., Touhami, A., Dufrene, Y., *Probing microbial cell surface charges by Atomic Force Microscopy.* Langmuir, 2002. **18**: p. 9937-9941.

132. Lulevich, V., et al, *Cell mechanics using atomic force microscopy-based single-cell compression.* Langmuir, 2006. **22**: p. 8151-8155.

133. Touhami, A., et al, *Nanoscale characterization and determination of adhesion forces of Pseudomonas aeruginosa pili by using atomic force microscopy.* Journal of Bacteriology, 2006. **188**(2): p. 370-377.

134. Bowen, W.R., Lovitt, R. W., Wright, C. J., *Direct Quantification of Aspergillus niger spore adhesion in liquid using an atomic force microscope.* Journal of Colloid and Interface Science, 2000. **228**: p. 483-433.

135. Engel, A., Muller, D. J., *Observing single biomolecules at work with the atomic force microscope.* Nature Structural Biology, 2000. 7(9): p. 715-718.

136. Engel, A., Gaub, H. E., Muller, D. J., *Atomic force microscopy: A forceful way with single molecules.* Current Biology, 1999. **9**: p. R133-R136.

137. Camesano, T.A., Abu-Lail, N. I., *Heterogeneity in bacterial surface polysaccharides, probed on a single-molecule basis.* Biomacromolecules, 2002. **3**(661-667).

138. Dupres, V., Alsteens, D., Andre, G., Verbelen, C., Dufrene, Y. F., *Fishing single molecules on live cells.* Nano Today, 2009. **4**: p. 262-268.

139. Tang, J., et al, *Atomic force microscopy imaging and single molecule recognition force spectroscopy of coat proteins on the surface of Bacillus subtilis spore.* Journal of Molecular Recognition, 2007. **20**: p. 483-489.

140. Cross, S.E., et al, *Nanomechanical properties of glucans and associated cell-surface adhesion of Streptococcus mutans probed by atomic force microscopy under in situ conditions.* Microbiology, 2007. **153**: p. 3124-3132.

141. Francius, G., et al, *Detection, localisation, and conformational analysis of single polysaccharide molecules on live bacteria.* ACS Nano, 2008. **2**(9): p. 1921-1929.

142. Abu-Lail, N.I., Camesano, T. A., *Role of ionic strength on the relationship of biopoymer conformation, DVLO contributions and steric interactions to bioadhesion of Pseudomonas putida KT2442.* Biomacromolecules, 2003. **4**(1000-1012).

143. Gotzinger, M., Weigl, B., Peukert, W., Sommer, K., *Effect of roughness on particle adhesion in aqueous solutions: a study of Saccharomyces cerevisiae and a silica particle.* Colloids and Surfaces B: Biointerfaces., 2007. **55**: p. 44-50.

144. Vadillo-Rodriguez, V., et al, *Role of lactobacillus cell surface hydrophobicity as probed by AFM in adhesion to surfaces at low and high ionic strength.* Colloids and Surfaces B, 2005. **41**: p. 33-41.

145. Gaboriaud, F., et al, *Probing the modifications of polystyrene surface properties after incubation with the Shewanella putrefaciens bacteria at two pH values (4,10) by atomic force microscopy.* Surface and Interaction Analysis, 2007. **39**: p. 648-652.

146. Leaphart, A.B., et al, *Transcriptome profiling of Shewanella oneidensis gene expression following exposure to acidic and alkaline pH.* Journal of Bacteriology, 2006. **188**(4): p. 1633-1642.

147. Gallardo-Moreno, A.M., Liu, Y., Gonzalez-Martin, M. L., Camesano, T. A., *Atomic force microscopy analysis of bacterial surface morphology before and after cell washing.* Journal of Scanning Probe Microscopy, 2006. **1**: p. 63-73.

148. Myers, C.R., Myers, J. M., *Cell surface exposure of the outer membrane cytochromes of Shewanella oneidensis MR-1.* Letters in Applied Microbiology, 2003. **37**: p. 254-258.

149. McLean, J.S., et al, *Oxygen-dependent autoaggregation in Shewanella oneidensis MR-1.* Environmental Microbiology, 2008. **10**(7): p. 1861-1876.

150. Paulick, A., et al, *Two different stator systems drive a single polar flagellum in Shewanella oneidensis MR-1.* Molecular Microbiology, 2009. **71**(4): p. 836-850.

151. Uchida, H., et al, *A new assay using surface plasmon resonance (SPR) to determine binding of the Lactobacillus acidophilus group to human colonic mucin.* Bioscience, Biotechnology and Biochemistry, 2004. **65**(5): p. 1004-1010.

152. Salminen, A., et al, *Inhibition of P-fimbriated Eschericia coli adhesion by multivalent galabiose derivatives studied by a live-bacteria application of surface plasmon resonance.* Journal of Antimicrobial Chemotherapy, 2007. **60**: p. 495-501.

153. Uchida, H., et al, *A new assay using surface plasmon resonance (SPR) to determine binding of the Lactobacillus acidophilus group to human colonic mucin.* Bioscience, Biotechnology and Biochemistry, 2004. **68**(5): p. 1004-1010.

154. Lockett, M.R., et al, *Carbon on metal films for surface plasmon resonance detection of DNA arrays.* Journal of the American Chemical Society, 2008. **130**(27): p. 8611-8613.

155. Cerf, A., Cau, J-C., Vieu, C., Dague, E., *Nanomechanical properties of dead or alive single-patterned bacteria.* Langmuir, 2008. **25**(10): p. 5731-5736.

156. Gaboriaud, F., et al, *Surface structure and nanomechanical properties of Shewanella putrefaciens bacteria at two pH values (4 and 10) determined by atomic force microscopy.* Journal of Bacteriology, 2005. **187**(11): p. 3864-3868.

157. Butt, H.J., Cappella, B., Kappl, M., *Force measurements with the atomic force microscope: Technique, interpretation and applications.* Surface Science Reports, 2005. **59**: p. 1-152.

158. Withers, J.R., Aston, D. E., *Nanomechanical measurements with AFM in the elastic limit.* Advances in Colloid and Interface Science, 2006. **120**: p. 57-67.

159. van der Mei, H.C., et al, *Direct probing by atomic force microscopy of the cell surface softness of a fibrillated and nonfibrillated oral streptococcal strain.* Biophysical Journal, 2000. **78**: p. 2668-2674.

160. Dufrene, Y.F., et al, *Probing molecular interactions and mechanical properties of microbial cell surfaces by atomic force microscopy.* Ultramicroscopy, 2001. **86**: p. 113-120.

161. Ouglova, A., Berthaud, Y., Francois, M., Foct, F, *Mechanical properties of an iron oxide formed by corrosion in reinforced concrete structures.* Corrosion Science, 2006. **48**: p. 3988-4000.

162. Pierson, H.O., *Handbook of carbon, graphite, diamond and fullerenes.* 1993, Park Ridge, New Jersey: Noyes Publications.

163. Halliday, R., Resnick, R., Walker, J., *Fundamentals of Physics.* 6th ed. 2001: Wiley.

164. Logan, B.E., et al, *Microbial fuel cells: methodology and technology.* Environmental Science and Technology, 2006. **40**(17): p. 5181-5192.

165. Kim, H.J., Hyun, S. M., Chang, I. S., Kim, B. H., *A microbial fuel cell type lactate biosensor using a metal-reducing bacterium, Shewanella putrefaciens.* Journal of Microbiology and Biotechnology, 1999. **9**(3): p. 365-367.

166. Myers, C.R., Myers, J. M., *The outer membrane cytochromes of Shewanella oneidensis MR-1 are lipoproteins.* Letters in Applied Microbiology, 2004. **39**: p. 466-470.

167. Lower, B.H., et al, *Antibody recognition force microscopy shows that outer membrane cytochromes OmcA and MtrC are expressed on the exterior surface of Shewanella oneidensis MR-1.* Applied and Environmental Microbiology, 2009. **75**(9): p. 2931-2935.

168. Shi, L., et al, *Isolation of a high-affinity functional protein complex between OmcA and MtrC: two outer membrane decaheme c-type cytochromes of Shewanella oneidensis MR-1.* Journal of Bacteriology, 2006. **188**(13): p. 4705-4714.

169. Baron, D., LaBelle, E., Coursolle, D., Gralnick, J. A., Bond, D. R., *Electrochemical measurement of electron transfer kinetics by Shewanella oneidensis MR-1.* Journal of Biological Chemistry, 2009. **284**(42): p. 28865-28873.

170. Borloo, J., et al, *A kinetic approach to the dependence of dissimilatory metal reduction by Shewanella oneidensis MR-1 on the outer membrane cytochromes c OmcA and OmcB.* FEBS Journal, 2007. **274**: p. 3728-3738.

Appendix – BIAcore regeneration protocol

In order to successfully re-use a sensor surface, a suitable regeneration solution is used to remove bound material from the functionalised surface. The suitability of regeneration solutions is determined through testing for two criteria:

- That the solution removes all of the bound material
- That the solution leaves the functionalised surface able to be used again without diminishing binding

In order to test for this a sensorgram is run using the functionalised surface. Analyte is injected, and then the regeneration solution under test. The volume of each solution injected is also considered (larger volume means longer time of contact between solution and sensor surface which can lead to more interaction depending on flow rates).

After the injection of regeneration solution is over, the sensorgram should return to the baseline level seen before the sample was injected.

A second batch of sample is then injected. The sensorgram should reach the same maximum as the first sample injection reached, and the same net response should be seen after the sample injection has finished.

The regeneration solution is then injected again. Once again the sensorgram should return to the baseline level seen at the very start once the regeneration solution injection is over.

This process is repeated one last time. Any decrease in net ΔRU after injection or maximum RU levels during injection of sample needs to be noted as this means that the regeneration solution is not ideal.

This process is repeated for different regeneration solutions, starting with the least abrasive in smaller volumes. If the least abrasive potential regeneration solution does not fit the first criterion then a more abrasive potential regeneration solution is tested, and so on. If a potential regeneration solution is too harsh and despite fitting the first criterion does not fit the second criterion then varying concentration, volume injected or flow rate need to be considered and tested.

There is a list of suggested regeneration solutions in the BIAcore X handbook, but it is not exhaustive. For some interactions considering the chemistry of the analyte and functionalised surface may indicate which

regeneration solutions are likely to work, or lead to the use of a regeneration solution that is not suggested by BIAcore.

Regeneration solutions tested for use in BIAcore studies in this research:

0.1M, 1M NaCl

0.001M, 0.01M, 0.1M, 1M NaOH

0.1M, 1M HCl

70% Ethanol

1M EDTA

50% Glycerol

BIAdesorb solution 1 (0.5% sodium dodecyl sulphate solution)